



R.M. Hoff



S.A. Christopher

Remote Sensing of Particulate Pollution from Space: Have We Reached the Promised Land?

Raymond M. Hoff

Department of Physics and the Joint Center for Earth Systems Technology/Goddard Earth Sciences and Technology Center, University of Maryland, Baltimore County, Baltimore, MD

Sundar A. Christopher

Department of Atmospheric Sciences and Earth System Science Center, University of Alabama–Huntsville, Huntsville, AL

ABSTRACT

The recent literature on satellite remote sensing of air quality is reviewed. 2009 is the 50th anniversary of the first satellite atmospheric observations. For the first 40 of those years, atmospheric composition measurements, meteorology, and atmospheric structure and dynamics dominated the missions launched. Since 1995, 42 instruments relevant to air quality measurements have been put into orbit. Trace gases such as ozone, nitric oxide, nitrogen dioxide, water, oxygen/tetraoxygen, bromine oxide, sulfur dioxide, formaldehyde, glyoxal, chlorine dioxide, chlorine monoxide, and nitrate radical have been measured in the stratosphere and troposphere in column measurements. Aerosol optical depth (AOD) is a focus of this review and a significant body of literature exists that shows that ground-level fine particulate matter ($PM_{2.5}$) can be estimated from column AOD. Precision of the measurement of AOD is $\pm 20\%$ and the prediction of $PM_{2.5}$ from AOD is order $\pm 30\%$ in the most careful studies. The air quality needs that can use such predictions are examined. Satellite measurements are important to event detection, transport and model prediction, and emission estimation. It is suggested that ground-based measurements, models, and satellite measurements should be viewed as a system, each component of which is necessary to better understand air quality.

IMPLICATIONS

Satellite measurements are going to be an integral part of the Global Earth Observing System of Systems. Satellite measurements by themselves have a role in air quality studies but cannot stand alone as an observing system. Data assimilation of satellite and ground-based measurements into forecast models has synergy that aids all of these air quality tools.

BACKGROUND

On Explorer VII, which was launched October 13, 1959,¹ Suomi² assessed infrared (IR) radiative heat balance measured from an orbiting satellite as a forcing agent for atmospheric circulation. This year marks one-half century of space-borne observations of the Earth's atmosphere. In 1961, meteorologists were first presented iconic images of the Earth from the first TIROS satellites.³ By showing clouds and weather systems that visually identified features only seen on synoptic weather charts, satellite meteorology was born and developed as a natural tool to identify present and future weather.

This critical review discusses the measurement of air-quality-related gases and aerosols from monitors orbiting above the atmosphere. The National Academy of Sciences (NAS) National Research Council "Decadal Survey"⁴ identifies a need to further involve satellite measurements in decision-making and applications for societal benefit. The NAS expectation of such observations to be integrated into routine monitoring and assessment for tropospheric pollution deserves a critical examination of the quality and utility of such measurements. There are several important constraints on the ability of satellite instruments to measure atmospheric composition. Orbit, atmospheric transparency, wavelength of observation, molecular spectroscopy, scattering, and absorption are among the variables that define whether a measurement can be made. This review begins with the physical principles underlying satellite observations.

SATELLITE ORBITS

The promise of space-borne atmospheric measurements has encouraged the launch of thousands of Earth-observing sensors in low (<2000 km, LEO [note that unfamiliar terms and abbreviations are listed in the glossary]; Table 1), medium (2000–25,000 km, MEO) and geosynchronous (35,786 km, GEO) orbits. Approximately 900 satellites are currently being tracked by the

Table 1. Glossary of terms.

Aerosol optical depth (AOD) or thickness	The integral of the atmospheric extinction coefficient from the surface to space (unitless)
Air mass (sunphotometry)	The inverse of the cosine of the solar zenith angle (i.e., an air mass of 1 is vertical and air mass of 5 is a solar angle zenith angle of 78°).
Albedo	From the Greek meaning "reflectance," albedo is the ratio of the scattered to scattered plus absorbed radiation. For the surface, the albedo is the percentage of the intercepted radiation that is scattered back to space. The Earth's average albedo is ~30% in the visible.
Anomaly	In a satellite orbit, the angle between the satellite and its position at the perigee.
Blackbody	An object that is in thermal equilibrium with its environment and radiates as much energy as it receives.
Emissivity	The fraction of emitted infrared radiation to that which would be expected from a perfect blackbody at temperature T .
Extinction	The sum of scattering and absorption; the extinction coefficient is a measure of light loss per meter of path (units m^{-1}).
Extrinsic (intrinsic) properties	Aerosol microphysical properties that depend (do not depend) on the number density of the aerosol.
Irradiance	The measurement of the flux of energy across a plane area (units $W \cdot m^{-2}$) or spectral irradiance, the flux within a limited range of wavelengths (units $W \cdot m^{-2} \cdot nm^{-1}$, visible, or $mW \cdot m^{-2} \cdot cm$, infrared).
LEO, MEO, GEO	Low, medium, and geostationary Earth orbit. Note GEO is also used for Geostationary Earth Observations and Global Earth Observations in other contexts.
Perigee, periapsis	The point in the path of an orbiting body that is closest to the surface.
Precess	Change in the orbital plane of an orbit with respect to the Earth's pole.
Product	The result of a satellite retrieval algorithm that describes a dataset from an instrument designed to represent a geophysical parameter.
Specific extinction coefficient	The mass weighted extinction or the extinction per unit concentration of an aerosol (units $m^2 \cdot g^{-1}$).
Spectral radiance	The physical measurement of radiation intensity within a defined solid angle and at a given wavelength (units $W \cdot m^{-2} \cdot nm^{-1} \cdot sr^{-1}$ in visible or $mW \cdot m^{-2} \cdot cm \cdot sr^{-1}$ in infrared). This is what a satellite uses as a signal.
Terminator	The line on the Earth between the illuminated and dark hemispheres

National Aeronautics and Space Administration (NASA), and thousands of pieces of space debris circle the planet.⁵ Figure 1a shows examples of these orbits. Satellite positions are defined by six variables: (1) the semi-major axis of the orbit, (2) the eccentricity, (3) the inclination of the orbit, (4) the longitude of the ascending node (the Earth longitude at which the satellite crosses the equator in a northbound direction), and the (5) periapsis and (6) mean anomaly.⁶ For a circular orbit (eccentricity = 0), the semi-major axis is the radius from the center of the Earth (in kilometers). GEO satellites must orbit the Earth precisely once for every rotation of the Earth (slightly different than a civil day or 86,400 sec) in an equatorial position to maintain a stationary position with respect to a fixed point on the planet. Communications satellites (television, telephony, intersatellite communications) often use this orbit to allow for the use of a fixed orientation dish on the ground to communicate with the satellite. GEO satellites with Earth sensors can provide multiple views (as short as every 5 min) of a large region of the globe per day. Some GEO satellites can image nearly the full hemispheric disk below the satellite. Spatial resolution of the sensors (the minimum area on the globe that the satellite instrument can retrieve data) can be as small as 1 km if a large telescope is used. The penalty of a sensor in GEO orbit is that a large, complicated satellite with high spatial and temporal resolution is heavy and expensive to launch into a high altitude orbit.

LEO satellites orbit the planet with a period of approximately 1.5 hr. Typical altitudes range from 250 to 700 km. Large, multi-instrument satellites are placed in LEO synchronous or asynchronous orbits. Figure 1b shows the example of a sun-synchronous orbit (typical of many satellites relevant to atmospheric composition measurements) or a satellite in an equivalent Keplerian orbit. A sun-synchronous orbit has an inclination of 96.1° (slightly to the west of the north pole) at 705 km altitude, which allows the Earth-Sun

vector to precess around the Sun exactly once per year. The ascending node is fixed so that the satellite crosses the Earth-Sun vector at the equator at the same local time each day. For satellite instruments that use reflected sunlight as a source, the ascending node equator crossing time (~22:30 for the NASA Terra satellite and 13:30 for the Aqua satellite) defines the viewing time of the satellite with respect to local solar time. The choice of the crossing times for Terra and Aqua gives images at approximately 10:30 a.m. and 1:30 p.m. (during the rising portion of the diurnal boundary layer and near maximum of the boundary layer) during each of the 16 daylight orbits daily. Figure 1c shows one day of orbits of the Terra LEO spacecraft with the time in coordinated universal time (UTC) marked on the ascending and descending orbits. Sensor swath widths (the cross-track extent of a measurement) vary from 70 m for some nadir pointing radar (e.g., CloudSat) and lidar instruments (e.g., CALIOP) to 2300 km for wide-swath imagers (MODIS). Orbits are approximately 2500 km apart (40,000 km circumference of the Earth divided by ~16 orbits per day). A single point on the Earth can be observed up to 4 times per day by wide-swath imagers, every 16 days or more for moderate-swath imagers, or very infrequently for the narrow-swath measurements. For sun-synchronous polar orbiters, the highest latitude reached is 82°, but at those latitudes many orbits cross and polar regions can be well mapped.

Heavier spacecraft get launched into low inclination asynchronous orbits (examples are shuttle launches, which use 39–57° orbits, or the TRMM, which is launched into a 39° orbit). There is a tradeoff between orbital coverage in the extent of the latitude range and the cost penalty in terms of weight that can be carried to orbit on a given launch vehicle. Typically, satellites are launched into the highest inclination orbit that weight and cost of the launch will allow.

MEO orbits combine some of the benefits and some of the deficits of GEO and LEO. MEO orbits have longer

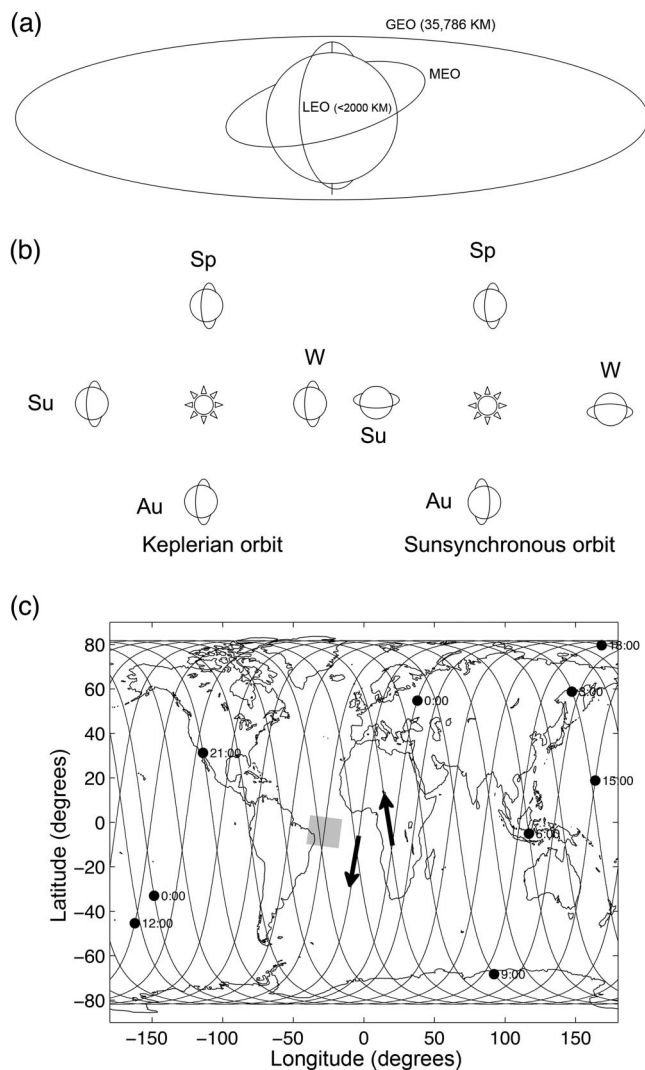


Figure 1. (a) Examples of LEO, MEO, and GEO orbits (not to scale). The LEO orbit shown is a polar sun-synchronous orbit. (b) A Keplerian orbit (left) as a function of season. The north pole of the Earth is out of the page at a 23° angle. The Keplerian orbit shown would have 12 hr of sunlight in summer and winter but would be along the Earth's terminator in spring and autumn. The sun-synchronous orbit (right) precesses once per year such that the orbit always has the ascending node (or descending node, depending on the orbit design) facing the sun. (c) The A-Train (Aqua) satellite orbit for 24 hr on February 24, 2007 with the time marked in UTC. The arrows show the descending and ascending tracks. The shaded square indicates the size of a MODIS 5-min granule of the data, which has 2330 km of cross-track information at 250- to 1000-m resolution depending on the wavelength of the instrument channels. An active instrument such as the CALIPSO lidar would have a footprint on the ground that is much narrower than the line width above, if scaled. Figure courtesy of K. McCann, University of Maryland, Baltimore County (UMBC).

periods, which allows for longer view times for a given ground point. MEO satellites orbit precess so they are neither fixed relative to the Sun nor a fixed point on the ground, losing those spatial and temporal benefits. Global positioning system (GPS) satellites are in MEO orbits because only 24 satellites are required in 6 fixed orbits to ensure that 6 or more satellites are visible from a single point on Earth at any time. This allows geopositioning. A

complication for MEO and GEO satellites is that they extend outside of the Van Allen belts surrounding the planet, and sensors on such satellites are much more likely to take radiation damage from solar ions and cosmic rays, which shortens their lifetime.

REMOTE SENSING FROM ORBIT

Earth observations are made at wavelengths from 260 nm in the ultraviolet (UV) through to radar wavelengths (0.1–10 cm). The ability to see through clouds exists only at radar wavelengths. Atmospheric transparency is needed to be able to probe down to the surface, therefore cloud cover is a significant limitation of satellite observations for air quality. Strong absorption by ozone (O_3) in the stratosphere obscures lower tropospheric measurements of several UV wavelength-absorbing gases that can be measured by surface-based remote sensing. Reflected solar radiation from the Earth-atmosphere system is probed for scattering by aerosols and clouds as well as the ability to measure a limited number of visibly absorbing gases. Bright surfaces (snow, deserts, urban areas) confound the ability to discern scattered light from the atmosphere. Observations of upwelling thermal IR radiation from the Earth and atmosphere give information on trace gases, dust aerosols, water, thermal structure of the atmosphere, and cloud amount, height, and type. There are now active instruments (radars and lidars) in orbit that generate the radiation detected by the satellite after scattering.

In the first grainy images of the planet from TIROS I,³ reflected visible solar radiation was viewed with a black and white television camera (a single visible wavelength channel encompassing 400–700 nm). Reflected sunlight from bright clouds contrasted with the darker surfaces from the ocean (which has low reflectivity for scattering angles up to ~40°). The motion of clouds was visualized, providing forecasters with the ability to correlate cloud motion with forecast models. In a prescient statement of the future of satellite observation, Wexler³ states, “Despite the ability of meteorologists to interpret more than a fraction of the information contained in the satellite cloud pictures, these have been proved to be quite useful in large-scale synoptic weather analysis and prediction.” It is hard to imagine that those instrument scientists would understand the terabytes of data that are down-linked from modern weather and composition satellites, yet the dilemma is the same because information must be gleaned from that stream of data.

In principle, remote sensing from space is not much more complicated than those early TIROS observations. Can the sensor on a satellite see enough contrast between photons emitted or reflected from the surface or underlying atmosphere and the photons that are being scattered or emitted back to the satellite from the pollutant of interest? And if these photons can be detected, is the physics of scattering, absorption, and emission well enough understood to specifically determine the number, temperature, and density of the molecules doing the scattering? These questions are determined from the radiative transfer through the atmosphere.

Fundamental one-dimensional (1D) radiative transfer in the visible part of the spectrum is described by Beer's Law:

$$I(\lambda) = I_o(\lambda)e^{-\alpha(\lambda)z} \quad (1)$$

where α is the extinction coefficient of the atmosphere (units m^{-1}), λ is the wavelength of light, and z is the physical path in meters. I_o is the source radiance and I is the measured radiance after passing through the path, z . If the path is vertical, z is the altitude of the source. For gases, the extinction is governed by the molecular (or atomic) spectra of the gas. The extinction is a sum of the contribution of electronic, vibrational, and rotational transitions in the molecule interacting with radiation. For aerosols, scattering and absorption (which sum to extinction) have spectral dependence governed by the particle size, particle complex index of refraction, and have an angular dependence between the source and scattered radiation. The physics behind light scattering by aerosols in relationship to visibility has been covered in an earlier critical review.⁷

Because the path through the entire atmosphere has a pressure-dependent α and the path z is an inconvenient unit, we define the optical depth (τ) of the atmosphere down to height z as

$$\tau_\lambda = \int_z^\infty \alpha(\lambda, z') dz' \quad (2)$$

At the surface, $z = 0$ and $\tau = \tau^*$, by definition, and $\tau = 0$ at the top of the atmosphere (TOA). The wavelength-dependent aerosol optical depth (AOD, or τ_a) is the total optical depth of the atmosphere corrected for absorption and scattering of gases in the atmosphere (e.g., Rayleigh scattering, O_3 , nitrogen dioxide [NO_2], and water absorption). In this review, the AOD is at 550 nm unless stated otherwise.

In atmospheric radiative transfer, the path is rarely vertical. Figure 2 shows the components of the radiation seen by the satellite for the Sun as a source in the visible and the Earth as a source in the IR. The components of the radiation path that are important are the incoming solar radiation at TOA, scattered radiation from gases and aerosols in the atmosphere, transmitted radiation through the atmosphere to the surface, reflected radiation from the Earth's surface, satellite retrieved TOA radiance from the surface, upwelling IR radiance from the surface, and the TOA IR radiance from the atmosphere.

The radiative transfer solution in a two-dimensional (2D) atmosphere derives from work by Schwartzschild in 1914 in stellar atmospheres.⁸ The radiative transfer equation for a plane-parallel atmosphere is generally written separately for a scattering (visible) atmosphere and an absorbing (IR) atmosphere.

Passive Remote Sensing in the IR Spectrum

Neglecting scattering, the upward (+) and downward (-) IR radiance at a height corresponding to optical depth τ , is given by⁹:

$$\mu \frac{dI^+(\tau, \mu)}{d\tau} = I^+(\tau, \mu) - B(T(\tau)) \quad (3)$$

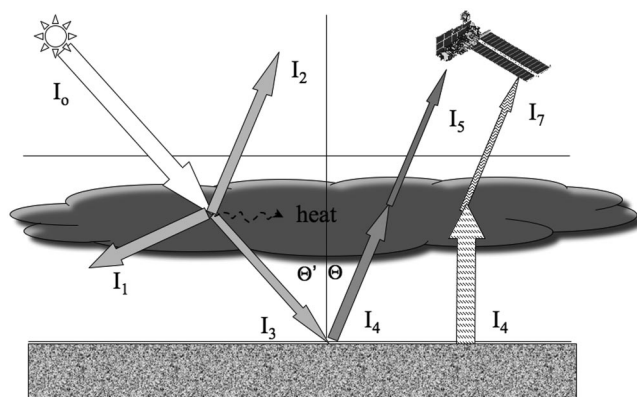


Figure 2. Sources of the radiance seen by a satellite sensor. The components of the radiation path that are important include the following: I_0 = incoming solar radiation at the TOA. I_1 = scattered radiation from gases and aerosols in the atmosphere. This component is dependent on the number density of air, trace gases, and aerosols as a function of height and is a loss mechanism for the source of radiation. I_2 = scattered radiation from gases and aerosols scattered into the field of view of the satellite (this component and I_1 sum to the total scattering in the radiative transfer equation). I_3 = transmitted radiation through the atmosphere to the surface. Directly related to Beer's law, the transmittance gives the one-way optical depth. A transmissometer such as a sunphotometer can directly measure τ .²²⁷ I_4 = reflected radiation from the Earth's surface. This component is largely the source of background radiation used by Earth-viewing satellites to compare with I_2 to retrieve aerosol and gas features. This term gives information on the surface characteristics and is the signal of interest for vegetation mapping, ocean color, etc. It is noise to the atmospheric scientist. I_5 = satellite-retrieved TOA radiance from the surface. Attenuated by scattering and absorption in the layer of interest, this value can be used for retrievals over bright scattering surfaces but generally is a background term that needs to be small for I_2 to be detected. I_6 = upwelling IR radiance from the surface, which is given by Planck's law. This is the largest source of background radiation for IR observation channels in space-borne platforms. Non-negligible at most IR wavelengths, except near the center of strong absorption lines, it must be known and the surface emissivity must be known for IR retrievals. I_7 = TOA IR radiance. Used for trace gas and water measurements in HIRS, these radiances are highly structured and dependent on the height of the source because of the highly varying atmospheric temperatures that emit in the IR. These wavelengths are important in cloud clearing because the temperature of high, thin clouds (cirrus) are much colder than the underlying surface, clouds, and aerosols below.

$$\mu \frac{dI^-(\tau, \mu)}{d\tau} = -I^-(\tau, \mu) + B(T(\tau)) \quad (4)$$

and $B(T)$ is the Planck function as a function of temperature T and wavelength λ

$$B(T(\tau)) = \frac{2hc^2}{\lambda^5 \left[e^{\frac{hc}{\lambda kT}} - 1 \right]} \quad (5)$$

k and h are the Boltzmann and Planck constants, and c is the speed of light.

Although not possible to fully develop here, eqs 3 and 4 can be shown to give

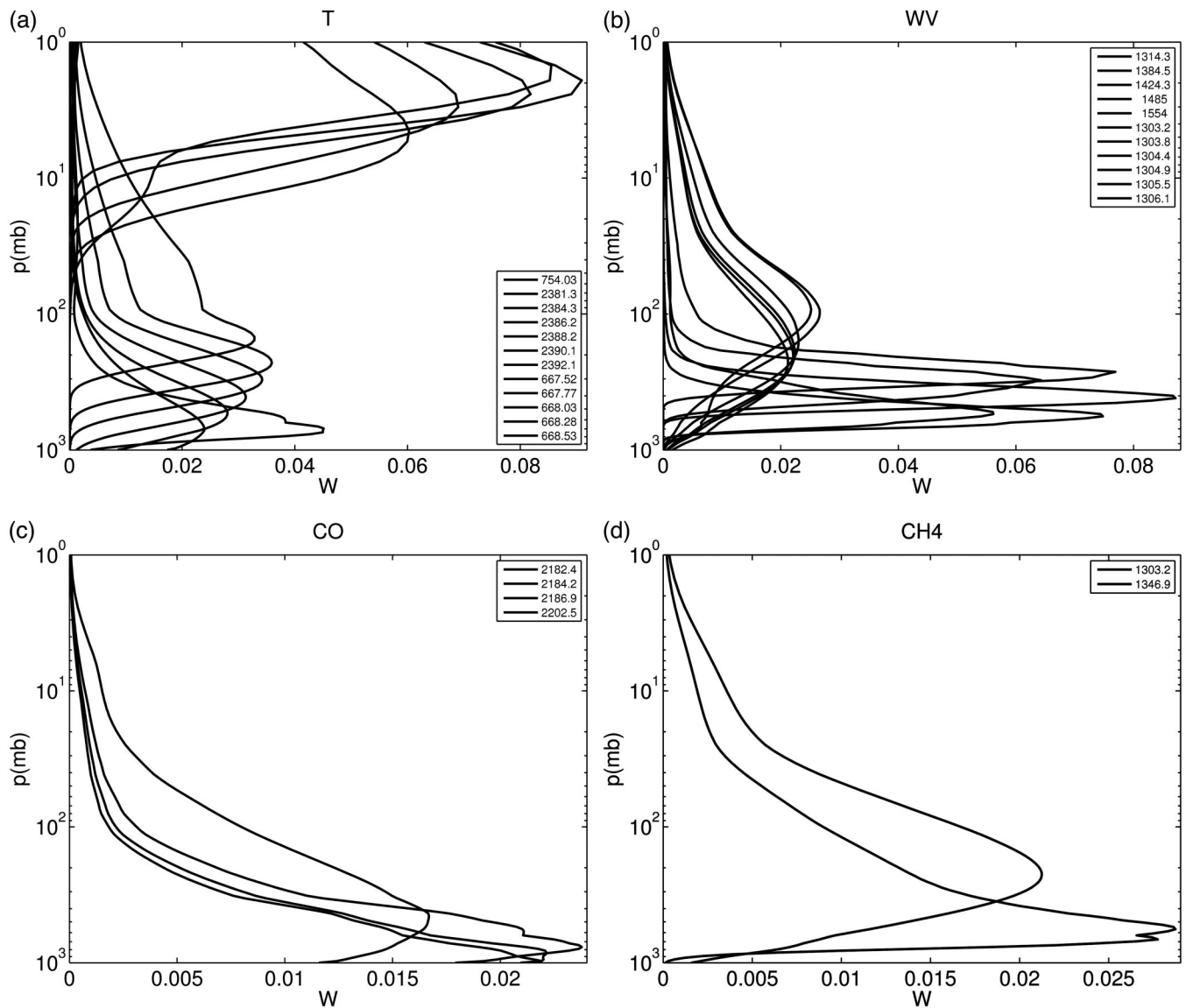


Figure 3. Weighting functions (W) for (a) temperature (T), (b) water (WV), (c) CO , and (d) CH_4 from the AIRS satellite. A representative, but not complete, set of weighting functions are shown. Numbers in the inset are the wavenumbers (cm^{-1}) for the AIRS channels. For the U.S. standard atmosphere, 100 mb is ~ 16.2 km, 10 mb = 31.2 km, and 1 mb = 48.2 km. Figure courtesy of S. DeSousa-Machado, UMBC.

$$I^+(\tau, \mu) = I^+(\tau^*, \mu) \mathbf{T}^+(\tau^*, \tau, \mu) + \int_{\tau^*}^{\tau} B(\tau') \frac{d\mathbf{T}^+}{d\tau'}(\tau', \tau, \mu) \frac{d\tau'}{\mu} \quad (6)$$

$$I^-(\tau, \mu) = I^-(0, \mu) \mathbf{T}^-(\tau, 0, \mu) + \int_0^{\tau} B(\tau') \frac{d\mathbf{T}^-}{d\tau'}(\tau', \tau, \mu) \frac{d\tau'}{\mu} \quad (7)$$

where the first term in eq 6 is the source radiance from the surface and the first term in eq 7 is the source radiance from the TOA (can be ignored except in the near-IR or microwave region). The second term in each is the thermal emission from the atmosphere. \mathbf{T} is the transmittance of the atmosphere and its derivative with respect to optical depth is called the weighting function, W . Examples

of weighting functions for temperature, water vapor, methane, carbon monoxide (CO), and carbon dioxide (CO_2) are shown in Figure 3. Although temperature and water vapor have channels that see down to the surface, signals from other gases may be dominated by thermal radiance from higher in the atmosphere.

Table 2 lists satellite measurements relevant to air quality. There were early users of satellite imagery in the air quality community.¹⁰⁻¹⁴ There is not space here to describe all of these historical measurements, but tutorials on remote sensing from space and the history of satellite measurements is available on NASA Web sites.^{15,16} Here we describe measurements from the most recent instruments (a list of satellite acronyms is given in Table 3). Two types of satellite instruments are used in the IR: imagers and sounders. An imager uses the entire column of radiance to retrieve information on the atmospheric path. The imager gives high (e.g., 1×1 km)

Table 2. Satellites and instruments relevant to air quality and composition^{224–226} (see Table 3 for acronyms).

Satellite	Orbit	Instrument	Years	Species
TIROS 1-10	Polar	Vidicon (TV)	1959–1965	Cloud imagery
TIROSN (NOAA 6-15)	Polar	TOVS	1978–present	H ₂ O, cloud imagery
Nimbus-1	Polar	IR radiometer	1964–1964	H ₂ O, cloud imagery
Nimbus-3	Polar	IRIS	1969–1970	T, H ₂ O, O ₃
		HRIR, MRIR	1969–1970	Imagery
		SIRS	1969–1970	IR radiation
		MUSE	1969–1970	UV radiation
Nimbus-4	Polar	SIRS	1970–1971	T, H ₂ O, O ₃
		BUV	1970–1977	O ₃
		FWS	1970–1971	Solar radiation
		IDCS	1970–1971	Clouds
		THIR	1970–1971	T, H ₂ O
Nimbus-5	Polar	ESMR	1973–1976	Cloud imagery
		ITPR	1975–1976	T
		NEMS	1972–1973	T, H ₂ O
		THIR	1972–1974	T, H ₂ O
Nimbus-6	Polar	ERB	1975–1976	IR radiation
		HIRS	1975–1976	T, H ₂ O
		LRIR	1975–1976	T, H ₂ O, geostrophic winds
		SCAMS	1975–1976	T, H ₂ O
Nimbus-7	Polar	CZCS	1978–1986	Ocean chlorophyll, aerosol correction
		ERB	1978–1993	IR radiation
		SMMR	1978–1987	T, H ₂ O, ocean winds from reflectivity
		SBUV/TOMS	1978–1991	O ₃
		SAM-II	1978–1991	Stratospheric aerosols
		SAMS	1978–1983	H ₂ O, N ₂ O, CH ₄ , CO, and NO in the stratosphere
		THIR	1978–1985	T, H ₂ O
ESSA1-9	PS	FPR	1966–1970	Cloud imagery, radiance
SMS-1	G15.5E	VISSR	1974–1975	Visible/IR imagery
SMS-2	G12E	VISSR	1975–1979	Visible/IR imagery
GOES 1-3	G135W, 75W	VISSR	1975–1979	Visible/IR imagery
GOES 4-7	G135W, 75W	VAS	1979–1994	T profiles
GOES 8-12 (I/M)	G135W, 75W	I/M imager	1994–present	Visible/IR imagery
		I/M sounder		T profiles
ERBS	L56.9	ERBE	1984–1991	Radiances
		SAGE-II	1984–1993	NO ₂ , O ₃ , aerosol extinction (horizontal path), H ₂ O
ERS-1	PS	ATSR	1991–1992	Cloud properties, T
ERS-2	PS	GOME	1995–present	NO, NO ₂ , H ₂ O, O ₂ /O ₄ , BrO, SO ₂ , HCHO, OCIO, ClO, and NO ₃
UARS	L56.9	HRDI	1991–2005	Upper atmospheric winds
		CLAES	1991–1993	T, H ₂ O, N ₂ O, NO, NO ₂ , N ₂ O ₅ , HNO ₃ , CFC-12, CFC-11, HCl, ClONO ₂ , O ₃ , and CH ₄
		SUSIM	1991–2005	O, O ₃
		HALOE	1991–2005	Profiles of H ₂ O, O ₃ , HCl, HF, NO, CH ₄ , HNO ₃ , and CO ₂ .
		ISAMS	1991–1992	Profiles of CO ₂ , H ₂ O, CO, NO, N ₂ O, O ₃ , HNO ₃ , N ₂ O ₅ , NO ₂ , and CH ₄
		MLS	1991–2005	Profiles of O ₃ , ClO, H ₂ O ₂ , O ₂
		WINDII	1991–2005	Upper atmospheric winds
TOMS-EP	PS	TOMS-EP	1996–1996	O ₃ , SO ₂
ADEOS	PS	TOMS	1996–1997	O ₃ , SO ₂
		ILAS	1996–1997	O ₃ , CH ₄ , N ₂ O, HNO ₃ , H ₂ O, NO ₂ , CFC-11
		POLDER	1996–1997	Aerosol properties by polarimetry
		AVNIR	1996–1997	Visible/IR imagery
		AMSR	1996–1997	H ₂ O, winds
		IMG	1996–1997	CH ₄ , CO ₂ , NO ₂
SeaStar	L90.7	SEAWIFS	1997–present	
TRMM	L35.0	TRMM radar	1997–present	Precipitation
Landsat 7	PS	ETM+	1999–present	Surface, aerosols
Terra	PS	MISR	1999–present	Aerosols
		MODIS	1999–present	H ₂ O, clouds, aerosols
		ASTER	1999–present	Visible/IR imagery
		CERES	1999–present	Visible/IR radiance
		MOPITT	1999–present	CO, CH ₄
EO-1	PS	Hyperion	2000–present	Hyperspectral imagery

Table 2. Cont.

Satellite	Orbit	Instrument	Years	Species
SAGE-III	L99.7	SAGE-III	2002–2006	Aerosols, O ₃ , H ₂ O, NO ₂
Aqua	PS, A-Train	AIRS	2002–present	H ₂ O, T, CH ₄ , CO, CO ₂
		MODIS	2002–present	H ₂ O, clouds, aerosols
		AMSU	2002–present	H ₂ O
		AMSR/E	2002–present	H ₂ O
		CERES	2002–present	Visible/IR radiance
ICESAT	L94.0	GLAS	2003–2006	Aerosols
Aura	PS, A-Train	HRDLS	2003–present	O ₃ , H ₂ O, CO ₂ , CH ₄ , NO _x , HNO ₃ , aerosols, and CFC
		MLS	2003–present	T, P, H ₂ O, HNO ₃ , O ₃ , CO, HNO ₂ , HCl, ClO, BrO, SO ₂ , OH
		OMI	2003–present	O ₃ , SO ₂ , NO ₂ , aerosols, CHOCHO
		TES	2003–present	CH ₄ , CO, H ₂ O, HDO, HNO ₃ , O ₃ , T
CALIPSO	PS, A-Train	CALIOP	2006–present	Lidar profiles of aerosols
		IIP	2006–present	IR clouds
CloudSat	PS, A-Train	Cloudsat	2006–present	Cloud radar
Envisat	PS	MERIS	2007–present	AOD
		MWR	2007–present	H ₂ O
		AATSR	2007–present	Surface T
		GOMOS	2007–2009	O ₃ , O ₂ , NO ₂ , NO ₃ , UV AOD in occultation
		SCIAMACHY	2007–present	O ₃ , NO ₂ , H ₂ O, N ₂ O, CO, CH ₄ , CHOCHO, OCIO, H ₂ CO, SO ₂ , aerosols, P, T
		MIPAS	2007–present	Trace gases
METOP	PS	IASI	2007–present	H ₂ O, CO ₂ , CH ₄ , T, NO ₂
		GOME-2	2007–present	O ₃ , aerosols, NO ₂ , BrO, OCIO, ClO
		AVHRR	2007–present	AOD
		Ibuki	2009–present	CO ₂ , GHGs
GOSAT	Polar	OCO	2009 failed to achieve orbit	CO ₂
OCO	NA			
Upcoming missions				
GLORY	PS		2009?	Aerosols
ADM/AEOLUS	PS	Aladin	2010?	Lidar profiles of aerosols
GCOM-W1	PS	SGGI	2013?	Aerosols
NPP	PS		2010?	Aerosols
LDCM	Polar		2010?	Aerosols
METOP-B	PS		2013?	
NPOESS	PS		2013?	Aerosols
GPM	2 + PS and L39		2013–2014	Precipitation
EARTHCARE	Polar	ATLid	2013?	Aerosols
		MSI	2013?	Aerosols
METOP-C	PS		2016?	
CLARREO	Polar		2016?	Radiance

Notes: G12° = geostationary at 12°E longitude, PS = polar sun-synchronous, L39° = low earth orbit with a 39° inclination angle, I/M = GOES sequence of satellites from I to M, N₂O₅ = dinitrogen pentoxide, T = temperature, P = pressure, H₂O = water, N₂O = nitrous oxide, O₄ = tetraoxygen, OCIO = chlorine dioxide, ClO = chlorine monoxide, NO₃ = nitrate radical, HF = hydrogen fluoride, H₂O₂, hydrogen peroxide, ClONO₂ = chlorine nitrate, HCl = hydrogen chloride, GHGs = greenhouse gases, OH = hydroxyl species, CFC = chlorofluorocarbon, HNO₃ = nitric acid, HNO₂ = nitrous acid, HDO = deuterated water, NA = not applicable.

horizontal spatial information but little unambiguous vertical information.

A particular application in the IR comes where the atmosphere is transparent because there are no absorbing gases or aerosols in the scene (second term in eq 6 is zero). The radiance seen arises from the surface temperature. IR sea surface temperature (SST) instruments (AVHRR, POES, ASTER, ERS-2, AIRS) operate on this principle. Over water, the surface emissivity is approximately 0.98; however, over land the IR emissivity of the surface is a complicated function of the mineral and vegetative cover and can vary from 0.7 to 0.98.^{17–19} Deriving land surface temperatures is complicated. ASTER was designed to examine retrieval of temperature over land.¹⁹ ASTER, launched in 1998, has relatively coarse spectral resolution in the IR, but was designed to give surface temperatures with a precision of ±1.5 K and ±0.015 in emissivity. Launched in 2002, AIRS

globally provides emissivity measurements at 0.05- μ m spectral resolution with 3% precision from 3 to 4 μ m and 1% precision at 10- to 12- μ m resolution.^{17,18} Because the surface emissivity enters into all calculations using eq 6 through the first term, emissivity uncertainty affects trace gas retrievals.

Equation 5 reduces to a linear relationship between temperature and microwave radiance at long wavelengths. Microwave thermal emission penetrates clouds. Instruments such as SMMI, TRMM, TMI, and AMSR utilize microwave retrievals for SST measurements.

Another application of surface temperature retrievals in the IR arises from thermal emission from fires. Measurements of emissions from fires have been made by “bottom-up” models (in which the areal extent of the fires, measured from the ground or estimated from space-borne imagery, is multiplied by biomass and fire-type emission factors).²⁰

Table 3. Acronyms of satellites and satellite instruments.

AATSR	Advanced Along Track Scanning Radiometer
ADEOS	Advanced Earth Observation Satellite
AIRS	Atmospheric Infrared Sounder
AMSR	Advanced Microwave Scanning Radiometer
AMSU	Advanced Microwave Sounding Unit-A
ASTER	Advanced Spaceborne Thermal Emission and Reflection radiometer
AtLid	Atmospheric Lidar
ATSR	Along Track Scanning Radiometer
AVHRR	Advanced Very High Resolution Radiometer
AVNIR	Advanced Visible and Near-Infrared Radiometer
BUV	Backscatter Ultraviolet
CALIOP	Cloud and Aerosol Lidar with Orthogonal Polarization
CALIPSO	Cloud and Aerosol Lidar for Pathfinder Spaceborne Observations
CERES	Clouds and Earth's Radiant Energy System
CLAES	Cryogenic Limb Array Etalon Spectrometer
CZCS	Coastal Zone Color Scanner
DesDynI	Deformation, Ecosystem Structure and Dynamics of Ice
ERB	Earth Radiation Budget
ERBE	Earth Radiation Budget Experiment
ERS-2	Second European Remote-Sensing Satellite
ESMR	Electrically Scanning Microwave Radiometer
ETM	Enhanced Thematic Mapper
FPR	Flat Plate Radiometer
FWS	Filter Wedge Spectrometer
GEOS	Geodetic and Earth Orbiting Satellite
GLAS	Geoscience Laser Altimeter System
GOES	Geostationary Operational Environment Satellite
GOME	Global Ozone Monitoring Experiment
GOMOS	Global Ozone Monitoring by Occultation of Stars
HALOE	Halogen Occultation Experiment
HIRDLS	High-Resolution Dynamics Limb Sounder
HRDI	High Resolution Doppler Imager
HRIR	High Resolution Infrared
HRIS	High Resolution Infrared Sounder
IASI	Infrared Atmospheric Sounding Interferometer
ICESAT	Ice, Cloud, and land Elevation Satellite
IDCS	Image Dissector Camera System
ILAS	Improved Limb Atmospheric Spectrometer
IMG	Imager
IRIS	Infrared Interferometer Spectrometer
ISAMS	Improved Stratospheric and Mesospheric Sounder
ITPR	Infrared Temperature Profile Radiometer
LIMS	Limb Infrared Monitor of the Stratosphere
LITE	Laser In-space Technology Experiment
LRIR	Low Resolution Infrared
MERIS	Medium Resolution Imaging Spectrometer
MIPAS	Michelson Interferometer for Passive Atmospheric Sounding
MLS	Microwave Limb Sounder
MODIS	Moderate Resolution Imaging Spectroradiometer
MOPITT	Measurements of Pollution in the Troposphere
MRIR	Moderate Resolution Infrared
MSI	Multispectral Imager
MUSE	Monitor of Ultraviolet Solar Energy
MWR	Microwave Radiometer
NEMS	Nimbus-5 Microwave Spectrometer Experiment
NPOESS	National Polar Orbiting Environmental Satellite System
OCO	Orbiting Carbon Observatory
OMI	Ozone Monitoring Instrument
PARASOL	Polarization and Anisotropy of Reflectance for Atmospheric Science coupled with Observations from a Lidar
POES	Polar Operational Environmental Satellite
POLDER	Polarization and Directionality of the Earth Reflectances
SAGE	Stratospheric Aerosol and Gas Experiment
SAM	Stratospheric Aerosol Mission

Table 3. Cont.

SBUV	Solar Backscatter Ultraviolet
SCAMS	Scanning Microwave Spectrometer
SCIAMACHY	SCanning Imaging Absorption SpectroMeter for Atmospheric Chartography
SEAWiFs	Sea-viewing Wide Field-of-view Sensors
SEVERI	Spinning Enhanced Visible and Infrared Imager
SIRS	Satellite Infra-Red Spectrometer
SMMR	Scanning Multichannel Microwave Radiometer
SMS	Synchronous Meteorological Satellite
SSM/I	Special Surface Microwave Imager
SUSIM	Solar Ultraviolet Spectral Irradiance Monitor
TES	Tropospheric Emission Spectrometer
THIR	Thermal Infrared
TIROS	Television Infrared Observation Satellite
TMI	Thermal Microwave Imager
TOMS	Total Ozone Mapping Spectrometer
TOMS-EP	Total Ozone Mapping Spectrometer-Earth Probe
TOVS	TIROS Operational Vertical Sounder
TRMM	Tropical Rainfall Measurements Mission
VAS	Visible Infrared Spin Scan Radiometer Atmospheric Sounder
VIIRS	Visible Infrared Imager Radiometer Suite
VISSR	Visible Infrared Spin Scan Radiometer
WINDII	Wind Imaging Interferometer

Other remote sensing techniques^{21–23} are based on the radiometric emissions from active fires in the 4- μm bands of multispectral satellites like the MODIS, the BIRD instrument, and the GOES. In these methods, the hypothesis is that the heat content of fires is proportional to the mass burned. Correlations between IR radiances and smoke mass emission estimates are relatively high, but there further validation of these estimates is needed. There are factors of 10 variability between emission estimates made from biomass consumption-based smoke estimates and those from the thermal radiance techniques.²³

MODIS²⁴ and GOES/AVHRR²⁵ fire detection algorithms are used operationally in the detection of fire occurrences by the U.S. Department of Agriculture (USDA) Remote Sensing Applications Center²⁶ and the National Oceanic and Atmospheric Administration (NOAA) National Environmental Satellite, Data and Information Service (NESDIS).²⁷ Arguably, fire detection in near real time is one of the most important satellite inputs to air quality assessment. A history of global fire frequency and extent is now archived at the Automated Biomass Burning Algorithm website at the University of Wisconsin²⁸ and the U.S. Navy.²⁹

Sounders invert the weighted Planck function from the second term in eq 6 to determine gas concentration from the differential transmission. Highly absorbing gases only receive radiances from high in the atmosphere and weakly absorbing gases may be visible all of the way down to the surface. With the advent of highly resolved Fourier transform spectrometers³⁰ and grating spectrometers in orbit,³¹ determination of highly resolved vertical profiles of gases are possible. AIRS has been able to determine temperature and water vapor in 1-km layers throughout the atmosphere. Figure 3 shows sets of weighting functions for temperature (Figure 3a), water vapor (Figure 3b), CO (Figure 3c) and methane (CH₄; Figure 3d). The broad trace gas weighting functions allow only a few pieces of truly independent information to be derived from these

AIRS channels. For CO, it is estimated that there is really only one independent weighting function from 300 to 700 mb pressure altitude.³² CO₂ also has only one weighting function, which peaks at 8-km altitude at midlatitude temperatures but has contributions from the surface to 20 km.³³ More details on the theory of IR inverse methods can be found in Goody and Yung.³⁴

Imagers (e.g., MODIS) and sounders (e.g., AIRS) can detect aerosols in the IR for coarse-mode or mechanically generated aerosols such as dust. Aerosols are possible to detect in the IR if their size is more than approximately 10 μm . Particulate light scattering of solar radiation is generally ignored at wavelengths greater than 1.5 μm . At longer wavelengths, scattering is replaced by thermal emission as the dominant source of radiation. Clouds and ice can be detected from their thermal emission at high altitudes contrasting with the surface temperature and many of the early instruments shown in Table 2 used IR radiances to detect types of clouds. Methods exist to discriminate ice from water clouds using far-IR wavelength radiance differences.³⁵ Dust has been detected in daytime and nighttime observations of sounders such as AIRS,³⁶ and polar orbiting and geostationary imagers such as the MODIS and SEVIRI instruments.^{36–40} Although the height of the aerosol is very important in the IR (because the effective temperature of the aerosol and the amount of water vapor above the dust layer must be known), optical depths retrieved in the IR have the advantage of not needing sunlight and therefore providing data that are not diurnally biased. However, accurate detection and calculation of dust aerosol properties such as optical depth require correct information on surface emissivity, surface temperature, water vapor, and mineralogy of the dust. Combination of instruments, such as the CALIPSO lidar (which derives aerosol height) and AIRS (which can derive AOD day and night provided the aerosol height is known), shows promise for dust emission detection and assessment.

Passive Remote Sensing in the Visible Range

In the UV (0.25–0.4 μm) and visible (0.4–0.7 μm) range of wavelengths, the Sun's input and reflected light dominate the radiance being emitted back to space. There are relatively few gases (O₃, sulfur dioxide [SO₂], NO₂, formaldehyde [HCHO], and glyoxal [CHOCHO]) that have absorption features that allow their detection at UV and visible wavelengths. Aerosols dominate visible radiative transfer. Because light scattering by aerosols is strongly dependent on the wavelength of light, and because the Mie extinction efficiency peaks in the accumulation mode below 1 μm in size⁷ (Mie scattering is largest where the particle size and wavelength are equal), particulate matter (PM) measurements use visible wavelengths.

The differential form of the 2D radiative transfer equation for visible radiation is⁹:

$$\mu \frac{dI(\tau, \Omega)}{d\tau} = I(\tau, \Omega) - \frac{\omega(\tau)}{4\pi} p(\Omega', \Omega) I_{\nu} e^{\tau} - \frac{\omega(\tau)}{4\pi} \int_0^{4\pi} p(\Omega', \Omega) I(\tau, \Omega') d\Omega' \quad (8)$$

where I is the radiance, τ is zero at TOA and is a variable of the downward path, $\mu = \cos\Theta$ (negative downwards), ω is the single-scatter albedo, and $p(\Omega', \Omega)$ is the scattering phase function from solid angle Ω' to Ω . The equation states that the rate of change of radiance with increasing optical depth is related to the downwelling radiance minus the lost direct radiance minus the diffuse scattering into 4π sr. There is a surface boundary condition for the reflected radiance⁹:

$$I(\tau^*, \Omega > 0) = \frac{1}{\pi} \int_0^{4\pi} \rho(\Omega', \Omega) I(\tau^*, \Omega' < 0) |\mu'| d\Omega' \quad (9)$$

where ρ is the bidirectional reflectance distribution function (BRDF) at the surface. Simplifications to the solution arise if ρ is zero (black surface) or the BRDF surface is Lambertian (isotropic). This is a fundamental uncertainty in the retrieval of the optical depth. Because surfaces generally have non-zero and non-Lambertian BRDF, retrieval of the AOD is an approximation.

Because $p(\Omega', \Omega)$ requires a Mie computation for aerosols, simplified solutions such as the Eddington, two-stream, and δ -Eddington approximations⁴¹ have been widely utilized in algorithms for satellite retrievals. There are no retrieval algorithms in operational use that make full Mie calculations. In these approximations, the atmosphere is considered 2D plane-parallel with no effects of clouds. The phase function is parameterized. With the multitude of complicated interactions between photons coming downward and reflected upward, numerical solutions for radiative transfer are computationally intensive. In the real world of satellite retrievals, shortcuts are taken where a range of expected gases and aerosol types, distributions, and optical properties are precomputed into look-up tables (LUTs), which are used to quickly search for solutions that best fit the observed radiance in orbit.⁴²

Three-dimensional (3D) solutions are required in the presence of clouds.⁴³ Multiple scattering within the cloud field, shadowing, and horizontal radiative transport within and between neighboring clouds are important. Recent work^{44–46} has examined the adjacency effect for aerosol retrievals in the presence of clouds and this effect is significant. The adjacency effect refers to the photons scattered from the neighboring pixels into the pixel of interest. It will be seen later that aerosol hydration and the radiative flux from clouds to aerosols is a significant limitation in the retrieval of AOD. In order not to include cloud effects in AOD retrievals, cloud masks are used and these masks have become more restrictive as the cloud-aerosol interaction effects are better understood.

Uplooking Instruments

Although not satellite instruments, instruments that measure the atmospheric column or optical depth from the ground are instructive for what can be accomplished with remote sensing measurements. These instruments are important in validating space-borne observations. The trace gas community has made column measurements of gases from spectral measurements of incoming solar radiation for almost 100 yr. The Dobson O₃ spectrophotometer has

operated since the 1920s (and in its current incarnation since 1963) by measuring the optical depth on 2–6 wavelengths from 305 to 345 nm.⁴⁷ By difference in absorption at these wavelengths, the column of O₃ can be determined from Beer's law. Because most of the absorption of O₃ occurs in the stratospheric O₃ layer, this column is relatively uniform with an optical path length of 300–400 milliatmosphere-cm (or Dobson units [DU]). Only a fraction of a centimeter of pure O₃ (at standard temperature and pressure [STP]) protects us from solar UV radiation. Currently, a newer instrument, the Brewer spectrophotometer, is being used widely to measure the O₃ column at 306.3, 310.1, 313.5, 316.8, and 320.1 nm.⁴⁸ These wavelengths are chosen so that SO₂ column retrievals and AOD can be determined in addition to the O₃ column.

The AOD of the atmosphere is monitored globally at over 90 sites with more than 4 yr of records using the Sun as a source and measuring the transmittance as a function of solar elevation angle (or equivalently the knowledge of the air mass).⁴⁹ The calibration of a sunphotometer is done via the Langley regression method,⁵⁰ whereby the Sun's radiance at the surface (preferably from an aerosol-free location) is measured as a function of the air mass (μ^{-1}). From eq 1, the logarithm of the signal has a slope that gives the instrumental response and an intercept (at zero air mass) that is related to the extraterrestrial solar radiance.

Sun photometers have been in use for almost 3 centuries.⁵¹ Major improvements in the technique over the last half century have come from sensitive and stable photodetectors, narrow band-pass filters for wavelength specificity, and robotic photometers,^{52–54} which can measure not only the direct radiation from the Sun but also the diffuse radiation from the sky throughout the solar hemisphere. The scattering term, I_2 , in Figure 1 comes from Rayleigh and Mie scattering at different angles. From multiwavelength measurements at numerous angles within the downwelling hemisphere of diffuse radiation, inversion techniques have been developed that allow determination of the particulate size distribution at 22 radii from 0.07 to 12 μm and indices of refraction of the scatterers.^{55,56}

Many large networks are available globally that use uplooking sunphotometry (Aerosol Robotic Network [AERONET],⁵³ Photométrie pour le Traitement Opérationnel de Normalization Satellitaire [PHOTONS],⁵⁷ SKYNET,⁵⁸ Multifilter Rotating Shadowband and Radiometer [MSRFR]⁵⁹ and World Meteorological Organization Global Atmosphere Watch Physikalisch-Meteorologisches Observatorium Davos [WMO/GAW/PMOD]⁵²). These networks serve as "truth" for satellite remote sensing because the instruments are stable, well-calibrated, well-characterized,⁵⁶ and can use sophisticated techniques to quality assure that clouds and noise are minimized. For space-borne remote sensing of AOD, most satellite instruments have been tested against sunphotometer results.^{60–70}

Occultation and Near-Nadir Viewing

Although Suomi's images clearly showed clouds and their motion, within less than a decade after those first TIROS images, gases and aerosols that are manmade and natural in origin were being monitored. In the 1970s and 1980s,

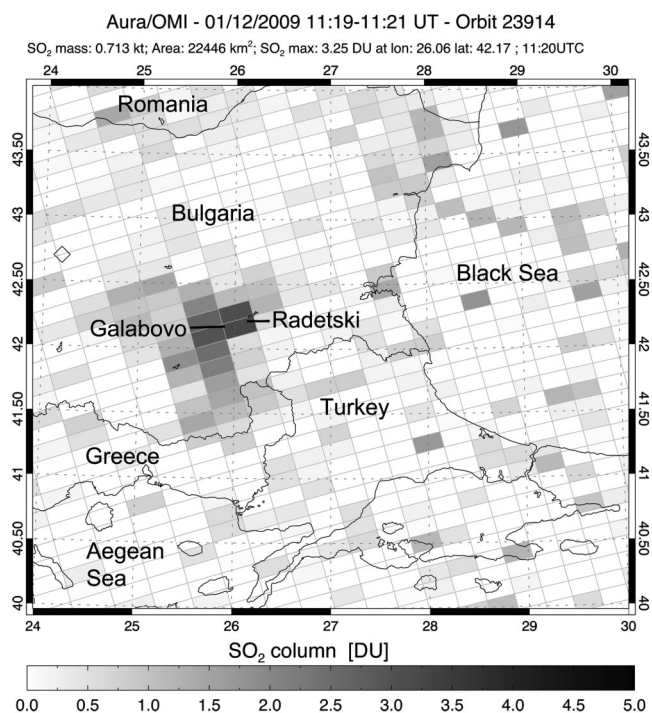


Figure 4. Detection of SO₂ from the Radetski and Galabovo power plants in Bulgaria from the OMI satellite.²²⁸ Axes are latitude (°N) and longitude (°E). Each pixel at nadir is 24 × 13 km and wider toward the edge of the swath. Figure courtesy of Nickolay Krotkov, UMBC.

the Nimbus satellites used occultation measurements to observe aerosols at 1- μm wavelength using the Sun as a source in the SAM measurement platform.⁷¹ Occultation uses the motion of a spacecraft to observe the rising or setting sun as the spacecraft crosses the terminator. Because occultation measurements occur in long horizontal paths through the atmosphere, the amount of absorption is enhanced. Limb scattering measurements of O₃ and water vapor were observed at millimeter wavelengths with the LIMS sounder.⁷²

Some trace gases (e.g., O₃, SO₂, NO₂, HCHO, and CHOCHO) can be detected in reflected UV/visible radiances. The strong Hartley absorption band of O₃ is used for differentially determining the transmittance at 0.3–0.35 μm . In 1987, the SBUV Instrument detected the O₃ hole over Antarctica by measuring the attenuation in the near UV.⁷³ A BUUV instrument utilizes the strong Rayleigh scattering of the atmosphere itself as a diffuse source of radiation from above the surface. The Rayleigh scattered photons are then absorbed by overlying gases and spectrally resolved through differential absorption. The detection of decreases in this column to levels below 100 DU in Antarctica were made in the 1980s from a satellite instrument, TOMS.⁷³ The iconic image of the low O₃ column in a large vortex over Antarctica was instrumental in mobilizing scientific and public opinion to reduce the production of chlorofluorocarbons in the 1980s. Although those column measurements were not related to surface concentrations of O₃, the value of column measurements to policy-making was demonstrated from a space-borne platform.

SBUV has evolved to the TOMS and OMI instruments (see Table 2) and, with the addition of narrower wavelength detection channels, more specificity between O₃ and SO₂ has been obtained. As an example, Figure 4 shows the recent detection of two strong power plants in Bulgaria using the OMI near-UV channels. NO₂ is observed at wavelengths between 440 and 450 nm.^{74–76} Additional examples on the measurement of NO₂ emissions were found from the controls imposed during the Beijing Olympics, also from the OMI instrument.⁷⁷ Other gases such as HCHO,⁷⁸ CHOCHO,^{79–81} and bromine oxide (BrO)^{82–84} are determined in column measurements from OMI, GOME, GOMOS, and SCIAMACHY (see Table 2). Millet has recently stated that the emissions of HCHO could be determined to 40% precision from satellite observations.⁸⁵ A 12-yr record of HCHO measurements has been published.⁸⁶ The ratio of HCHO to CHOCHO is an important indicator of oxidant chemistry in biomass emission plumes.⁸¹ BrO concentrations are important to Arctic O₃ chemistry.⁸⁷

Measurement of tropospheric trace gases from space in the UV requires the gas to be in high concentration (as in the example above or in volcanic plume detections) or present above approximately 2 km. Work by Liu⁸⁸ has shown promise in removing the overburden of stratospheric O₃ from tropospheric UV O₃ measurements. Because UV instruments cannot see all of the way down to the surface, correlation of the results from these instruments with air quality concentrations at the surface will continue to be difficult because of the underlying controlling physics. Tropospheric O₃ column retrieval from space has been addressed in detail in two recent reviews.^{89,90}

AOD is the integral of the aerosol extinction due to scattering and absorption in a vertical column. Horizontal visibility in kilometers has been related to extinction since 1923.^{7,91–93} There is a wide body of literature that shows that there are strong correlations between visibility and PM measurements.^{94–96} The Interagency Monitoring of Protected Visual Environments (IMPROVE) network^{97,98} reconstructs extinction (and inversely visibility) from concentration measurements of particulate species comprising fine PM (PM_{2.5}) and coarse PM (PM₁₀).⁹⁹ The important factor in such a relationship is the significant constraint that deposition, condensation, and coagulation put on suspended particle sizes in the atmosphere. Because light scattering, to first order, is proportional to the cross-sectional area of the scatterer (with some significant modifications by Mie scattering), and the volume is proportional to the cube of the radius (times the particle density), the relationship between scattering and mass is approximately linearly related to particle size. If particle size is constrained to submicrometer modes where light scattering is most important and illumination is highest, strong correlations between scattering and mass will exist.⁹⁴ The earliest versions of nephelometers had both scattering and mass on the front dial of the instrument with a simple proportion of 3.2 m²/g (known as the specific scattering coefficient of the aerosol) to scale from one value to the other.¹⁰⁰ Many decades of research have ensued to understand the intricacies in the relationship between particle size, humidification, speciation, etc. and light scattering (or extinction), but the physics of the light

scattering problem has not changed since those early years.

The reflected solar radiation in the presence of aerosols is a complex function of surface, atmospheric, and aerosol properties. When the surface is dark and homogeneous, aerosols above this background are readily apparent in midvisible imagery. Multispectral satellite imagery provides radiance measurements that must be converted to AOD, which is therefore an inverse problem. To accomplish this, clouds are first identified and removed from satellite imagery and surface reflectance is obtained. Radiative transfer algorithms with specified surface, aerosol, and atmospheric properties are used to calculate LUTs from which AOD is retrieved. For submicron aerosols, over oceans, multiple wavelengths between 0.47 and 2.1 μm are used to retrieve AOD by characterizing the ocean surface as a function of roughness, wind speed, solar angle, and other parameters. Over land, because the background reflectance underneath the aerosol layer is required, approximations are necessary. The assumption that submicron aerosols are transparent to solar radiation at 2.13 μm and that the surface reflectance (ρ) at 470 nm and 660 nm can be derived using empirical relationships such as $\rho_{0.47} = 0.25 \rho_{2.13}$ and $\rho_{0.66} = 0.50 \rho_{2.13}$ led to the original MODIS algorithms.^{69,101,102} Recently, other refinements have been proposed to this method.^{103–106} MODIS retrieves AOD at 0.47 and 0.660 μm independently and interpolates these values to 0.55 μm because no established relationships exist between 0.55 and 2.13 μm for estimating surface reflectance. Therefore for each pixel identified as aerosols by the algorithm, for a specific Sun-satellite viewing geometry, the multispectral reflectances from satellites are used to obtain AOD from the LUTs.

The forcing of climate by solar radiation and aerosols has been related to the optical depth, and global coverage of AOD has been a desired element in climate studies for the last 3 decades.^{107,108} The radiative effect of “natural aerosols” such as dust is called *radiative efficiency*, which is the change in TOA radiative fluxes between clear and aerosol skies per unit AOD. The term *radiative forcing* or *climate forcing* of aerosols is for anthropogenic sources. The global distributions of optical depth coupled with radiative transfer algorithms¹⁰⁹ or in conjunction with broadband measurements such as those from CERES¹¹⁰ are used to calculate the total radiative effect of all aerosols or the climate forcing of anthropogenic aerosols.¹¹¹ These satellite-based methods are the benchmark for assessing the performance of global simulations of aerosol effects on climate.¹¹²

Aerosol microphysical features (size, index of refraction, humidification, etc.) can be examined by measuring the phase function of the aerosol. The Multiangle Imaging Spectroradiometer¹¹³ (MISR) uses the aerosol phase function to improve on the ability to detect aerosols over varying terrain reflectivity. With nine cameras pointed fore and aft, MISR has shown that the oblique views of aerosols over a scene provide more precision than MODIS in retrieving AOD.¹¹⁴ A disadvantage of the MISR instrument is the narrow swath (360 km when compared with the 2400 km for MODIS) that the cameras view and a week-long repeat cycle near the equator before a region

can be surveyed. Therefore, MISR has less ability than MODIS to fill the gaps between ground sensors.

The POLDER series of satellites, including the current PARASOL instrument in the A-Train, has a strong heritage of retrieving AOD.^{115–121} Because the Mie scattering phase function of the aerosol is dependent on all of the intrinsic factors, measurement of the angular scattering behavior of sunlight from the aerosol can be an effective alternative to retrieving AOD. In the POLDER class of instruments, aerosol polarimetry is used to measure the phase function of the aerosol in backscatter. Measuring the polarized components of reflected light from the aerosol provides a means of determining the aerosol scattering phase function. The fringes in the polarimeter's scene have spacings that are related to particle size and index of refraction. This technique will be used in the upcoming Glory mission¹²² scheduled to be launched this fall by NASA. Aerosol retrievals during the Glory mission will move beyond only the retrievals of AOD and other parameters such as particle size. Using both the radiance measurements in multiple bands, the Stokes parameters that describe the polarization state of the reflected radiation and multi-angle measurements will increase the number of independent variables that can be retrieved. Spectral optical thickness, particle size, particle shape, single scattering albedo, and spectral behavior of the aerosol refractive index will be obtained.

There are other measures in addition to the AOD that are useful in determining intrinsic aerosol properties. The GOME and OMI instruments have a product to measure the aerosol absorption optical depth (AAOD).^{123,124} Less sensitive to the surface than the OMI AOD or aerosol index (AI) product, the AAOD is very sensitive to black carbon (BC) in aerosols and has been used to detect smoke aerosol plumes. Although this product is useful for plume delineation and transport, the AAOD may still be less sensitive at the surface because of the atmospheric opacity due to Rayleigh scattering. This needs to be further tested to see if it is useful for ground-based PM assessment.

Active Remote Sensing from Space and the Ground (Lidar)

Lidar measures the backscatter coefficient of the aerosol. The lidar backscatter coefficient may be sufficient to determine the aerosol profile. In principle, lidar can be used to infer the vertical profile of extinction and then integrate to obtain the optical depth. However, the returned signal is not only proportional to the backscatter coefficient of the aerosol but also to the two-way transmittance out to that range and back. For a single wavelength backscatter lidar, the backscatter and total extinction (scattering plus absorption) must be known. With the use of a "lidar ratio" between backscatter and absorption, it is possible to derive an extinction profile.¹²⁵ Some researchers use the optical depth as a constraint to determine the lidar ratio. This "weights" the extinction within the lidar profile such that stronger extinction gets preferentially detected. Circular reasoning results from trying to determine optical depth by using an optical depth.

Raman scattering by nitrogen (N_2) in the atmosphere (the profile of which is well known) can enable an exact determination of the extinction as a function of

height.¹²⁶ This technique is used in the European Aerosol Research Lidar Network to Establish an Aerosol Climatology (EARLINET) lidar network in Europe with a significant literature describing these measurements.^{127–129}

Because the measurement of extinction in a column is closely related to the scattering coefficient (if absorption is a small fraction of the extinction, which is generally true for sulfates), the derivation of $PM_{2.5}$ from extinction is similar to the nephelometer estimates discussed above. In principle, lidar profiles may be as useful (or more useful) than a column measurement because one could examine the extinction closest to the surface rather than integrated over the observation path.

In 1994, NASA launched the LITE on the Space Shuttle Discovery.^{130,131} For a 9-day period, clouds and aerosols were observed with unprecedented detail. Detection of desert dust, biogenic, anthropogenic, and sea-salt aerosols were mapped over the period with 30-m vertical resolution. In a grand finale, the LITE instrument was operated for five orbital passes over the Atlantic Ocean giving a picture of Saharan dust transport to the United States. The LITE experiment showed that a laser could be operated in space for extended periods and gave us a view of aerosol spatial extent that was not previously available.

In 2003, NASA launched the GLAS¹³² on the ICESAT satellite. The prime focus of the mission was to measure ice sheets around the globe with centimeter-scale precision on the height of those surfaces. To ensure that clouds, snow, and ice crystals were not detected as the ice surface, GLAS had two wavelength (532 and 1064 nm) profiling channels that were used for detection of clouds and aerosols. Operating over a 5-yr period, GLAS obtained periods of up to a month duration, each of which had sensitivity similar to the LITE lidar. GLAS lasers were operated near their rated capacity and power on the instrument degraded quickly. The useful lifetime of the lasers for detecting clouds and aerosols was approximately 90 days of continuous operation, and although GLAS carried on with its primary mission of measuring ice, the use of GLAS for air quality purposes was limited.^{133,134} GLAS data were used to measure the transport of large fires in California in 2003 toward the U.S. northeast and over the ocean to Europe.¹³⁵ From the GLAS measurements, the optical depth of this fire plume over Maine was 0.48, the Angstrom coefficient was 1.8, and a mass flux estimate of the amount of smoke in the plume was $900 \pm 350 \text{ t} \cdot \text{sec}^{-1}$ heading eastward toward Europe.

In 2006, the CALIPSO satellite was launched in a sun-synchronous polar orbit. In a station-keeping orbit with a suite of other Earth observing satellites called the A-Train (because these satellites are led by the AQUA satellite and trailed by the AURA satellite), CALIPSO provides continuous observation of the planet with 30-m vertical resolution and one 70-m diameter spot every 330 m horizontally along the ground track.¹³⁶ The CALIPSO laser is less powerful than LITE and in a 705-km instead of 260-km orbit. This leads to significantly higher noise and lower signal than was seen in the LITE experiment. CALIPSO's observations are much better at night when the solar background is absent than they are in the daytime. Comparison to the AOD retrievals from the MODIS or GASP instruments requires daytime data. Significant averaging to improve the signal to noise ratio

(S/N) and products are available as profiles with 5- and 40-km horizontal resolution. Aerosol and clouds are identified in a feature finder at 330-m (single shot) and 1-, 5-, 20-, 40-, and 80-km resolutions using a technique called "overpainting." The signal is averaged for 80 km to detect the faintest layers of aerosol and then at 40-, 20-, 5-, and 1-km resolution more and more intense features are painted over the weaker ones.

CALIPSO is now producing a provisional (beta) product that provides extinction profiles at 40-km horizontal scale as well as a layer extinction product at 5-km horizontal spatial scale.¹³⁷ There is evidence that the 40-km profile product is not reproducing optical depth well in comparison with MODIS, with an underestimate in the CALIPSO AOD.¹³⁸ Comparisons with MODIS AOD and the CALIPSO AOD from the 5-km layer product¹³⁹ suggest that the two products are within 20% of each other on average when globally aggregated at $2^\circ \times 2^\circ$ horizontal resolution. At this time, however, AOD results from CALIPSO have not compared well to surface measurements and the reasons for the discrepancies are being evaluated.

SATELLITE OBSERVATIONS FOR AIR QUALITY MONITORING

Several reviews^{89,90,101} examine observations of trace gas species and aerosols from space. The 1999 review of King et al.¹⁰¹ focused on the use of satellite retrievals of aerosol properties for radiative forcing and climate applications. Nearly 10 yr later, their conclusions still hold about the need for more precision in satellite measurements and more breadth of measurements as a requirement to address global aerosol forcing. Proponents of the use of satellite measurements make several suppositions about the usefulness of satellite data for air quality applications. Fishman et al.⁸⁹ lead with an assertion "Geostationary satellite observations of chemically reactive trace gases will provide unique insight into the evolution and extent of air pollution with the temporal resolution necessary to address air quality on a daily basis." Those authors explain the opportunities and limitations for measuring O₃, CO, HCHO, and NO₂ from space. They conclude with the recommendation from the National Research Council (NRC) Decadal Survey that geostationary observations are of highest priority to bring satellite composition measurements into a decision-making framework. Martin⁹⁰ reviews the methods of determining the four gases above but also includes a discussion of the retrieval of IR active gases, SO₂, and aerosols. The focus of that review is largely methodological but discusses issues of near-surface (boundary layer) retrievals, validation needs, improvement in the algorithms used to retrieve composition, and the assimilation of satellite data into large-scale numerical models. He concludes, also quoting the NRC report, "These recommendations include development of a geostationary mission to provide continuous observations, to improve air quality forecasts, monitor pollutant emissions, and to understand pollutant transport. High priority should be given to supporting the next generation of satellite observations."

In the NRC report and these reviews, the diversity of air quality information needs is often blurred. Near-real-time forecasting of O₃ and PM, identification of large-scale, long-

range transport (LRT) events, source identification, long-term composition measurements, regulatory compliance, management of haze impairment in Class I areas, and exposure measurements for health concerns are all air quality-related issues. Not all of these can be addressed by satellite air quality measurements and, at this time, few are. There are significant temporal- and spatial-scale differences between those needs. Chow et al.^{140,141} have addressed the dichotomy between health exposure assessment needs and the scales of aerosol measurements needed by air quality agencies. They identified implementation of a standard, compliance with air quality standards, alerts, atmospheric process research, determination of health effects, ecological effects, and visibility impairments as reasons for the formation and maintenance of an air quality monitoring system. They said that not all of these needs are compatible. Health exposure needs tend to focus on spatial scales ranging from 1 to 100 m and time scales of minutes to months. Neither surface network monitoring or satellite measurements can deal with that spatial scale. Satellite measurements of air quality begin generally at the 4- to 10-km horizontal spatial scale. Polar orbiting measurements are nearly instantaneous and represent only one or two measurements per day in any location. Geostationary satellite data can be averaged to hourly or daily values because many observations are made at a given point on the ground, thus the recommendations above that geostationary satellite data observations should be further developed.

Air quality compliance, atmospheric composition and trends, alerts, near-real-time forecasting, and determination of visibility impairment are addressed in some fashion by satellite measurements.

Enforcement of Standards and Compliance with Air Quality Standards

In 2007, the A&WMA Critical Review by Bachmann discussed the history of the National Ambient Air Quality Standards (NAAQS).¹⁴² The 39-yr history of those standards parallels the time period that satellite meteorology and observations have developed and yet, to date, no satellite measurements have been used to quantitatively address the NAAQS. From the review conducted here, only one congressional statute has been identified, which addresses the use of satellite measurements for air quality purposes. NASA is empowered with a regulatory requirement under Title VI of the Clean Air Act to monitor the stratospheric O₃ layer. This rule provides NASA with the legislative requirement for instruments such as the OMI monitoring the stratospheric O₃ column. There are no clear legislative mandates for any agency to do satellite monitoring climate and NASA, NOAA, the U.S. Environmental Protection Agency (EPA), and the U.S. Department of Energy (DOE) are all claiming some role in observing climate. In congressional testimony, one of the authors of the Decadal Survey told congress in March 2009, that "Our ability as a nation to sustain climate observations has been complicated by the fact that no single agency has both the mandate and requisite budget for providing ongoing climate observations."¹⁴³ That testimony called for referral of issues of jurisdiction in satellite measurements to the Intergovernmental Working Group on Global Earth Observations. The exact same concern can be voiced by changing the word "climate" to "air quality" above.

EPA has taken a satellite observations role for itself in the Exceptional Events Rule.¹⁴⁴ If a region can show conclusively that they are being impacted by an event (a fire, a dust storm, etc.) that is outside of their jurisdiction to regulate, the event can be flagged as a nonexceedance event. This provides a significant motivation for regional air quality districts to examine transport from other areas to see whether there are such extenuating circumstances. The rule states:

“Information demonstrating the occurrence of the event and its subsequent transport to the affected monitors. This could include, for instance, documentation from land owners/managers, satellite-derived pixels (portions of digital images) indicating the presence of fires; satellite images of the dispersing smoke and smoke plume transport or trajectory calculations (calculations to determine the direction of transport of pollutant emissions from their point of origin) connecting fires with the receptors.”

AOD tracking from day to day can provide evidence that may help make such a case. However, there is the onus to show that the event was significant enough that had it not occurred (the “but for” test), the site would have been in compliance with the EPA air quality guidelines. We examine next the precision of satellite surrogate measurements of $PM_{2.5}$ as they might apply to the “but for” test.

The Gaps in Data

Rural versus Urban Measurements and Spatial Holes in the Surface Networks. As of 2007, EPA’s Air Quality System (AQS) consists of 947 filter-based daily and 591 continuous stations run by federal, state, local, and tribal agencies.¹⁴⁵ For real-time forecasting requirements, there are significant portions of the United States that have no continuous monitors. Most real-time monitors in air quality networks are urban-based. These measurements focus on high-density urban sources (transportation, industry, etc.). For measurements of regional haze and compliance over longer term measurements, IMPROVE,¹⁴⁶ the Chemical Speciation Network (CSN),¹⁴⁵ the Clean Air Status Trends Network (CASTNET),¹⁴⁷ and the Southeastern Aerosol Research and Characterization Study (SEARCH)¹⁴⁸ networks provide data with more regional and national perspective. In the EPA planning documents for PM and other criteria pollutants, effort was placed on adding non-urban sites to the NAAQS networks, especially CASTNET.¹⁴⁹ It was suggested that perhaps 25% of the stations for O_3 should be rural to avoid titration issues from nitric oxide (NO) from the cities and document regional conditions.

Because it is available in near real time, satellite information can be used to alleviate these gaps between sensors. Al-Saadi et al.¹⁵⁰ mapped the smoke plumes emanating from fires in the U.S. northwest in September 2007. Figure 5 shows an example of where there were gaps in real-time surface measurements in Kansas, Oklahoma, and Arkansas. In all four panels, clouds are shown in white/gray from the MODIS visible imagery. The spatial distribution of AOD is overlaid on the cloud image, in

which low values are in blue and high values showing high concentrations of pollution in orange and red. The vertical bars in various colors denote the $PM_{2.5}$ air quality by EPA category. The plume from the Washington state fires had first been detected in AIRNow observations on September 10 over the Great Lakes. On September 11, part of this plume turned southward and looped through the southern United States before heading eastward again. On September 11, a major branch of this plume fell between the AIRNow stations in Texas and Louisiana. On September 12 and 13, the plume was observed over much of the East Coast. Al-Saadi used a Bayesian technique to bridge the gap between AIRNow data that were available for the U.S. East Coast.

This example shows that satellite observations can play a part in the “alert” role for air quality monitoring. Because the AOD data product is available 1–3 hr after the overpass of the satellite, air quality forecasters and analysts have increasingly been interested in having such tools available. Training sessions on how to access these data have been given at the EPA/National Association of Clean Air Agencies (NACAA) National Air Quality Conference.¹⁵¹

Although satellite imagery coupled with ground information is useful for qualitatively assessing $PM_{2.5}$, the abovementioned example shows the utility of satellite data filling in the gaps where there are no ground monitors or minimal coverage. Therefore, in the next section we discuss how the satellite AOD has been compared quantitatively with ground-based $PM_{2.5}$ over various locations worldwide to see whether satellite information can be used as a proxy.

Use of AOD to Assess Ground-Based Concentrations: $PM_{2.5}$ /AOD Relationships

AOD is correlated with ground-based $PM_{2.5}$ mass. Assuming cloud-free skies, well-mixed boundary layer of height (H) with no overlying aerosols, and aerosols that have similar optical properties, the AOD can be written as¹⁵²:

$$AOD = PM_{2.5} H f(RH) \frac{3Q_{ext,dry}}{4\rho r_{eff}} = PM_{2.5} H S \quad (10)$$

where $f(RH)$ is the ratio of ambient and dry extinction coefficients, ρ is the aerosol mass density ($g \cdot m^{-3}$), $Q_{ext,dry}$ is the Mie extinction efficiency, and r_{eff} is the particle effective radius (the ratio of the third to second moments of the size distribution). S is the specific extinction efficiency ($m^2 \cdot g^{-1}$) of the aerosol at ambient relative humidity (RH).

In reviewing the more than 30 papers that have addressed this topic, the columnar satellite-derived AODs have been compared with surface $PM_{2.5}$ mass measurements on a station-by-station basis. Most papers have addressed $PM_{2.5}$ /AOD and a few PM_{10} /AOD. The results from these studies are compared in Table 4. Matchups in the spatial location have been typically restricted to less than 50-km offset although there is variability in how the collocation of the data has been done by investigators. MODIS AOD retrievals are at 10- by 10-km spatial scales and $PM_{2.5}$ ground measurements are point measurements

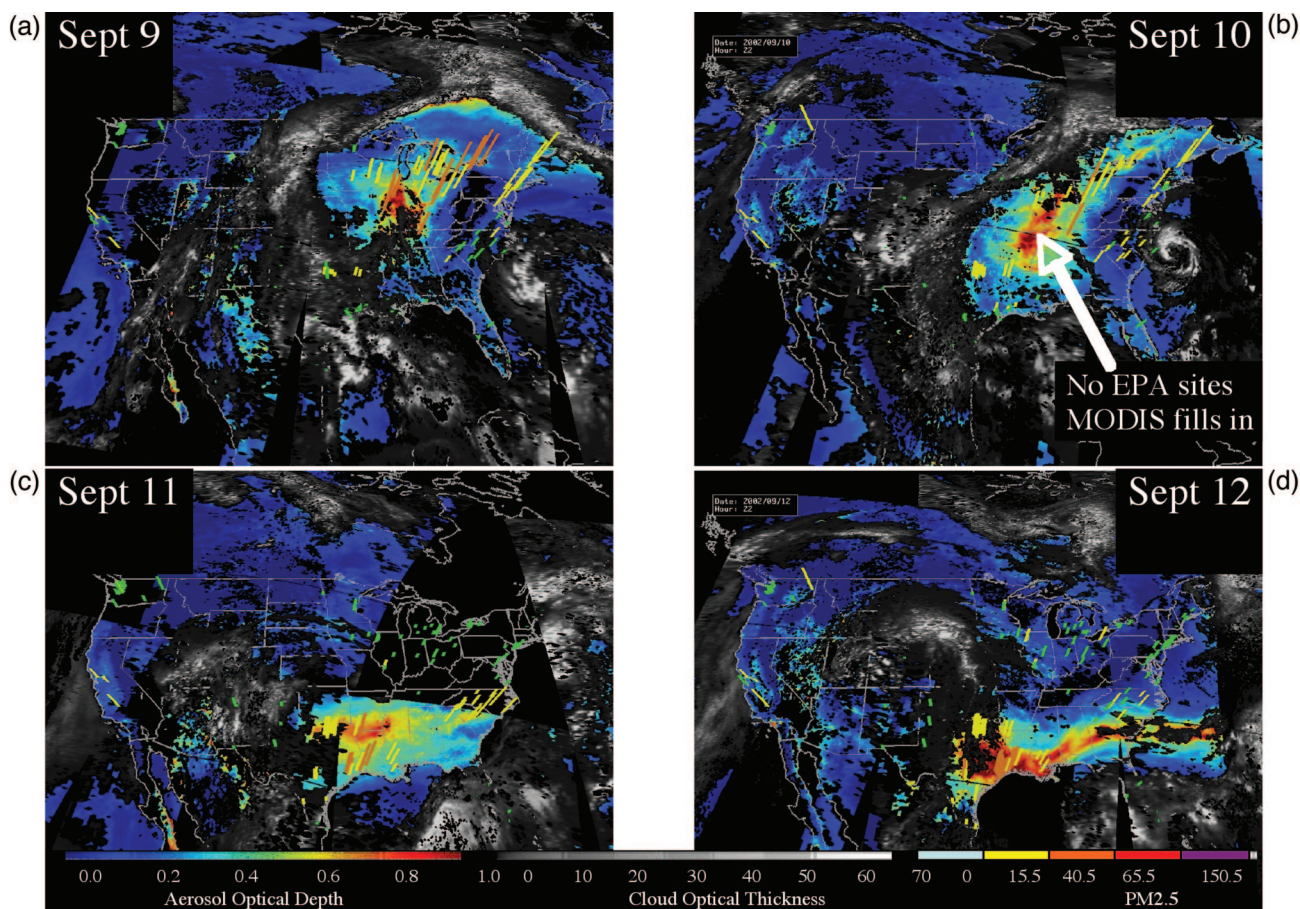


Figure 5. Example of MODIS gap filling from a smoke plume that was generated in Washington but impacted the southeastern United States on (a) September 9, (b) September 10, (c) September 11, and (d) September 12, 2007. Clouds are shown in shades of gray in which white denotes an optically thick cloud. The spatial distribution of MODIS AOD is shown in color and the vertical bars are $PM_{2.5}$ from the EPA network color coded according to concentrations. The panel for September 10 shows that there was a region where no ground-based Speciation Trends Network samplers (shown by the vertical histograms) were available but the MODIS AOD data filled in the gap. Reproduced with permission from Chu et al.²²⁹ Copyright 2008 SPIE.

with a high temporal resolution. At a $10\text{-km} \cdot \text{hr}^{-1}$ wind speed, it takes the aerosol 1 hr to cross a pixel. This corresponds to hourly surface measurements. MODIS AOD results have been compared with both hourly and 24-hr $PM_{2.5}$ measurements. More sophisticated approaches use meteorological and surface information to further refine this relationship.

Early in the MODIS aerosol mission, Chu et al.¹⁵³ found that the correlation between PM_{10} and AOD was high for a single site in northern Italy. The ratio of $PM_{2.5}$ to AOD (P/A) ratio was $54.7 \mu\text{g} \cdot \text{m}^{-3}$ with a linear correlation coefficient (R) of 0.82. The predominance of the papers below reported R, not R^2 , which is a measure of the variance of the data.

Wang and Christopher's¹⁵⁴ study in Jefferson County, AL compared the AOD results from the Terra and Aqua satellites and 1- and 24-hr averaged $PM_{2.5}$ mass from 7 locations within 100 km. Linear correlation coefficients combined from all seven sites between AOD and $PM_{2.5}$ for hourly data were 0.70, and when aggregated to daily means the correlations increased to 0.98.

Hutchison^{155,156} showed the use of MODIS AOD and imagery for a dust event in Texas in 2002 and a haze event in September of the same year but P/A correlations were

not assessed. The Texas Commission on Environmental Quality (TCEQ) uses MODIS AOD and imagery to assess air quality and transport of pollutants. Hutchison et al.^{157–159} improved the existing P/A correlations by better addressing the cloud masking in MODIS and taking into account the vertical profile of aerosols.

In 2004–2006, in a series of papers that covered regional measurements to national measurements, Engel-Cox et al.^{160–163} examined the linear regression of P/A. In the first study to look at the entire United States they showed that the correlations in P/A had a systematic behavior with the best correlations coming in the U.S. northeast (correlation coefficients >0.8) and the poorest in the U.S. northwest (correlation coefficients <0.2).¹⁶¹ The conclusions were that where the aerosol type, mixing height, and loading were the most uniform (the east), the P/A correlation could have a regression coefficient of greater than 0.8–0.9. In the west, the correlations were poorer because of a wider variation in aerosol types (more nitrate than sulfate), more smoke than the east, higher surface reflectivities making AOD retrieval difficult, and more elevated plumes in the AOD signatures. These results are shown in Figure 6.

Table 4. Literature survey of P/A ratios, intercepts, and correlation coefficients.

Author	Sensor	Date	Region	Number of Ground Monitors	PM _{2.5} /PM ₁₀	Linear Regression	R
Wang ¹⁵⁴	MODIS (Terra)	2002	Alabama	7	PM _{2.5} (24 hr) ^a	77.0τ - 0.23	0.67
	MODIS (Aqua)	2002	Alabama	7	PM _{2.5} (24 hr) ^a	68.6τ + 1.93	0.76
	Average	2002	Alabama	7	PM _{2.5} (24 hr) ^a	72.3τ + 0.85	0.98
Chu ¹⁵³	MODIS	August–October 2000	Italy	1	PM ₁₀	54.7τ + 8.0	0.82
Engel-Cox ¹⁶¹	MODIS	April–September 2002	United States	1338	PM _{2.5}	22.6τ + 6.4	0.4
					PM _{2.5} (24 hr)	18.7τ + 7.5	0.43
Liu ²⁰⁸	MISR	2003	St. Louis	22	PM _{2.5}	NA	0.8
Engel-Cox ¹⁶³	MODIS	July 1 to August 30, 2004	Baltimore	4	PM _{2.5}	31.1τ + 5.2	0.65
					PM _{2.5} (<PBL)	48.5τ + 6.2	0.65
					PM _{2.5} (24 hr)	25.3τ + 11.1	0.57
					PM _{2.5} (24 hr < PBL)	64.8τ + 1.76	0.76
Liu ¹⁶⁹	MISR	2001	Eastern United States	346	PM _{2.5}		–
Al-Saadi ¹⁶⁴	MODIS	Review	United States		PM _{2.5}	62.0τ	NA
Gupta ¹⁷¹	MODIS	2002 and July–November 2003	Global cities	26	PM ₁₀ ^a	141.0 τ	0.96
Koelemeijer ¹⁵²	MODIS	2003	Europe	88 (PM _{2.5})	PM _{2.5} ^a	NA	0.63
					PM ₁₀ ^a	214.0τ - 42.3	0.58
Kacenenbogen ¹¹⁸	POLDER	April–October 2003	France	28	PM _{2.5}	26.6τ + 13.2	0.7
Gupta ¹⁷³	MODIS	February 2000 to December 2005	Southeastern United States	38	PM _{2.5}	29.4τ + 8.8	0.62
					PM _{2.5} (24 hr)	27.5τ + 15.8	0.52
Hutchison ¹⁵⁸	MODIS	August–November 2003 and 2004	Texas	28	PM _{2.5} (August) ^a	68.8τ - 39.9	0.47
					PM _{2.5} (September) ^a	59.7τ - 17.2	0.98
Paciorek ¹⁷⁷	GOES-12	2004	United States	Not given	PM _{2.5} (24 hr)	NA	0.5
					PM _{2.5} (yearly)	NA	0.75
An ¹⁷⁹	MODIS	April 3–7, 2005	Beijing	6	PM ₁₀ ^a	21.7τ + 6.1	0.92
Schaap ¹⁸⁰	MODIS	August 2006 to May 2007	Cabauw, Netherlands	1	PM _{2.5} ^a	31.1τ + 5.1	0.92
					PM _{2.5}	120τ + 5.1	0.72

Notes: ^aSlope and intercept converted from an AOD to PM (A/P) ratio. The P/A ratio is the slope of PM_{2.5} to AOD in a linear regression model.

After these papers were published, a team of researchers developed an application called Infusing Satellite Data into Environmental Applications (IDEA).¹⁶⁴ Initially delivered from the University of Wisconsin, this product has been transferred to an operational environment at NOAA/NESDIS, where maps of AOD from MODIS on Terra (10:30 a.m. nominal crossing time), Aqua (1:30 p.m. nominal crossing time), and GASP (every 30 min) are made available to users such as air quality forecasters on a daily basis.^{165,166} The IDEA product uses the single P/A relationship developed by Chu et al.¹⁵³ across the United States. Trajectories are used to estimate where today's high AOD will be in the following 48 hr. There are comparative panels that show the correlation between P/A by station in the AQS network. There are time series that show the previous 2 months of P/A relationships. IDEA has added source data from the GOES Aerosol and Smoke Product (GASP)^{167,168} as a separate panel with animations of AOD movement.

Because simple linear relationships between AOD and PM_{2.5} were applicable only for certain seasons and locations, Liu et al.¹⁶⁹ combined the MISR and 346 EPA daily averaged ground monitors in the eastern United States with other variables such as planetary boundary layer (PBL) height and RH from the GEOS-3 model to improve PM_{2.5} estimations from satellite AOD. In this study, nearly half of the data were randomly assigned and

used to develop a relationship between PM_{2.5} and MISR AOD (with ancillary information such as PBL, RH, etc.), and these relationships were used to test the remaining half of the data. Using a power-law fit with AOD and PBL height and RH as parameters (derived from GEOS-3), they found that AOD had a positive power-law dependence but was sublinear with the exponent averaging 0.45. The probability density functions of PM_{2.5} mass, AOD, and PBL height were all lognormal and the RH was roughly normally distributed. The multiplier for RH was $\exp(-0.634RH)$ and for the PBL height had a -0.36 power dependence. The negative value for PBL height indicates that fine particles from the surface are diluted in the boundary layers as PBL increases. The negative value for RH indicates that because the satellite AOD retrievals are for ambient conditions and those from a tapered element oscillating microbalance (TEOM)¹⁷⁰ are at 40% RH, the same AOD values at higher RH levels may correspond to smaller PM_{2.5} concentrations. In other words, as the PBL increased, the PM decreased by roughly the cube root of PBL. The sublinear response to AOD in this nonlinear model is interesting because it may explain some of the large positive intercepts seen in the linear models from data derived at high AOD. It also would predict that P/A would be largest for small AOD and flatter for large AOD.

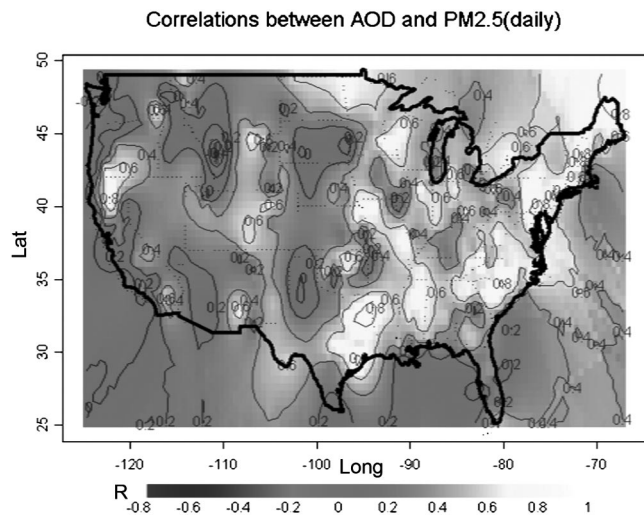


Figure 6. Linear correlation coefficient (R, gray scale) between daily $PM_{2.5}$ and Terra-MODIS AOD across the United States.¹⁶¹ Correlations are determined by regressing daily $PM_{2.5}$ and satellite AOD over 1000 ground monitors and then contouring using kriging techniques. Axes are latitude ($^{\circ}$ N) and longitude ($^{\circ}$ W). Figure courtesy of J.A. Engel-Cox, Battelle Memorial Institute.

Moving from primarily U.S. studies to 26 cities in five countries, Gupta et al.¹⁷¹ found a high P/A ratio with appreciable offset from the aggregated data from five cities (Hong Kong, Basel/Bern in Switzerland, Delhi, Sydney, and New York). Correlation coefficients were reported for each station and when averaged over all locations, the correlation coefficient was 0.96. In 2007, Gupta et al.¹⁷² showed that the correlation coefficient for smoke from bush fires over Sydney varied from r values of 0.11 to 0.48, probably because of the fact that the smoke may have been elevated that the surface monitors did not observe. They showed that over 7 yr of measurements in the U.S. southeast, P/A slopes were similar to those found by Engel-Cox and the range of slopes varied from 21 to 36 $\mu\text{g} \cdot \text{m}^{-3}$.¹⁷³

Van Donkelaar et al.¹⁷⁴ showed good agreement between model-predicted AOD and the measured AOD when chemistry transport model-derived vertical structure was used. The spatial correlation improved from 0.36–0.37 to 0.58–0.69 when the vertical profile of aerosol extinction was used in the AOD- $PM_{2.5}$ relationship. The NASA GEOS-CHEM model predicted the aerosol microphysics and the mass used in the correlations. The authors found a similar underestimate of surface $PM_{2.5}$ using AERONET AOD (considered as a reference value) of 0.59 $PM_{2.5}$ from the Canadian National Air Pollution Surveillance (NAPS)/AQS network. The slope improves to 0.89, removing much of the bias if California is eliminated from the international comparison. It is difficult to combine these data with those of the other studies because the GEOS-CHEM model is so intricately woven into the calculation of $PM_{2.5}$ in this paper.

Using the POLDER instrument,¹¹⁶ which is flying in the A-Train suite of satellites, Kacenenbogen¹¹⁸ reported similar P/A relationships to studies that used MODIS. However, their results from 28 ground monitors in France report the root mean square (RMS) error on the slope was

$5.3 \mu\text{g} \cdot \text{m}^{-3}$ and this is one of the only reported measures of precision of the slope estimate.

Kumar, in one of two papers reporting essentially the same data,^{175,176} found that in India, the P/lnA (note the logarithmic form) has a slope of 0.33–0.48. This is consistent with the finding of Liu above of a sublinear slope of P/A, but the results are difficult to reconcile with a linear model. The paper also finds a constant in the regression of –62 to –72, which makes little sense at $\tau = 1$ (i.e., PM would be negative).

Paciorek et al.¹⁷⁷ studied the AOD relationship with $PM_{2.5}$ using the GOES-12 GASP. This product is primarily available only over the continental United States. The GASP provides data at a higher temporal resolution (every 30 min) when compared with once-a-day polar orbiting MODIS and MISR sensors. They matched the GASP AOD with nearly 100,000 data points from EPA ground monitors and examined their results over all 4 seasons. Simple two-variate regressions between AOD and $PM_{2.5}$ were compared against AOD- $PM_{2.5}$ relationships adjusted for RH and PBL. Although they did not give the explicit relationship that they used for the comparison in the paper, they did state that they could improve the correlation coefficient in the P/A relationship from using just the raw AOD data from 0.5 to 0.75 by correcting for RH, the PBL height, and seasonality.

Zhang et al.¹⁷⁸ completed a similar adjustment for location and season by determining independent P/A relationships for MODIS on Terra and Aqua for the new Collection 5 MOD04 AOD algorithm (as well as the older heritage Collection 4 algorithm) for each of the nine EPA air quality regions by season. The Collection 5 algorithms are a new generation of satellite retrievals that use improved surface and aerosol characterization with improved AOD accuracies when compared with AERONET. The intent of the Zhang study is to use the seasonality and regional differences to provide more specificity in the NOAA NESDIS IDEA product than the current single relationship used for the entire United States ($62 \mu\text{g} \cdot \text{m}^{-3}$ per unit AOD with zero intercept).

In 2007, An et al.¹⁷⁹ compared MODIS AOD near Beijing with ground-based $PM_{2.5}$ and PM_{10} from the six networks near the city. They also conducted Community Multiscale Air Quality (CMAQ) model runs (April 3–7, 2005) of precursor gases and aerosols for the Beijing area in preparation for the 2008 Olympic Games. Their P/A ratio was converted from the inverse of this ratio shown in their paper and, therefore, the R value shown is on the AOD/ $PM_{2.5}$ ratio. Because they regressed the aerosol column versus the CMAQ aerosol column, we have used 2000 m (from their model runs) as the mixing height for this value in a well-mixed boundary layer. Their results also indicate that the simulated SO_2 concentrations from CMAQ and columnar AODs are well correlated with ground and satellite observations respectively ($r > 0.7$).

Schaap et al.¹⁸⁰ compared $PM_{2.5}$ from a TEOM in Cabauw, Netherlands, with AERONET and MODIS retrievals of AOD from August 2006 to May 2007. They found slopes in the P/A relationship of $120 \mu\text{g} \cdot \text{m}^{-3}/\text{unit AOD}$ when they carefully screened 67 cases with a lidar at the site. It should be noted, however, that the authors used a

modification to the TEOM with a filter dynamics measurements system (FDMS) that accounts for volatile nitrate loss from the TEOM at the standard crystal temperature of 40 °C. One of the authors stated that this loss could be 40% of the particulate mass in Holland.¹⁸¹ It is difficult, then, to compare this result to other PM_{2.5} measurements in North America and Asia where this correction has not been made.

Liu et al.,¹⁶⁹ Paciorek et al.,¹⁷⁷ and Kacenelenbogen et al.¹¹⁸ have all used eq 10 to estimate the aerosol relationship. Charlson et al.¹⁸² used a global value of S of 5.5 m² · g⁻¹ (at 85% average RH) to estimate global climate forcing by aerosols. Assuming a representative PBL height over the United States is 1.5 km, this gives a P/A of 121 μg · m⁻³ per unit optical depth. Few of the values retrieved in practice (Table 4) have slopes that are this large. The assumption in eq 10 that one has a well-mixed boundary layer does not often hold. Factors that lead to differing correlations in eq 10 are types of aerosol, surface type, whether overlying aerosols have been removed from the regression, whether the aerosol is really on the surface, definitions of PM_{2.5}, and satellite precision in determining AOD.

Several authors have tried to address the issue of overlying aerosols. Engel-Cox et al.¹⁶³ used lidar to determine cases in the Baltimore-Washington area to screen elevated aerosols. Doing so increased the linear correlation coefficient slightly (~5%) but left considerable uncertainty. Al-Saadi et al.¹⁵⁰ showed an improvement in the correlation in P/A by using the AOD/ H as the regression variable, deriving H from a model prediction of the PBL height during February 2007. Correlations between AOD and PM_{2.5} over the Californian San Joaquin Valley were improved from 0.36 to 0.75 by using this method. However, a problem arises because modelers are concerned about the accuracy of the current PBL prediction schemes in models¹⁸³ and require the use of lidar PBL heights, when available, as a validation for the model output. It is not clear whether a lidar-derived PBL height or a model height will add more precision to the P/A prediction.

The inexplicability of the generally positive intercept in P/A regressions deserves some examination. There should be no significant PM_{2.5} that does not scatter some light. Although nucleation-mode aerosols would not scatter much light, they also do not carry much mass per unit volume. Dust particles can be scatterers with sufficient mass, but not in the PM_{2.5} size range. So having a 5- to 15-μg · m⁻³ intercept on AOD indicates uncertainty. If the intercept were negative, one might assume that the AOD has some noise in a clear atmosphere. But this is not what the preponderance of these studies show. One explanation may be seen conceptually in Figure 7, where Liu et al.¹⁶⁹ predicted a sublinear dependence of P/A with a power-law slope of +0.45 is plotted. With positive curvature to the P/A relationship and such nonlinearity, much of the variability in the linear regressions can be explained by the range of P/A values sampled. Where AOD is low, one might expect higher slopes (which has been seen where RH is low or corrected).¹⁶³ This behavior would also explain the positive intercept in the regressions of MODIS data. MODIS has a stated precision of

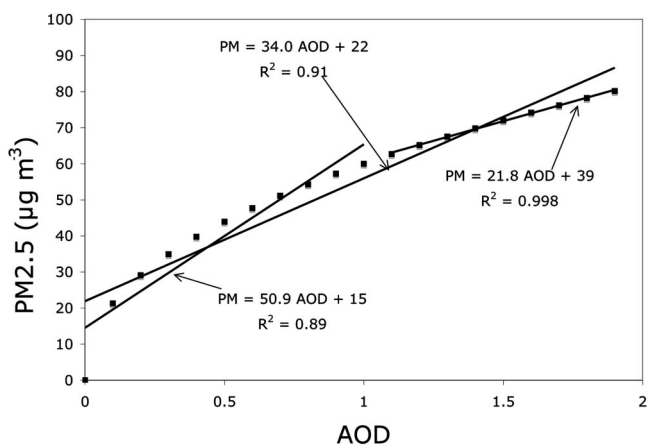


Figure 7. Hypothetical example of the slopes for low and high optical depths in which the model relationship follows Liu's¹⁶⁹ derived relationship (but scaled) $PM_{2.5} = 60 \times AOD^{0.45}$. Although the overall slope of the linear regression of all of the data is 34 μg · m⁻³, it could be as high as 50.9 for the values <1 AOD and 21.8 for values from AOD of 1 to 2. The range of AOD observed would highly influence the slope and intercept in a linear model.

$\Delta\tau = \pm 0.05 + 0.2 \tau_{550}$, where τ_{550} is the AOD at 550 nm. Below 0.1 AOD, MODIS' error would be >70% of the AOD. If this nonlinear behavior is real (and this deserves more study), one would expect a positive intercept because these low AOD values would be sparse in the datasets used in Table 4. It would also improve correlation at higher PM_{2.5} and higher AOD (even neglecting the additional factor that instrumental precision also improves at higher values).

Gupta¹⁷³ looked at two alternatives to a linear correlation (LC). Using a multiple linear regression (MLR) technique, he allowed additional variables (PBL height, location, temperature, RH) to aid P/A assessment. This study used 2 yr of satellite data over 85 ground monitors in the southeastern United States. The greatest improvement in the correlation (from 0.6 to 0.7) between PM_{2.5} and AOD occurred when surface temperature was added followed by PBL height to the multiple regression equations. Because both of these variables may not truly be independent (PBL height is driven by convection, which is highest at highest temperatures), it is not clear what physical change is happening to the scattering to improve the correlation.

Gupta further analyzed this relationship using neural network techniques to relate eight expected dependencies on two input variables (PM_{2.5} and AOD) with four hidden variable layers in the neural net.¹⁸⁴ The integrated satellite, surface, and ancillary database contained 32,834 samples. The samples were divided into testing (10%), training (50%), and validation (40%) categories. The overall correlation for the U.S. southeast increased from 0.41 in the LC technique to 0.7 in the MLR and 0.83 in the neural net for validation data. There was some skill in the neural net in removing some outliers (see Figure 8), but one of the shortcomings of the technique is that it is difficult, if not impossible, to discover what pathway the network used to remove the outlying points.

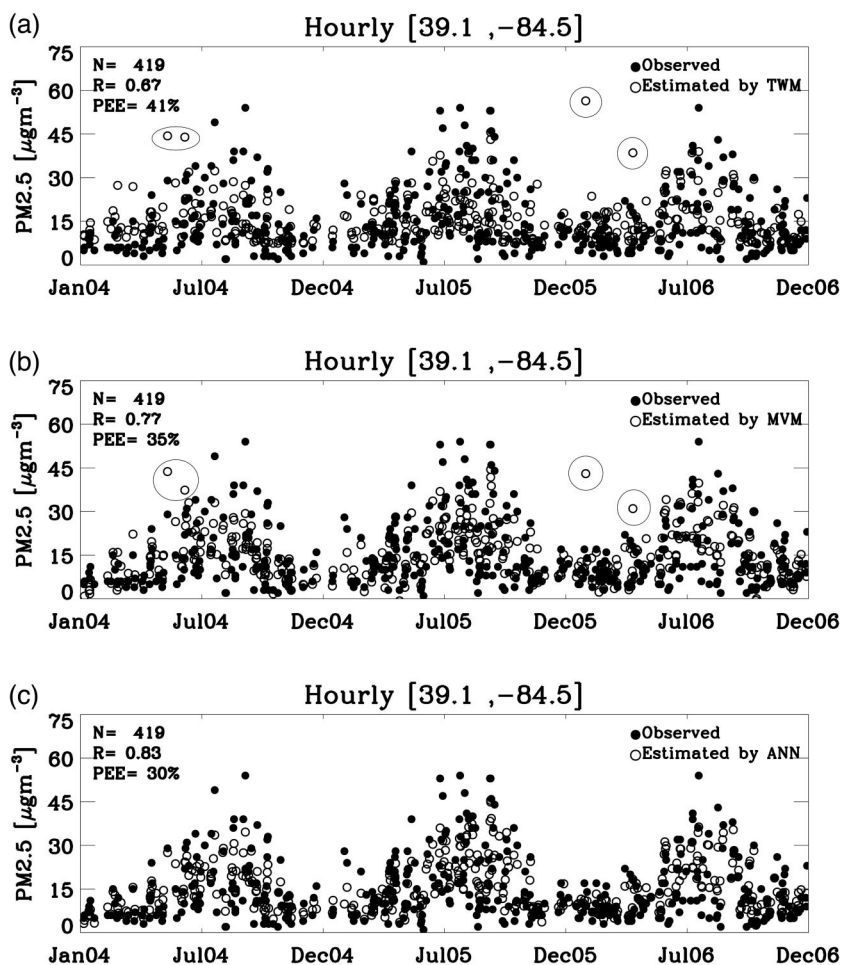


Figure 8. Comparisons of the $PM_{2.5}$ predictions \circ to observed $PM_{2.5}$ \bullet from a (a) linear, (b) multilinear, and (c) neural network model.¹⁸⁴ The circled points in the top and middle panel are outliers that the neural network was able to eliminate. Reproduced with permission of the author.

In Table 4, the large range of relationships in P/A will bring skepticism that one can make a quantitative prediction of $PM_{2.5}$ with sufficient accuracy to be useful in regulatory compliance or in the “but for” test under the Exceptional Events Rule. Satellite AOD measurements are still in their infancy with less than a 10-yr overall record. What is missing in many of the studies above are better statistical measures of precision on the slope and intercept from the P/A relationship. From those measures, precision of the $PM_{2.5}$ estimate could be computed. At $40 \mu\text{g} \cdot \text{m}^{-3}$, An’s Beijing¹⁷⁹ and Engel-Cox’s U.S. East Coast¹⁶³ slopes are identical and predict $\tau = 1.1$ at that ground concentration. Engel-Cox’s national average¹⁶¹ would predict $29 \mu\text{g} \cdot \text{m}^{-3}$ and Gupta¹⁷³ would predict $38.2 \mu\text{g} \cdot \text{m}^{-3}$. For three of these studies, the variability is less than 5% but extrapolating across the United States the precision drops to 25%. The IDEA product¹⁶⁶ will be a useful tool to examine the precision with which $PM_{2.5}$ can be estimated at over 500 ground stations in the United States as long as a single national P/A relationship is no longer used. Those changes are being incorporated into IDEA this year and will allow better assessment of the precision of the estimate in the future.

Rather than just looking at the $PM_{2.5}$ prediction, Gupta also showed¹⁸⁴ that AOD could predict the same EPA hazard classification (0–14.4 is “good” or green, 14.5–

$40.4 \mu\text{g} \cdot \text{m}^{-3}$ is “moderate” or yellow, 40.5 – $65.4 \mu\text{g} \cdot \text{m}^{-3}$ is “unhealthy for sensitive groups” or orange, etc.) 98% of the time. It is possible to create maps of the EPA color classifications from the AOD measurements coupled with ancillary information such as aerosol height and meteorology, but it requires some assessment of the need for smoothing to eliminate noise from the 2% of the pixels that may be misclassified. For an AIRNow-type presentation of the EPA color scheme,¹⁸⁵ it appears that satellite AOD measurements can achieve this.

Events, Atmospheric Process Research, and Trends

Two recent intensive air quality studies illustrate how satellite information was critical in piecing together a story of LRT influencing local air quality.

The NOAA Northeast Air Quality Study–Intercontinental Transport and Chemical Transformation Experiment/Intercontinental Transport Experiment. In 2004, NOAA and NASA sponsored a joint experiment to estimate the outflow of pollutants and their precursors through the northeast. The NOAA Northeast Air Quality Study–Intercontinental Transport and Chemical Transformation Experiment (NEAQS-ITCT)

was run in conjunction with the Intercontinental Transport Experiment (INTEX-NA). Designed to measure outflow of pollutants from the United States and follow those pollutant plumes as far as Europe, the 2004 study was highly influenced from major forest fires in Alaska. Column measurements of AOD and CO were consistent in tracing the input of a major plume from these fires and helped discriminate local pollution from LRT.

Analysis of this case¹⁸⁶ showed that there was significant impact of the CO from these fire plumes on INTEX DC-8 aircraft measurements made in the U.S. east including both trace gases and BC (Figure 9). Those column measurements were well aloft for much of their travel to the U.S. East Coast. In Figure 10, we have superimposed 3 days of the University of Wisconsin HSRL profiles for this period.¹⁸⁶ The lidar profiled the lowest 15 km of the atmosphere and showed a large plume of material passing over Madison, WI, on July 18, 2004. Shown below the HSRL lidar data are three panels of MODIS AOD.¹⁸⁷ The AOD data showed that the plume passed over Wisconsin early on July 18 and had passed through by July 19. Five ground-based monitors making PM_{2.5} measurements in Wisconsin are also shown in this figure and the three times from MODIS are noted as arrows. Although there is a slow increase of PM through the period from July 16 to 20, the impact of the plume on ground-based PM was minimal in Wisconsin. In Maryland, smoke impacted the boundary layer on July 20 in the afternoon.^{163,186} This example shows that the column measurement is important to investigate LRT components to local pollution and that the vertical dimension cannot be ignored. If plumes do not contact the surface (or only mix down for limited periods as this plume did on July 18 evening), ground-based concentrations will not be impacted. Without having the HSRL results available, it would have been impossible to understand why such a large AOD plume had so little impact on PM_{2.5} at the ground.

TEXAS Air Quality Study. In the 2006 second Texas Air Quality Study (TEXAQs-II), model estimates of O₃ and PM_{2.5} were compared with measurements from an intensive air and ground sampling program. Although the overall results from the study gave results that were comparable to model predictions, there were cases in which PM north of Houston exceeded the predictions. When looked at with satellite information, dust intrusions from the Caribbean were shown to enhance the ground concentrations. CALIPSO results showed that the dust was from the Sahara in Africa (Figure 11 shows a multiday set of CALIPSO cross sections tracking the dust plume into the Caribbean and up into Texas).¹⁸⁸ In addition to the LRT import of dust, McMillan et al.¹⁸⁹ have shown again that fire plumes from Montana impacted the study during the TEXAQs period.

Trends. In the future, satellite measurements may have a significant input in trend determination, but the time series for most satellites is short. There are no published trends in AOD from MODIS. Xia et al.¹⁹⁰ have published data showing a weekday-weekend difference in AOD from AERONET and MODIS. Longer-term satellite-derived trend data for NO₂ in Europe shows a decreasing trend in

emissions that is consistent with the European Monitoring and Evaluation Programme emissions inventory.¹⁹¹ The increased emissions of NO₂ in China and trends on other continents have been documented by Richter et al.^{89,192}

To What Extent Does AOD Improve Modeling?

Numerical modeling and forecasting of aerosols and trace gases rely on accurate emission locations. Most simulation frameworks require meteorological models to obtain atmospheric dynamic conditions for the period of forecast that is used as input to the core of a model that requires transport, chemistry, and deposition information.¹⁹³⁻¹⁹⁸ In situ and satellite datasets are useful to evaluate these simulations.

These simulations generally capture the average spatial trends and the dynamic range in PM_{2.5} when compared with in situ measurements, but overestimates and/or underestimates are possible because of various issues, including uncertainties in emission inventories, physics, chemistry, and meteorology.¹⁹³⁻¹⁹⁶ Assumptions in boundary conditions and poorly quantified emissions within the model domain are among the major uncertainties in simulations. McKeen et al.¹⁹⁵ evaluated seven air quality forecast models using data collected during a field experiment and discussed the biases between and among these models. These simulations were compared against 118 PM_{2.5} monitors and 342 O₃ monitors between July 14, 2004 and August 17, 2004. These studies did not use satellite data for model verification or for assimilation purposes. Their results showed that the PM_{2.5} forecasts had better skill relative to the O₃ forecasts although the models did not capture the diurnal behavior of PM_{2.5} in urban and rural locations.

Most of these models also do not account for aerosols transported from outside of the model domain.¹⁹³ Studies indicate that when compared with ground truth, models underestimate PM_{2.5} by a factor of 2 during biomass burning events because of smoke transported from outside of the model domain.¹⁹⁵ Satellite remote sensing can help with this issue because near-real-time information on fire locations and emissions are available. Hot spots/fire locations are routinely identified by polar orbiting¹⁹⁹ and geostationary sensors²⁵ that are then used to obtain PM_{2.5} emissions.^{20,200,201} These fire source functions can then be used to improve model forecasts. Wang et al.²⁰² showed the utility of using fire emissions from Central America in a forecast model to estimate PM_{2.5} concentrations in the United States. Stein et al.²⁰³ recently used the Hybrid Single-Particle Lagrangian Integrated Trajectory (HYSPPLIT) model to estimate PM_{2.5} concentrations from various fire events. These models assess surface PM_{2.5} due to aerosols transported from outside of the domain.

Satellite remote sensing products can also be assimilated into numerical models to improve predictive capabilities. For example, Mathur¹⁹⁴ used the MODIS AOD during the 2004 fires in Alaska to improve the characterization of pollution from outside of the model domain. For each model grid, the PM_{2.5} mass was estimated from the satellite AOD using a priori PM_{2.5}-AOD relationships. The difference in PM_{2.5} between the base model runs (no fire emissions) and the PM_{2.5} from the satellite AOD are

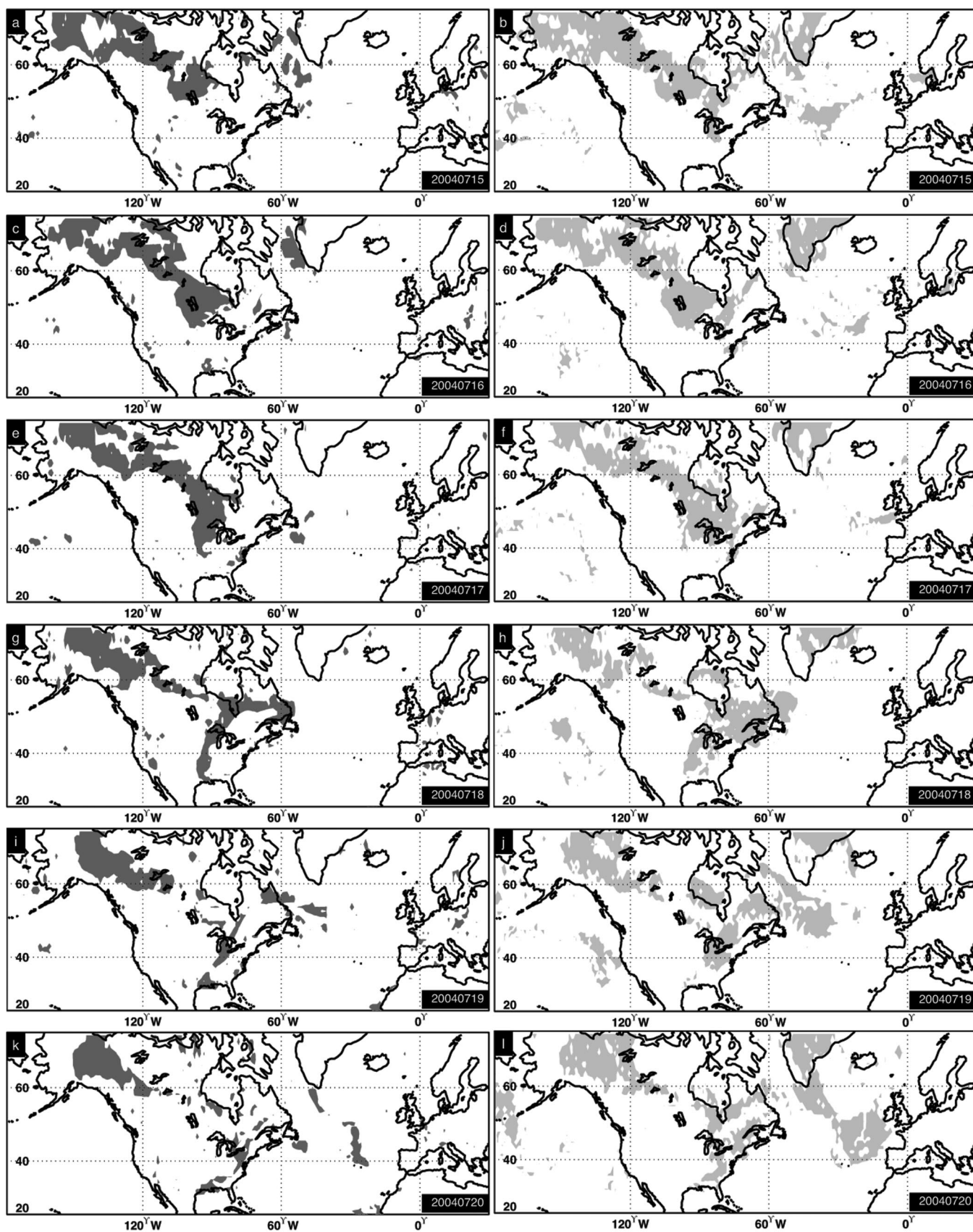


Figure 9. MODIS AOD (panels a, c, e, g, i, k: $\tau > 0.65$) and AIRS CO 500-mb mixing ratio (panels b, d, f, h, j, and l: CO > 150 ppb) for July 15–20, 2004, during the INTEX-A study, showing the injection of a major smoke plume from Alaska into the INTEX study area.¹⁸⁶

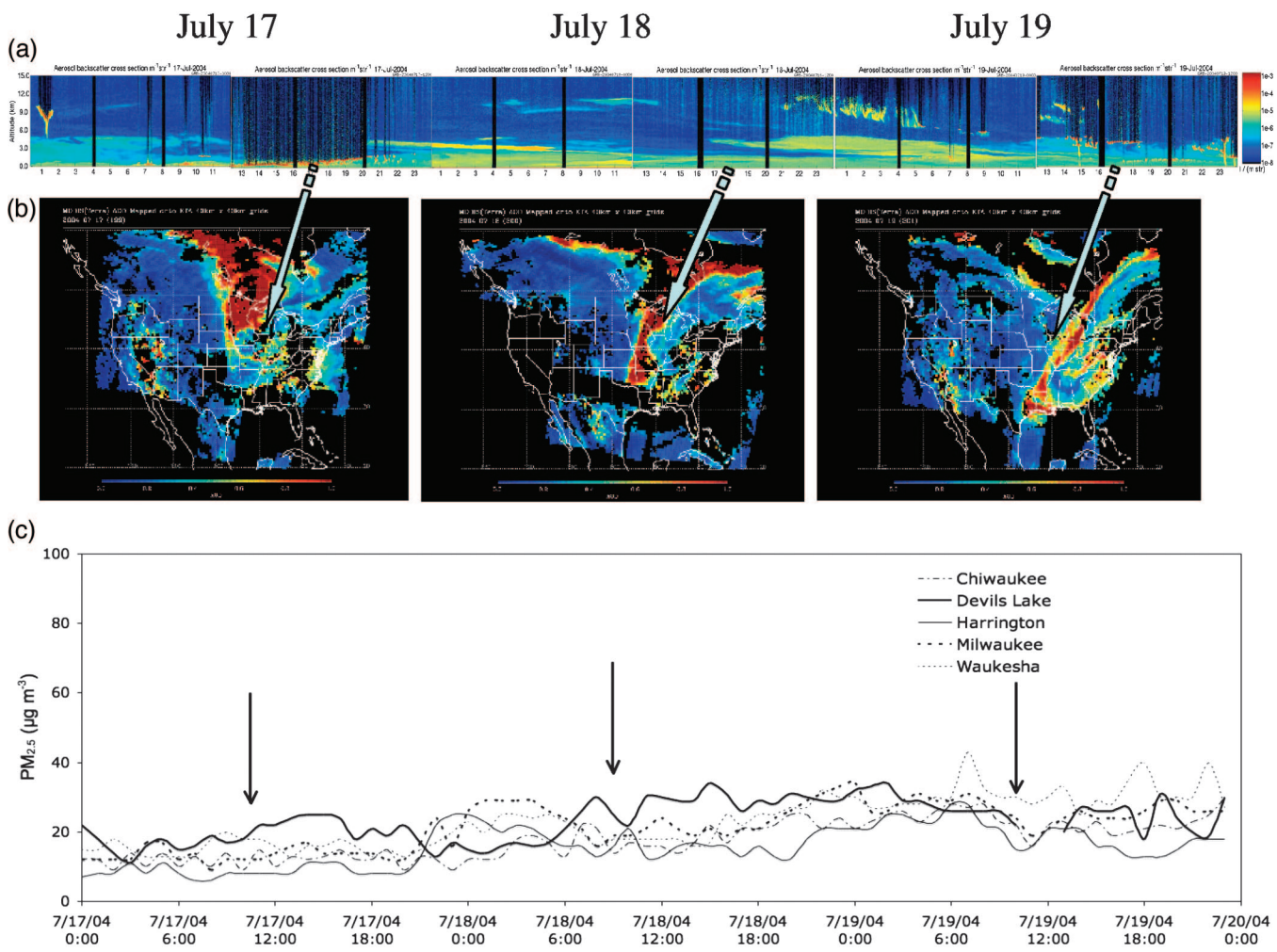


Figure 10. The same case showing (a) the University of Wisconsin HSRL lidar profiles that were based in Madison, WI; (b) the MODIS Terra AOD; and (c) the ground-based PM_{2.5} for five stations in Wisconsin from the AIRNow technology database. The times of the overpasses are marked with arrows on the PM_{2.5} time series.

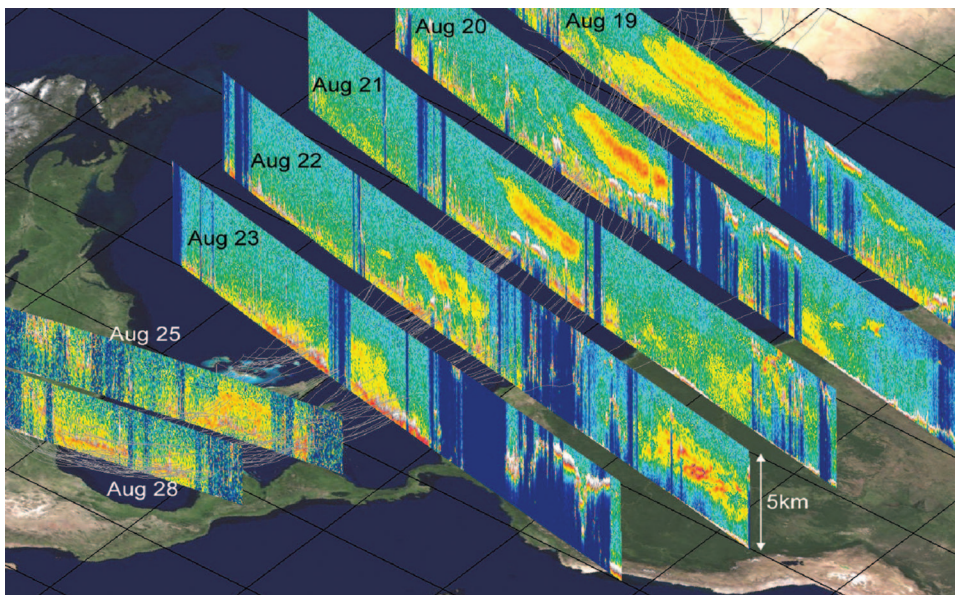


Figure 11. Injection of Saharan dust into the TEXAQS 2006 study area on August 28, 2006.¹⁸⁸

calculated and then vertically distributed for various species for further simulations. This first attempt at simulating AOD requires correct P/A relationships that are not applicable for all meteorological situations. For example, the a priori relationship assumes that the aerosols are in a well-mixed boundary layer that yields good $PM_{2.5}$ /AOD relationships, but this may not be true in all cases. It also requires assumptions on taking column measurements and distributing it vertically using a priori information. Another source of uncertainty arises from taking column satellite AOD retrievals with no speciation information and allocating these into various species for the model.

Because the vertical distribution of aerosols is critical for assessing $PM_{2.5}$, another technique is to take the column-integrated satellite AOD and distribute it vertically on the basis of the model-predicted distributions of aerosols. This assumes that the physics, chemistry, radiation, and the mechanics of the PBL height characterization in the model are correct.¹⁹⁸ Probably the "best" solution is to take measured vertical distributions of aerosols from a space-borne lidar or a ground-based lidar to partition the satellite AOD into various model layers¹⁹⁹; however, there are challenges in this approach as well. The CALIOP two-wavelength polarization-sensitive lidar (on the CALIPSO satellite) with a footprint of 70 m does not have global daily coverage and precludes characterization of vertical distributions over the entire modeling domain. Also, ground-based lidars need to be available in a near-continuous manner to improve model performance.

Kondragunta et al.²⁰⁴ compared the CMAQ simulations of aerosols with GOES AOD during the summer 2004 International Consortium for Atmospheric Research on Transformation/New England Air Quality Study (ICARTT/NEAQS) field campaign. This period was dominated by LRT of smoke from fires in Canada/Alaska and regional-scale sulfate event over the eastern United States. The CMAQ simulations did not include boundary conditions for these smoke aerosols. For clear sky conditions, the GOES AOD was compared with simulated AOD. The forecast accuracy was between 0 and 20% for exceedances of $PM_{2.5}$ (AOD > 0.55) and between 40 and 90% for nonexceedances (AOD < 0.55). In general, accuracies were better from the sulfate events when compared with the smoke events because the CMAQ did not include emissions from LRT of smoke aerosols. Although some European models are actively using chemical data assimilation,^{205,206} several challenges remain, including lack of observations about vertical structure and a better understanding of aerosol composition, emission locations, sources, and magnitudes. In cloud-free skies, AOD is available on a daily near-real-time basis that can be considered in an assimilation system.

Detection of source emissions from event-driven and intermittent sources may be one of the greatest strengths of satellite measurements. Measurements of emissions from fires have been made by "bottom-up" models (where the areal extent of the fires is multiplied by emission factors from biomass type and fire type).²⁰ Other techniques^{22,23} are based on the radiometric emissions from active fires in the 4- μ m bands of multispectral satellites such as MODIS and GOES. Correlations of the emissions in the IR and smoke mass are relatively high, but there is

the need for validation of these emissions and the quality assurance of the fire detections to ensure that glint (specular reflection) and other issues are dealt with.

Trace gas emissions of NO_2 have been observed from large urban regions. Oxides of nitrogen (NO_x) and SO_2 emissions have been reported from Beijing,²⁰⁷ and recently, emission controls in that region during the Olympics were observed from space-borne measurements.⁷⁷ If robust emissions data can be gleaned from satellite observations, better model predictions can be expected in the future.

In summary, the use of satellite data products for forecasting $PM_{2.5}$ in chemical models is in its infancy. Using fire locations and emissions of smoke aerosols from biomass burning fires has shown success in assessing $PM_{2.5}$. There is no reason why these datasets should not be included in models. These satellite-based datasets are especially useful for assessing $PM_{2.5}$ air quality from LRT.²⁰² Near-daily retrievals of columnar AOD are also available on a continuous basis from several satellites. In clear sky conditions, these data products can be used for model assessment or as input to models. Although ancillary information about the vertical structure of aerosols is critical, space-borne and ground-based lidars provide this information when available. This is an asset that needs to be utilized for modeling studies, especially when aerosol injection height information is needed.

FUTURE MISSIONS AND PROSPECTS FOR IMPROVING ON THE PHYSICS

The examples above and the extensive literature that has developed on the use of satellite instruments for air quality assessment show a promising future for the use of these data in air quality research and applications. But, in answer to the title of this review, we have not yet reached the promised land. There are still significant issues to address before these measurements will be as routinely used as a $PM_{2.5}$ monitor in a network.

Some Fundamental Problems in Satellite Remote Sensing

Extrinsic versus Intrinsic Property Requirements. The use of satellite data needs to address the fundamental mismatch in the regulatory need to measure a mass concentration (or in the case of trace gases, a mixing ratio at the surface) from a column measurement of an optical radiance property. For trace gases, in principle, the problem is somewhat easier because the conversion of mixing ratio to extinction requires the knowledge of the absorption coefficient of the gas at a given pressure and temperature. Because many of our visible absorption measurements for O_3 , SO_2 , and NO_2 are relatively wide spectral measurements, the absorption coefficient is reasonably well known and easy to characterize. For these gases, the column measurement from passive instruments may be sufficient to characterize a mass budget, especially if integrated horizontally by the measurement and vertically by the column measurement to give fluxes of the gas across a plane.

Aerosols provide a more difficult challenge because the intrinsic (or microphysical) property of the pollutant

is not constant as it is for a gas. For aerosols, the composition, sizes, indices of refraction, and hydration properties are not constant. Not only do the extrinsic properties (i.e., the number of particles per cubic meter, the height of the mixed layer, the profile, etc.) have to be known, but the PM_{2.5} (or PM₁₀) intrinsic property differences (composition, size distribution, density, indices of refraction, hygroscopicity) is also problematic. To the extent that PM_{2.5} is used in the regulatory environment, there will still be significant scientific issues between what is measured and the pollution problem (acid rain, health, etc.) that is being addressed. With that in mind, the use of an optical surrogate for PM_{2.5} is probably no more challenging an issue.

The use of the AOD as a measure for mass concentration has skill in some regions but less in others and does not provide a uniform way to measure aerosols across the United States. We discussed in Table 4 the range of measurements from across the globe and the wide range of correlations between AOD and mass. It may be possible to reduce that range of uncertainty by further intrinsic measurements. It is unlikely that we will further reduce that uncertainty by statistical regressions. Within a given region, the types of aerosols may be more limited, the heights of the boundary layer may be more uniform, the ranges of humidity that the aerosol experiences more limited, and these factors may make the correlation of AOD to PM more accurate in some regions.^{163,184,208} Study of the controlling extrinsic factors will aid in understanding the P/A relationship. It is not at all obvious that these can be extrapolated to other regions with similar certainty of the predictability of PM_{2.5}. However, some regions of the globe have no PM measurements at all. Central, South America, and Africa have few stations measuring PM. The current uncertainty in the P/A ratios could be acceptable for estimates in those regions.

Clouds. Clouds cover 60–70% of the planet at any time.^{209,210} Clouds obscure the surface and make detection of aerosols at the surface impossible. Gupta²¹¹ examined this possible bias and determined that for the U.S. southeast for a 7-yr period, the PM_{2.5} levels on days with and without clouds have the same probability density functions; yearly means have average values of PM_{2.5} that differ by less than 2 μg · m⁻³. This would indicate that clouds do not significantly bias the measurement of PM_{2.5} in broken cloud fields on an annual mean basis. However, cloud obscuration cannot be neglected, and satellite observations cannot be used to detect exceedances for regions that have extensive cloud cover. This limitation is significant during winter months at midlatitudes and during the rainy seasons in the tropics.

Snow. Similar to clouds, the high surface reflectivity of snow is problematic at wavelengths that rely on dark surfaces for detection of extinction contrast. NO₂ retrievals are possible over snow-covered surfaces because the NO₂ absorption features are close together in wavelength (<10 nm) and, over this wavelength range, reflectivity from the surface is constant. OMI AAOD retrievals are similarly unaffected by snow or low clouds because the effective scattering height for these UV wavelengths is 2–3

km or more. However, all other visible retrievals are precluded over snow.

Bright Surfaces. Bright surfaces like deserts or bare soil do not provide enough contrast with the added radiance from aerosols to be able to retrieve AOD. In the “Deep Blue” algorithm,¹⁰⁶ Hsu and her colleagues used the shortest wavelength from MODIS to push the contrast between the surface reflectance and aerosol reflectance beyond the traditional MODIS AOD retrieval. Deserts and bright surfaces are still a challenge for aerosol retrievals. De Castanho and Martins⁶³ used a “critical reflectance” method for bright surfaces (such as urban areas with hardened asphalt and concrete surfaces). In that method, there is a critical reflectance for which the range of expected AODs in a plot of reflectances at 0.65 μm crosses.^{212,213} If, for a given surface pixel, this critical reflectance can be determined, radiance ratios at higher or lower reflectivities can be mapped to AODs. In other words, aerosols over bright surfaces may darken the scene, over dark surfaces brighten the scene, and the degree to which they do so is wavelength dependent.

Lyapustin et al.²¹⁴ have developed algorithms that use more sophistication in the knowledge from the BRDF at the surface. In a routine designed to better detect overlying clouds, the Multiangle Implementation of Atmospheric Correction (MAIAC) algorithm²¹⁵ uses the concept that the surface reflectivity is fixed and varies on time scales of days, whereas the atmosphere is moving with a time scale of minutes. Using the 2D covariance fields from clear and hazy scenes, the algorithm is able to pick out scene elements that are atmospheric in nature over highly structured underlying surface scenes. This technique is likely to show important new results from geostationary sensors that have more wavelength channels and show motion over scales of minutes.

Noncontinuity in Observations. Polar orbiting satellites are generally placed in sun-synchronous orbits with equator crossing times in the morning or afternoon. At 7.1 km/sec orbital velocity, observation of a 10- by 10-km MODIS pixel takes 1.5 sec. At most, a given site would be observed less than 4 times per day from a polar orbiter. Although these orbits are designed to be representative of the diurnal cycle variations in the PBL, the lack of hourly observations throughout the day limits the usefulness for exceedances of the AQS.

The geostationary satellites—GOES-12 and GOES-11—have an AOD product that can be related to AOD. GASP measures AOD every half hour across the United States at 4- by 4-km resolution. This high temporal resolution allows not only visualization of aerosol plume movement, but is also potentially useful for timing of exceedances. GASP, however, does not have the precision of MODIS’ AOD primarily because it has only one broad visible channel. The GASP retrieval is based on discrimination of the radiance in that channel from the minimum radiance detected over the previous 28 days of measurement. If the minimum in such radiance is not from a very aerosol-free day, there will be some bias in the retrieval. By 2015, NOAA proposes to launch the GOES-R series of satellites. This series has MODIS-like channels and will

allow retrievals of a more precise AOD every 5–30 min, depending on the observation mode of the satellite. This is a factor in the Decadal Survey recommendation for geostationary platforms quoted above.

Precision. The AOD P/A ratio, even if refined to a high degree of correlation, still has error estimates in the literature on the order of $5\text{--}10 \mu\text{g} \cdot \text{m}^{-3}/\text{unit AOD}$ (15–30%). It should be incumbent on future papers written about this regression to include such estimates of the precision. MODIS AOD has precision⁴² of $\pm 0.05 + 0.2\tau$, which indicates that the precision of the AOD retrieval itself dominates the P/A relationship. For surface networks in Class I areas, the precision of the $\text{PM}_{2.5}$ measurement should be better than $2 \mu\text{g} \cdot \text{m}^{-3}$ or 5% and better than 10% in Class II and Class III areas.²¹⁶ Satellite measurements are not at that level of maturity and it is unlikely that they will meet that precision in the near future. Satellite observations of column measures of trace gases similarly will be difficult to relate to regulatory compliance needs. One exception to this may be NO_2 , for which significant correlations to ground-based NO_x and NO_y observations can be made if the NO_2/NO_y ratio is estimated.^{217,218} In fact, satellites such as GOME, SCIAMACHY, and OMI may actually measure ambient rural NO_2 more completely than the ground networks. In 2001–2006, only 243 of 4177 site-years (~5%) of NO_2 data in the United States were not in metropolitan statistical areas.²¹⁹

Errors in the AOD measurement directly propagate into the precision with which PM can be estimated. There are some areas in which AOD retrievals can be improved. As in the 7–9 wavelength AERONET retrievals of aerosol size, single scattering albedo, and indices of refraction, it may be possible in the future with hyperspectral satellite instruments (hundreds of wavelengths) to develop algorithms with more accuracy in determining the microphysical (intrinsic) properties of the aerosol, which would make the retrieval of AOD or extinction (the extrinsic properties) more robust. However, wavelength channels are expensive to implement in orbit, and the future NPOESS missions have taken the unfortunate path of having fewer instead of more channels.

Combined Measurements

Combination of sensors shows promise in reducing the uncertainty in column retrievals. Use of profiling instruments such as lidars from the ground and from space allows more certain placement of the pollutant in the vertical. For CO and CH_4 algorithms, knowing the height of the pollutant constrains the range of IR temperatures that affect retrievals. Similarly, dust profiling in the IR needs an estimate of the aerosol height.³⁶ The OMI AOD can be improved if knowledge of the plume height is known.⁷⁰ However, profiling instruments with variable pointing ability are unlikely in the next few decades simply because the combination of power, agility, and weight would make such an instrument difficult to carry to space. Without having horizontal spatial coverage (similar to the MISR difficulty), most areas of the globe would not be covered each day and interpolation between orbits with over 1500-km spacing would cause even extended, significant features to be missed because the orbit path was not

appropriate on that day. For example, during the Southern California wildfires of October 2007, the CALIPSO satellite detected the smoke only twice over a 7-day period because of the vagaries of the orbital coverage with respect to the fires.¹⁶⁶ Future lidar satellite missions should consider active pointing capability to target specific significant events such as fires (natural and Homeland Security related) and volcanoes.

Measurement of the vertical humidity profile is desirable in conjunction with an AOD retrieval. Hygroscopic growth can change extinction by factors of 3–5, therefore it is expected that AOD would have a strong humidification effect (e.g., eq 10). Hygroscopic effects near the edges of clouds is an active research topic and it may be that the hydration of aerosols can extend outward from cloud edges by up to 10 km horizontally.⁴⁶ Combination of ground-based lidars and satellite measurements may prove useful in determining the horizontal scales involved. Whiteman²²⁰ has proposed an airborne water vapor Raman lidar that is currently in the testing phase. Such a system is being evaluated for use from a spaceborne orbit. AIRS and TES do provide profile measurements of water vapor in the free troposphere but have difficulty near the surface where understanding the hydration of aerosols is most needed. Models can provide the information needed to better account for the hydration effect of aerosols to relate to dry $\text{PM}_{2.5}$.^{173,208}

Unlike the lidar on the CALIPSO satellite, which measures a broad elastic scattering feature from both Rayleigh scattering and aerosol backscatter, NASA has flown a prototype instrument similar to the ground-based HSRL shown in Figure 10. The NASA Langley HSRL¹⁸⁸ works by simultaneously measuring the Rayleigh-scattered and aerosol-scattered components of elastic scattering. The ratio of these signals is proportional to the aerosol mixing ratio and the extinction as a function of height. HSRL lidars are under consideration for the Atmospheric Chemistry Experiment (ACE) mission, a part of the Decadal Survey planned missions.

Several satellites are planned that have advanced multicomponent profiling capability. The European Space Agency's Aladin wind and aerosol lidar will be the first to launch in 2010 on the Atmospheric Dynamics Mission (ADM)-Aeolus platform and will be followed in 2013 by the ATLid on the EARTH CARE mission.^{221,222} Although the United States plans to launch ICESAT-II in this time frame and a lidar on the DesDynI mission, both will be used only for surface detection (ice and vegetation, respectively). There are no realistic plans to launch atmospheric lidar in NASA's plans before the ACE mission, which cannot credibly be launched before 2020 at the current NASA funding profile. This is a considerable transition of capability in profiling aerosols to Europe over the next decade.

The GOES-R series of satellites have been designed to mimic the spectral features available on MODIS or the VIIRS instruments that are run in LEO and polar orbits. The GOES-R Advanced Baseline Imager (ABI) is an important development for AOD retrievals.²²³ In a geostationary orbit, GOES-R ABI will be able to view the United States every half hour while the Sun is up. The GOES-R ABI algorithm is being designed to give similar precision

to MODIS but instead of 2 realizations (MODIS Terra and MODIS Aqua) each day, we will have 14–28 images taken. For forecasting and analysis, this will revolutionize our ability to address aerosol transport and monitoring. GOES-R will not launch until 2015. It is unfortunate that so many of the NASA Earth Observing System (EOS) instruments are nearing or past the planned lifetime for these instruments. If instruments start to fail in orbit, the United States will be poorly placed to continue in air quality monitoring from space and will have to rely on its international partners.

One impediment to such combinations of datasets is the diverse nature of the data formats, spatial and temporal scale, and access. Not all satellite data, especially from foreign agencies, are publicly available. Another impediment is that satellite science teams tend to have narrow foci with no mission funding to combine measurements from other sensors.

CONCLUSIONS

Satellite air quality measurements are in their infancy with 50 yr of history of atmospheric composition measurements but less than 10 yr of record with modern multisensor platforms from polar and geostationary orbits. The physics behind remote sensing of gases and aerosols uses Beer's law to convert radiances measured in orbit to mixing ratios or concentrations. IR retrievals and visible measurements have fundamentally different approaches to solving for the concentrations. In the IR, broad weighting functions make the vertical resolution of the profile of the target species vary from 1 to 10 km depending on the gas. Horizontal resolution of the measurements is comparable to visible column measurements (1–10 km horizontally).

Success has been shown at retrieving the column of several gases in visible and IR wavelengths (e.g., O_3 , NO_2 , SO_2 , HCHO, CHOCHO, BrO, water, CO, CH_4 , CO_2). However, the lowest part of the troposphere is too optically thick to accurately measure O_3 and SO_2 all of the way to the surface. Aerosols have been quantified using the AOD and the relationship between AOD and $PM_{2.5}$ is being actively investigated.

Although the desire for the use of satellite data for air quality purposes is widely stated, the reality is that many of the measurements have not yet met the promise that they can be operationally used for today's air quality monitoring requirements. Precision in measuring AOD is $\pm 20\%$, and the relationship to $PM_{2.5}$ is at best $\pm 30\%$ in controlled measurements in which overlying aerosols, aerosol type, and boundary layer structure are known. This is not currently sufficient for regulatory use. The interest in using such data in the EPA Exceptional Event Rule needs investigation, but with the precision above, the "but for" provision in the rule makes the use of satellite data possible in significant exceedances only. Applications such as event identification, transport, and atmospheric composition determination are strengths of satellite measurements. Where high precision is required (compliance monitoring, the "but for" test, and quantitative measurement of visibility effects on Class I areas), satellite data are presently of limited utility.

Strengths of satellite measurement are found in emissions identification (fires especially), event tracking and transport, definition of boundaries of large-scale pollution features, and providing some evidence for profiles of pollutants well above the surface. Satellite observations fill gaps in areas where there are no ground sensors (e.g., much of the third world). Satellite measurements have been very useful in defining production, oxidation, and evolution processes from biomass burning. Satellite imagery can provide iconic views of major events such as forest fires, volcanic plumes, and stagnant haze masses over highly industrialized areas. In conveying the extent of pollution to the public, visual imagery from space is important.

Combining multiple measurements and models improves the understanding of the physics of the measurement and improves the precision. Use of forecast and analysis models is synergistic with satellite and surface measurements, improving understanding of the prediction and the measurement. Assimilation of existing satellite air quality and ground data into models needs serious evaluation, and the United States lags Europe in such research. More new missions for air quality will be launched in Europe and Japan than in the United States for the next decade. Although the promise of satellite measurements has not been fully met at this time, spaceborne remote sensing will be one way of seeing the promised land.

ACKNOWLEDGMENTS

The authors thank Drs. Pawan Gupta, Jill Engel-Cox, Kevin McCann, Nickolay Krotkov, James Szykman, and Wallace McMillan for providing graphics that were used in this review. Helpful comments were received from Meloe Kacenenbogen and Amy Huff in early drafts of the review. Comments of the reviewers (George Hidy, John Watson, Judy Chow, Thomas Overcamp, Luis Diaz-Robles, and Peter Mueller) contributed greatly to the focus and structure of the review. The authors dedicate this work to a colleague who devoted her life to the measurement of air pollution from space. Cheiko Kittaka left this planet far too soon, and she is remembered for her enthusiasm about air quality remote sensing.

REFERENCES

1. Explorer Series of Spacecraft; National Aeronautics and Space Administration (NASA); NASA History Division; available at <http://history.nasa.gov/explorer.html> (accessed January 30, 2009).
2. Weinstein, M.; Suomi, V.E. Analysis of Satellite Infrared Radiation Measurements on a Synoptic Scale; *Mon. Weather Rev.* **1961**, *89*, 419–428.
3. Wexler, H. TIROS Observational Results; *Space Sci. Rev.* **1962**, *1*, 7–67.
4. *Earth Science and Applications from Space: National Imperatives for the Next Decade and Beyond*; National Research Council; National Academies: Washington, DC, 2007.
5. *J-Track 3-D Satellite Tracking*; National Aeronautics and Space Administration; available at <http://scisites.msfc.nasa.gov/realtime/jtrack/3d/JTrack3D.html> (accessed January 29, 2009).
6. Kidder, S.Q.; Vonder Haar, T.H. *Satellite Meteorology: an Introduction*; Academic: San Diego, CA, 1995.
7. Watson, J.G. Visibility: Science and Regulation; *J. Air & Waste Manage. Assoc.* **2002**, *52*, 628–713.
8. Thomas, G.; Stamnes, K. *Radiative Transfer in the Atmosphere and Ocean*; Cambridge University Press: Cambridge, MA, 1999.
9. Lenoble, J. *Atmospheric Radiative Transfer*; A. Deepak: Hampton, VA, 1993.
10. Volz, F.E. Satellite Remote Sensing of Atmospheric Aerosol; *J. Air Pollut. Control Assoc.* **1973**, *23*, 527.

11. Nakata, J.K.; Wilshire, H.G.; Barnes, C.G. Origin of Mojave Desert Dust Plumes Photographed from Space; *Geology* **1976**, *4*, 644-648.
12. Lyons, W.A.; Dooley, J.C., Jr.; Whitby, K.T. Satellite Detection of Long-Range Pollution Transport and Sulfate Aerosol Hazes; *Atmos. Environ.* **1978**, *12*, 621-631.
13. Chung, Y.S. Air Pollution Detection by Satellites: the Transport and Deposition of Air Pollutants over Oceans; *Atmos. Environ.* **1986**, *20*, 617-630.
14. Takayama, Y.; Takashima, T. Aerosol Optical Thickness of Yellow Sand over the Yellow Sea Derived from NOAA Satellite Data; *Atmos. Environ.* **1986**, *20*, 631-638.
15. Remer, L. *Remote Sensing: Introduction and History*; National Aeronautics and Space Administration; Earth Observatory; available at <http://earthobservatory.nasa.gov/Features/RemoteSensing/remote.php> (accessed January 31, 2009).
16. Short, N. *Remote Sensing Tutorial*; National Aeronautics and Space Administration; available at <http://rst.gsfc.nasa.gov/> (accessed January 31, 2009).
17. Seemann, S.W.; Borbas, E.E.; Knuteson, R.O.; Stephenson, G.R.; Huang, H. L. Development of a Global Infrared Land Surface Emissivity Database for Application to Clear Sky Sounding Retrievals from Multispectral Satellite Radiance Measurements; *J. Appl. Meteor. Clim.* **2008**, *47*, 108-123.
18. Pequignot, E.; Chedin, A.; Scott, N.A. Infrared Continental Surface Emissivity Spectra Retrieved from AIRS Hyperspectral Sensor; *J. Appl. Meteor. Clim.* **2008**, *47*, 1619-1633.
19. Gillespie, A.; Rokugawa, S.; Matsunaga, T.; Cothorn, J.S.; Hook, S.; Kahle, A.B. A Temperature and Emissivity Separation Algorithm for Advanced Spaceborne Thermal Emission and Reflection Radiometer (ASTER) Images; *IEEE Trans. Geosci. Remote Sens.* **1998**, *36*, 1113-1126.
20. Zhang, X.Y.; Kondragunta, S.; Schmidt, C.; Kogan, F. Near Real Time Monitoring of Biomass Burning Particulate Emissions (PM_{2.5}) across Contiguous United States Using Multiple Satellite Instruments; *Atmos. Environ.* **2008**, *42*, 6959-6972.
21. Ichoku, C.; Kaufman, Y. J. A Method to Derive Smoke Emission Rates from MODIS Fire Radiative Energy Measurements; *IEEE Trans. Geosci. Remote Sens.* **2005**, *43*, 2636-2649.
22. Ichoku, C.; Giglio, L.; Wooster, M.J.; Remer, L.A. Global Characterization of Biomass-Burning Patterns Using Satellite Measurements of Fire Radiative Energy; *Rem. Sens. Environ.* **2008**, *112*, 2950-2962.
23. Jordan, N.S.; Ichoku, C.; Hoff, R.M. Estimating Smoke Emissions over the U.S. Southern Great Plains using MODIS Fire Radiative Power and Aerosol Observations; *Atmos. Environ.* **2008**, *42*, 2007-2022.
24. Kaufman, Y.J.; Justice, C.O.; Flynn, L.P.; Kendall, J.D.; Prins, E.M.; Giglio, L.; Ward, D.E.; Menzel, W.P.; Setzer, A.W. Potential Global Fire Monitoring from EOS-MODIS; *J. Geophys. Res. Atmos.* **1998**, *103*, 32215-32238.
25. Weaver, J.F.; Lindsey, D.; Bikos, D.; Schmidt, C.C.; Prins, E. Fire Detection Using GOES Rapid Scan Imagery; *Weather Forecast.* **2004**, *19*, 496-510.
26. *MODIS Active Fire Maps*; U.S. Department of Agriculture; available at <http://activefiremaps.fs.fed.us/> (accessed January 30, 2009).
27. *NOAA Hazard Mapping System*; National Oceanic and Atmospheric Administration; available at <http://www.osdpd.noaa.gov/ml/land/hms.html> (accessed January 30, 2009).
28. Schmidt, C. *Biomass Burning*; Cooperative Institute for Meteorological Satellite Studies Space Science and Engineering Center; University of Wisconsin-Madison; available at <http://cimss.ssec.wisc.edu/goes/burn/abba.html> (accessed January 30, 2009).
29. *Fire Locating and Modeling of Burning Emissions (FLAMBE)*; U.S. Naval Research Laboratory; available at <http://www.nrlmry.navy.mil/flambe/index.html> (accessed January 30, 2009).
30. Turquety, S.; Hadji-Lazaro, J.; Clerbaux, C.; Hauglustaine, D.A.; Clough, S. A.; Casse, V.; Schlusser, P.; Megie, G. Operational Trace Gas Retrieval Algorithm for the Infrared Atmospheric Sounding Interferometer; *J. Geophys. Res. Atmos.* **2004**, *109*, D21301; doi: 10.1029/2004jd004821.
31. Aumann, H. AIRS/AMSU/HSB on the Aqua Mission: Design, Science Objectives, Data Products, and Processing Systems; *IEEE Trans. Geosci. Remote Sens.* **2003**, *41*, 253-264.
32. Xiong, X.Z.; Barnet, C.; Maddy, E.; Sweeney, C.; Liu, X.P.; Zhou, L.H.; Goldberg, M. Characterization and Validation of Methane Products from the Atmospheric Infrared Sounder (AIRS); *J. Geophys. Res. Biogeosci.* **2008**, *113*, G00A01; doi: 10.1029/2007jg000500.
33. Maddy, E.S.; Barnet, C.D.; Goldberg, M.; Sweeney, C.; Liu, X. CO₂ Retrievals from the Atmospheric Infrared Sounder: Methodology and Validation; *J. Geophys. Res. Atmos.* **2008**, *113*, D11301; doi: 10.1029/2007jd009402.
34. Goody, R.M.; Yung, Y.L. *Atmospheric Radiation: Theoretical Basis*; Oxford University: New York, 1995.
35. Rolland, P.; Liou, K.N.; King, M.D.; Tsay, S.C.; McFarquhar, G.M. Remote Sensing of Optical and Microphysical Properties of Cirrus Clouds Using Moderate-Resolution Imaging Spectroradiometer Channels: Methodology and Sensitivity to Physical Assumptions; *J. Geophys. Res. Atmos.* **2000**, *105*, 11,721-11,738.
36. DeSouza-Machado, S.G.; Strow, L.L.; Hannon, S.E.; Motteler, H.E. Infrared Dust Spectral Signatures from AIRS; *Geophys. Res. Lett.* **2006**, *33*, L03801; doi: 10.1029/2005gl024364.
37. Ackerman, S.A. Remote Sensing of Aerosols Using Satellite Infrared Observations; *J. Geophys. Res. Atmos.* **1997**, *102*, 17,069-17,080.
38. Sokolik, I.N. The Spectral Radiative Signature of Wind-Blown Mineral Dust: Implications for Remote Sensing in the Thermal IR Region; *Geophys. Res. Lett.* **2002**, *29*, 2154; doi: 10.1029/2002gl015910.
39. Brindley, H.E.; Russell, J.E. Improving GERB Scene Identification Using SEVIRI: Infrared Dust Detection Strategy; *Rem. Sens. Environ.* **2006**, *104*, 426-446.
40. Legrand, M.; Plana-Fattori, A.; N'Doume, C. Satellite Detection of Dust Using the IR Imagery of Meteosat 1. Infrared Difference Dust Index; *J. Geophys. Res. Atmos.* **2001**, *106*, 18,251-18,274.
41. Joseph, J.H.; Wiscombe, W.J.; Weinman, J.A. The Delta-Eddington Approximation for Radiative Flux Transfer; *J. Atmos. Sci.* **1976**, *33*, 2452-2459.
42. Remer, L.A.; Tanré, D.; Kaufman, Y.J. *Algorithm for Remote Sensing of Tropospheric Aerosol from MODIS: Collection 005*; National Aeronautics and Space Administration; Goddard Space Flight Center: Greenbelt, MD, 2009.
43. Cahalan, R.F.; Oreopoulos, L.; Marshak, A.; Evans, K.F.; Davis, A.B.; Pincus, R.; Yetzer, K.H.; Mayer, B.; Davies, R.; Ackerman, T.P.; Barker, H.W.; Clothiaux, E.E.; Ellingson, R.G.; Garay, M.J.; Kassianov, E.; Kinne, S.; Macke, A.; O'Hirok, W.; Partain, P.T.; Prigarin, S.M.; Rublev, A.N.; Stephens, G.L.; Szczap, F.; Takara, E.E.; Varnai, T.; Wen, G.Y.; Zhuravleva, T.B. The 13RC—Bringing Together the Most Advanced Radiative Transfer Tools for Cloudy Atmospheres; *Bull. Am. Meteor. Soc.* **2005**, *86*, 1275-1293.
44. Wen, G.Y.; Marshak, A.; Cahalan, R.F.; Remer, L.A.; Kleidman, R.G. 3-D Aerosol-Cloud Radiative Interaction Observed in Collocated MODIS and ASTER Images of Cumulus Cloud Fields; *J. Geophys. Res. Atmos.* **2007**, *112*, D13204; doi: 10.1029/2006jd008267.
45. Marshak, A.; Wen, G.; Coakley, J.A.; Remer, L.A.; Loeb, N.G.; Cahalan, R. F. A Simple Model for the Cloud Adjacency Effect and the Apparent Bluing of Aerosols near Clouds; *J. Geophys. Res. Atmos.* **2008**, *113*, D14517; doi: 10.1029/2007jd009196.
46. Koren, I.; Remer, L.A.; Kaufman, Y.J.; Rudich, Y.; Martins, J.V. On the Twilight Zone between Clouds and Aerosols; *Geophys. Res. Lett.* **2007**, *34*, L08805; doi: 10.1029/2007gl029253.
47. Komhyr, W.D.; Grass, R.D.; Leonard, R.K. Dobson Spectrophotometer 83—a Standard for Total Ozone Measurements, 1962–1987; *J. Geophys. Res. Atmos.* **1989**, *94*, 9847-9861.
48. Kerr, J.B. New Methodology for Deriving Total Ozone and Other Atmospheric Variables from Brewer Spectrophotometer Direct Sun Spectra; *J. Geophys. Res. Atmos.* **2002**, *107*, 4731; doi: 10.1029/2001jd001227.
49. *WMO/GAW Experts Workshop on a Global Surface-Based Network for Long Term Observations of Column Aerosol Optical Properties*; World Meteorological Organization: Geneva, Switzerland, 2005.
50. Tanaka, M.; Nakajima, T.; Shiobara, M. Calibration of a Sunphotometer by Simultaneous Measurements of Direct-Solar and Circumsolar Radiations; *Appl. Opt.* **1986**, *25*, 1170-1175.
51. Shaw, G.E. Sun Photometry; *Bull. Am. Meteor. Soc.* **1983**, *64*, 4-10.
52. Wehrli, C. Calibrations of Filter Radiometers for Determination of Atmospheric Optical Depth; *Metrologia* **2000**, *37*, 419-422.
53. Holben, B.N.; Eck, T.F.; Slutsker, I.; Tanre, D.; Buis, J.P.; Setzer, A.; Vermote, E.; Reagan, J.A.; Kaufman, Y.J.; Nakajima, T.; Lavenu, F.; Jankowiak, I.; Smirnov, A. AERONET—a Federated Instrument Network and Data Archive for Aerosol Characterization; *Rem. Sens. Environ.* **1998**, *66*, 1-16.
54. Sano, I.; Mukai, S.; Yamano, M.; Takamura, T.; Nakajima, T.; Holben, B. Calibration and Validation of Retrieved Aerosol Properties based on AERONET and SKYNET; *Adv. Space Res.* **2003**, *32*, 2159-2164.
55. Dubovik, O.; Lapyonok, T.; Kaufman, Y.J.; Chin, M.; Ginoux, P.; Kahn, R. A.; Sinyuk, A. Retrieving Global Aerosol Sources from Satellites Using Inverse Modeling; *A.C.P.* **2008**, *8*, 209-250.
56. Dubovik, O.; Smirnov, A.; Holben, B.N.; King, M.D.; Kaufman, Y.J.; Eck, T.F.; Slutsker, I. Accuracy Assessments of Aerosol Optical Properties Retrieved from Aerosol Robotic Network (AERONET) Sun and Sky Radiance Measurements; *J. Geophys. Res. Atmos.* **2000**, *105*, 9791-9806.
57. Goloub, P.; Arino, O. Verification of the Consistency of POLDER Aerosol Index over Land with ATSR-2/ERS-2 Fire Product; *Geophys. Res. Lett.* **2000**, *27*, 899-902.
58. Sano, I. Optical Thickness and Angstrom Exponent of Aerosols over the Land and Ocean from Space-Borne Polarimetric Data; *Adv. Space Res.* **2004**, *34*, 833-837.
59. Alexandrov, M.D.; Laci, A.A.; Carlson, B.E.; Cairns, B. Remote Sensing of Atmospheric Aerosols and Trace Gases by Means of Multifilter Rotating Shadowband Radiometer. Part II: Climatological Applications; *J. Atmos. Sci.* **2002**, *59*, 544-566.
60. Abdou, W.A.; Diner, D.J.; Martonchik, J.V.; Bruegge, C.J.; Kahn, R.A.; Gaitley, B.J.; Crean, K.A.; Remer, L.A.; Holben, B. Comparison of Coincident Multiangle Imaging Spectroradiometer and Moderate Resolution Imaging Spectroradiometer Aerosol Optical Depths over Land

- and Ocean Scenes Containing Aerosol Robotic Network Sites; *J. Geophys. Res. Atmos.* **2005**, *110*, D10S07; doi: 10.1029/2004jd004693.
61. Brindley, H.E.; Ignatov, A. Retrieval of Mineral Aerosol Optical Depth and Size Information from Meteosat Second Generation SEVIRI Solar Reflectance Bands; *Rem. Sens. Environ.* **2006**, *102*, 344-363.
 62. Chu, D.A.; Kaufman, Y.J.; Ichoku, C.; Remer, L.A.; Tanre, D.; Holben, B.N. Validation of MODIS Aerosol Optical Depth Retrieval over Land; *Geophys. Res. Lett.* **2002**, *29*, 1617; doi: 10.1029/2001gl013205.
 63. de Almeida Castanho, A.A.D.; Vanderlei Martins, J.; Artaxo, P. MODIS Aerosol Optical Depth Retrievals with High Spatial Resolution over an Urban Area Using the Critical Reflectance; *J. Geophys. Res. Atmos.* **2008**, *113*, D02201; doi: 10.1029/2007JD008751.
 64. Fan, X.H.; Goloub, P.; Deuze, J.L.; Chen, H.B.; Zhang, W.X.; Tanre, D.; Li, Z.Q. Evaluation of PARASOL Aerosol Retrieval over North East Asia; *Rem. Sens. Environ.* **2008**, *112*, 697-707.
 65. Hao, W.M.; Ward, D.E.; Susott, R.A.; Babbitt, R.E.; Nordgren, B.L.; Kaufman, Y.J.; Holben, B.N.; Giles, D.M. Comparison of Aerosol Optical Thickness Measurements by MODIS, AERONET Sun Photometers, and Forest Service Handheld Sun Photometers in Southern Africa during the SAFARI 2000 Campaign; *Int. J. Rem. Sens.* **2005**, *26*, 4169-4183.
 66. Ichoku, C.; Remer, L.A.; Eck, T.F. Quantitative Evaluation and Inter-comparison of Morning and Afternoon Moderate Resolution Imaging Spectroradiometer (MODIS) Aerosol Measurements from Terra and Aqua; *J. Geophys. Res. Atmos.* **2005**, *110*, D10S03; doi: 10.1029/2004jd004987.
 67. Kahn, R.A.; Gaitley, B.J.; Martonchik, J.V.; Diner, D.J.; Crean, K.A.; Holben, B. Multiangle Imaging Spectroradiometer (MISR) Global Aerosol Optical Depth Validation Based on 2 Years of Coincident Aerosol Robotic Network (AERONET) Observations; *J. Geophys. Res. Atmos.* **2005**, *110*, D10S04; doi: 10.1029/2004jd004706.
 68. Kleidman, R.G.; O'Neill, N.T.; Remer, L.A.; Kaufman, Y.J.; Eck, T.F.; Tanre, D.; Dubovik, O.; Holben, B.N. Comparison of Moderate Resolution Imaging Spectroradiometer (MODIS) and Aerosol Robotic Network (AERONET) Remote-Sensing Retrievals of Aerosol Fine Mode Fraction over Ocean; *J. Geophys. Res. Atmos.* **2005**, *110*, D22205; doi: 10.1029/2005jd005760.
 69. Remer, L.A.; Tanre, D.; Kaufman, Y.J.; Ichoku, C.; Mattoo, S.; Levy, R.; Chu, D.A.; Holben, B.; Dubovik, O.; Smirnov, A.; Martins, J.V.; Li, R.R.; Ahmad, Z. Validation of MODIS Aerosol Retrieval over Ocean; *Geophys. Res. Lett.* **2002**, *29*, 1618; doi: 10.1029/2001gl013204.
 70. Torres, O.; Bhartia, P.K.; Sinyuk, A.; Welton, E.J.; Holben, B. Total Ozone Mapping Spectrometer Measurements of Aerosol Absorption from Space: Comparison to SAFARI 2000 Ground-Based Observations; *J. Geophys. Res. Atmos.* **2005**, *110*, D10S18; doi: 10.1029/jd004611.
 71. Russell, P.B.; McCormick, M.P.; Swissler, T.J.; Chu, W.P.; Livingston, J.M.; Fuller, W.H.; Rosen, J.M.; Hofmann, D.J.; McMaster, L.R.; Woods, D.C.; Pepin, T.J. Satellite and Correlative Measurements of the Stratospheric Aerosol. II: Comparison of Measurements Made by SAM II, Dustsondes and an Airborne Lidar; *J. Atmos. Sci.* **1981**, *38*, 1295-1312.
 72. Gille, J.C.; Russell, J.M., III. The Limb Infrared Monitor of the Stratosphere—Experiment Description, Performance, and Results; *J. Geophys. Res. Atmos.* **1984**, *89*, 5125-5140; doi: 10.1029/JD089iD04p05125.
 73. Stolarski, R.S.; Krueger, A.J.; Schoeberl, M.R.; McPeters, R.D.; Newman, P.A.; Alpert, J.C. Nimbus 7 Satellite Measurements of the Springtime Antarctic Ozone Decrease; *Nature* **1986**, *322*, 808-811.
 74. Bovensmann, H.; Burrow, J.P.; Buchwitz, M.; Frerick, J.; Noel, S.; Rozanov, W.; Chance, K.V.; Goede, A.P.H. SCIAMACHY: Mission Objectives and Measurement Modes; *J. Atmos. Sci.* **1999**, *56*, 127-150.
 75. Wenig, M.; Spichtinger, N.; Stohl, A.; Held, G.; Beirle, S.; Wagner, T.; Jahne, B.; Platt, U. Intercontinental Transport of Nitrogen Oxide Pollution Plumes; *Atmos. Chem. Phys.* **2003**, *3*, 387-393.
 76. Wenig, M.; Kuhl, S.; Beirle, S.; Bucsel, E.; Jahne, B.; Platt, U.; Gleason, J.; Wagner, T. Retrieval and Analysis of Stratospheric NO₂ from the Global Ozone Monitoring Experiment; *J. Geophys. Res. Atmos.* **2004**, *109*, D04315; doi: 10.1029/2003jd003652.
 77. New Satellite Data Reveal Impact of Olympic Pollution Controls; National Aeronautics and Space Administration; available at http://www.nasa.gov/topics/earth/features/Olympic_pollution.html (accessed January 31, 2009).
 78. Chance, K.; Palmer, P.I.; Spurr, R.J.D.; Martin, R.V.; Kurosu, T.P.; Jacob, D.J. Satellite Observations of Formaldehyde over North America from GOME; *Geophys. Res. Lett.* **2000**, *27*, 3461-3464.
 79. Fu, T.M.; Jacob, D.J.; Wittrock, F.; Burrows, J.P.; Vrekoussis, M.; Henze, D.K. Global Budgets of Atmospheric Glyoxal and Methylglyoxal, and Implications for Formation of Secondary Organic Aerosols; *J. Geophys. Res. Atmos.* **2008**, *113*, D15303; doi: 10.1029/2007jd009505.
 80. Volkamer, R.; Molina, L.T.; Molina, M.J.; Shirley, T.; Brune, W.H. DOAS Measurement of Glyoxal as an Indicator for Fast VOC Chemistry in Urban Air; *Geophys. Res. Lett.* **2005**, *32*, L08806; doi: 10.1029/2005gl022616.
 81. Wittrock, F.; Richter, A.; Oetjen, H.; Burrows, J.P.; Kanakidou, M.; Myriokefalitakis, S.; Volkamer, R.; Beirle, S.; Platt, U.; Wagner, T. Simultaneous Global Observations of Glyoxal and Formaldehyde from Space; *Geophys. Res. Lett.* **2006**, *33*, L16804; doi: 10.1029/2006gl026310.
 82. Chance, K. Analysis of BrO Measurements from the Global Ozone Monitoring Experiment; *Geophys. Res. Lett.* **1998**, *25*, 3335-3338.
 83. Noel, S.; Bovensmann, H.; Burrows, J.P.; Frerick, J.; Chance, K.V.; Goede, A.P.H. Global Atmospheric Monitoring with SCIAMACHY; *Phys. Chem. Earth C Solar-Terr. Planet. Sci.* **1999**, *24*, 427-434.
 84. Wagner, T.; Leue, C.; Wenig, M.; Pfeilsticker, K.; Platt, U. Spatial and Temporal Distribution of Enhanced Boundary Layer BrO Concentrations Measured by the GOME Instrument aboard ERS-2; *J. Geophys. Res. Atmos.* **2001**, *106*, 24,225-24,235.
 85. Millet, D.B.; Jacob, D.J.; Boersma, K.F.; Fu, T.M.; Kurosu, T.P.; Chance, K.; Heald, C.L.; Guenther, A. Spatial Distribution of Isoprene Emissions from North America Derived from Formaldehyde Column Measurements by the OMI Satellite Sensor; *J. Geophys. Res. Atmos.* **2008**, *113*, D02307; doi: 10.1029/2007jd008950.
 86. De Smedt, I.; Muller, J.F.; Stavrou, T.; van der A, R.; Eskes, H.; Van Roozendaal, M. Twelve Years of Global Observations of Formaldehyde in the Troposphere using GOME and SCIAMACHY Sensors; *Atmos. Phys. Chem.* **2008**, *8*, 4947-4963.
 87. Wagner, T.; Platt, U. Satellite Mapping of Enhanced BrO Concentrations in the Troposphere; *Nature* **1998**, *395*, 486-490.
 88. Liu, X.; Chance, K.; Kurosu, T.P. Improved Ozone Profile Retrievals from GOME Data with Degradation Correction in Reflectance; *Atmos. Phys. Chem.* **2007**, *7*, 1575-1583.
 89. Fishman, J.; Bowman, K.W.; Burrows, J.P.; Richter, A.; Chance, K.V.; Edwards, D.P.; Martin, R.V.; Morris, G.A.; Pierce, R.B.; Ziemke, J.R.; Al-Saadi, J.A.; Creilson, J.K.; Schaack, T.K.; Thompson, A.M. Remote Sensing of Tropospheric Pollution from Space; *Bull. Am. Meteor. Soc.* **2008**, *89*, 805-821.
 90. Martin, R.V. Satellite Remote Sensing of Surface Air Quality; *Atmos. Environ.* **2008**, *42*, 7823-7843.
 91. Koschmeider, H. Theorie der Horizontalen Sichtweite; *Beitr. Phys. Freie Atmosph.* **1924**, *12*, 33-53.
 92. Horvath, H.; Noll, K.E. The Relationship between Atmospheric Light Scattering Coefficient and Visibility; *Atmos. Environ.* **1969**, *3*, 543-552.
 93. Chow, J.C.; Bachmann, J.D.; Wierman, S.S.G.; Mathai, C.V.; Malm, W.C.; White, W.H.; Mueller, P.K.; Kumar, N.; Watson, J.G. Visibility: Science and Regulation—Discussion; *J. Air & Waste Manage. Assoc.* **2002**, *52*, 973-999.
 94. Waggoner, A.P.; Weiss, R.E. Comparison of Fine Particle Mass Concentration and Light Scattering Extinction in Ambient Aerosol; *Atmos. Environ.* **1980**, *14*, 623-626.
 95. Wolff, G.T.; Ferman, M.A.; Kelly, N.A.; Ruthkosky, M.S.; Stroup, D.P. The Relationships between the Chemical Composition of Fine Particles and Visibility in the Detroit Metropolitan Area; *J. Air Pollut. Control Assoc.* **1982**, *32*, 1216-1220.
 96. Tomasi, C. Evaluation of the Atmospheric Content of Particulate Mass from Visibility Observations; *Il Nuovo Cimento C* **1982**, *5*, 223-246.
 97. Malm, W.C. Characteristics and Origins of Haze in the Continental United States; *Earth Sci. Rev.* **1992**, *33*, 1-36.
 98. Hyslop, N. An Evaluation of Interagency Monitoring of Protected Visual Environments (IMPROVE) Collocated Precision and Uncertainty Estimates; *Atmos. Environ.* **2008**, *42*, 2691-2705.
 99. Malm, W.C.; Molenar, J.V.; Eldred, R.A.; Sisler, J.F. Examining the Relationship among Atmospheric Aerosols and Light Scattering and Extinction in the Grand Canyon Area; *J. Geophys. Res.* **1996**, *101*, 19,251-19,265.
 100. Charlson, R.J.; Ahlquist, N.C.; Selvig, H.; McCready, P.B. Monitoring the Atmospheric Aerosol Parameters with the Integrating Nephelometer; *J. Air Pollut. Control Assoc.* **1969**, *19*, 837-842.
 101. King, M.D.; Kaufman, Y.J.; Tanre, D.; Nakajima, T. Remote Sensing of Tropospheric Aerosols from Space: Past, Present, and Future; *Bull. Am. Meteor. Soc.* **1999**, *80*, 2229-2259.
 102. Kaufman, Y.J.; Gobron, N.; Pinty, B.; Widlowski, J.L.; Verstraete, M.M. Relationship between Surface Reflectance in the Visible and mid-IR Used in MODIS Aerosol Algorithm—Theory; *Geophys. Res. Lett.* **2002**, *29*, 2116; doi: 10.1029/2001gl014492.
 103. Levy, R.C.; Remer, L.A.; Dubovik, O. Global Aerosol Optical Properties and Application to Moderate Resolution Imaging Spectroradiometer Aerosol Retrieval over Land; *J. Geophys. Res. Atmos.* **2007**, *112*, D13210; doi: 10.1029/2006jd007815.
 104. Levy, R.C.; Remer, L.A.; Mattoo, S.; Vermote, E.F.; Kaufman, Y.J. Second-Generation Operational Algorithm: Retrieval of Aerosol Properties over Land from Inversion of Moderate Resolution Imaging Spectroradiometer Spectral Reflectance; *J. Geophys. Res. Atmos.* **2007**, *112*, D13211; doi: 10.1029/2006jd007811.
 105. Hsu, N.C.; Tsay, S.C.; King, M.D.; Herman, J.R. Aerosol Properties over Bright-Reflecting Source Regions; *IEEE Trans. Geosci. Remote Sens.* **2004**, *42*, 557-569.
 106. Hsu, N.C.; Tsay, S.C.; King, M.D.; Herman, J.R. Deep Blue Retrievals of Asian Aerosol Properties during ACE-Asia; *IEEE Trans. Geosci. Remote Sens.* **2006**, *44*, 3180-3195.
 107. Yu, H.; Kaufman, Y.J.; Chin, M.; Feingold, G.; Remer, L.A.; Anderson, T.L.; Balkanski, Y.; Bellouin, N.; Boucher, O.; Christopher, S.; DeCola, P.; Kahn, R.; Koch, D.; Loeb, N.; Reddy, M.S.; Schulz, M.; Takemura, T.; Zhou, M. A Review of Measurement-Based Assessments of the

- Aerosol Direct Radiative Effect and Forcing; *Atmos. Chem. Phys.* **2006**, *6*, 613-666.
108. Forster, P.; Ramaswamy, V.; Artaxo, P.; Bernsten, T.; Betts, R.; Fahey, D.W.; Haywood, J.; Lean, J.; Lowe, D.C.; Myhre, G.; Nganga, J.; Prinn, R.; Raga, G.M.S.; Van Dorland, R. *Changes in Atmospheric Constituents and in Radiative Forcing*; Cambridge: New York, 2007.
 109. Remer, L.A.; Kaufman, Y.J.; Kleidman, R.G. Comparison of Three Years of Terra and Aqua MODIS Aerosol Optical Thickness over the Global Oceans; *JGRS Lett.* **2006**, *3*, 537-540.
 110. Loeb, N.G.; Kato, S. Top-of-Atmosphere Direct Radiative Effect of Aerosols over the Tropical Oceans from the Clouds and the Earth's Radiant Energy System (CERES) Satellite Instrument; *J. Clim.* **2002**, *15*, 1474-1484.
 111. Christopher, S.A.; Zhang, J.L.; Kaufman, Y.J.; Remer, L.A. Satellite-Based Assessment of Top of Atmosphere Anthropogenic Aerosol Radiative Forcing over Cloud-Free Oceans; *Geophys. Res. Lett.* **2006**, *33*, L15816; doi: 10.1029/2005gl025535.
 112. Myhre, G.; Berglen, T.F.; Johnsrud, M.; Hoyle, C.R.; Bernsten, T.K.; Christopher, S.A.; Fahey, D.W.; Isaksen, I.S.A.; Jones, T.A.; Kahn, R.A.; Loeb, N.; Quinn, P.; Remer, L.; Schwarz, J.P.; Yttri, K.E. Radiative Forcing of the Direct Aerosol Effect Using a Multi-Observation Approach; *Atmos. Chem. Phys.* **2009**, *9*, 1365-1392.
 113. Kahn, R.A.; Li, W.H.; Moroney, C.; Diner, D.J.; Martonchik, J.V.; Fishbein, E. Aerosol Source Plume Physical Characteristics from Space-Based Multiangle Imaging; *J. Geophys. Res. Atmos.* **2007**, *112*, D11205; doi: 10.1029/2006jd007647.
 114. Liu, Y.; Koutrakis, P.; Kahn, R. Estimating Fine Particulate Matter Component Concentrations and Size Distributions Using Satellite-Retrieved Fractional Aerosol Optical Depth. Part 1: Method Development; *J. Air & Waste Manage. Assoc.* **2007**, *57*, 1351-1359; doi: 10.3155/1047-3289.57.11.1351.
 115. Deuze, J.L.; Herman, M.; Goloub, P.; Tanre, D.; Marchand, A. Characterization of Aerosols over Ocean from POLDER/ADEOS-1; *Geophys. Res. Lett.* **1999**, *26*, 1421-1424.
 116. Gerard, B.; Deuze, J.L.; Herman, M.; Kaufman, Y. J.; Lallart, P.; Oudard, C.; Remer, L.A.; Roger, B.; Six, B.; Tanre, D. Comparisons between POLDER 2 and MODIS/Terra Aerosol Retrievals over Ocean; *J. Geophys. Res. Atmos.* **2005**, *110*, D24211; doi: 10.1029/2005jd006218.
 117. Hodzic, A.; Vautard, R.; Chepfer, H.; Goloub, P.; Menut, L.; Chazette, P.; Deuze, J.L.; Apituley, A.; Couvert, P. Evolution of Aerosol Optical Thickness over Europe during the August 2003 Heat Wave as Seen from CHIMERE Model Simulations and POLDER Data; *Atmos. Chem. Phys.* **2006**, *6*, 1853-1864.
 118. Kacenelenbogen, M.; Leon, J.F.; Chiapello, I.; Tanre, D. Characterization of Aerosol Pollution Events in France Using Ground-Based and POLDER-2 Satellite Data; *Atmos. Chem. Phys.* **2006**, *6*, 4843-4849.
 119. Leon, J.F.; Chazette, P.; Dulac, F. Retrieval and Monitoring of Aerosol Optical Thickness over an Urban Area by Spaceborne and Ground-Based Remote Sensing; *Appl. Opt.* **1999**, *38*, 6918-6926.
 120. Myhre, G.; Stordal, F.; Johnsrud, M.; Ignatov, A.; Mischenko, M.I.; Geogdzhayev, I.V.; Tanre, D.; Deuze, J.L.; Goloub, P.; Nakajima, T.; Higurashi, A.; Torres, O.; Holben, B. Intercomparison of Satellite Retrieved Aerosol Optical Depth over the Ocean; *J. Atmos. Sci.* **2004**, *61*, 499-513.
 121. Vachon, F.; Royer, A.; Aube, M.; Toubbe, B.; O'Neill, N.T.; Teillet, P.M. Remote Sensing of Aerosols over North American Land Surfaces from POLDER and MODIS Measurements; *Atmos. Environ.* **2004**, *38*, 3501-3515.
 122. Mishchenko, M. I.; Cairns, B.; Kopp, G.; Schueler, C.F.; Fafaul, B.A.; Hansen, J.E.; Hooker, R. J.; Itchkawich, T.; Maring, H.B.; Travis, L.D. Accurate Monitoring of Terrestrial Aerosols and Total Solar Irradiance—Introducing the Glory Mission; *Bull. Am. Meteor. Soc.* **2007**, *88*, 677-691.
 123. de Graaf, M.; Stammes, P.; Torres, O.; Koelmeijer, R.B.A. Absorbing Aerosol Index: Sensitivity Analysis, Application to GOME and Comparison with TOMS; *J. Geophys. Res. Atmos.* **2005**, *110*, D01201; doi: 10.1029/2004jd005178.
 124. Torres, O.; Tanskanen, A.; Veihelmann, B.; Ahn, C.; Braak, R.; Bhartia, P.K.; Veeckind, P.; Levelt, P. Aerosols and Surface UV Products from Ozone Monitoring Instrument Observations: an Overview; *J. Geophys. Res. Atmos.* **2007**, *112*, D24547; doi: 10.1029/2007jd008809.
 125. Ackermann, J. The Extinction-to-Backscatter Ratio of Tropospheric Aerosol: a Numerical Study; *J. Atmos. Oceanic Tech.* **1998**, *15*, 1043-1050.
 126. Ansmann, A.; Riebesell, M.; Wandinger, U.; Weitkamp, C.; Voss, E.; Lahmann, W.; Michaelis, W. Combined Raman Elastic-Backscatter Lidar for Vertical Profiling of Moisture, Aerosol Extinction, Backscatter, and Lidar Ratio; *Appl. Phys. B* **1992**, *54*, 1-11.
 127. Papayannis, A.; Amiridis, V.; Mona, L.; Tsaknakis, G.; Balis, D.; Bosenberg, J.; Chaikovski, A.; De Tomasi, F.; Grigorov, I.; Mattis, I.; Mitev, V.; Muller, D.; Nickovic, S.; Perez, C.; Pietruczuk, A.; Pisani, G.; Ravetta, F.; Rizi, V.; Sicard, M.; Trickl, T.; Wiegner, M.; Gerding, M.; Mamouri, R.E.; D'Amico, G.; Pappalardo, G. Systematic Lidar Observations of Saharan Dust over Europe in the Frame of EARLINET (2000–2002); *J. Geophys. Res. Atmos.* **2008**, *113*, D10204; doi: 10.1029/2007jd009028.
 128. Mattis, I.; Ansmann, A.; Muller, D.; Wandinger, U.; Althausen, D. Multiyear Aerosol Observations with Dual-Wavelength Raman Lidar in the Framework of EARLINET; *J. Geophys. Res. Atmos.* **2004**, *109*, D13203; doi: 10.1029/2004jd004600.
 129. Mattis, I.; Muller, D.; Ansmann, A.; Wandinger, U.; Preissler, J.; Seifert, P.; Tesche, M. Ten Years of Multiwavelength Raman Lidar Observations of Free-Tropospheric Aerosol Layers over Central Europe: Geometrical Properties and Annual Cycle; *J. Geophys. Res. Atmos.* **2008**, *113*, D20202; doi: 10.1029/2007jd009636.
 130. Kent, G.S.; Trepte, C.R.; Skeens, K.M.; Winker, D.M. LITE and SAGE II Measurements of Aerosols in the Southern Hemisphere Upper Troposphere; *J. Geophys. Res. Atmos.* **1998**, *103*, 19,111-19,127.
 131. Osborn, M.T.; Kent, G.S.; Trepte, C.R. Stratospheric Aerosol Measurements by the Lidar in Space Technology Experiment; *J. Geophys. Res. Atmos.* **1998**, *103*, 11447-11453.
 132. Zwally, H.J.; Schutz, B.; Abdalati, W.; Abshire, J.; Bentley, C.; Brenner, A.; Bufton, J.; Dezio, J.; Hancock, D.; Harding, D.; Herring, T.; Minster, B.; Quinn, K.; Palm, S.; Spinhirne, J.; Thomas, R. ICESat's Laser Measurements of Polar Ice, Atmosphere, Ocean, and Land; *J. Geodyn.* **2002**, *34*, 405-445.
 133. Hart, W.D.; Spinhirne, J.D.; Palm, S.P.; Hlavka, D.L. Height Distribution between Cloud and Aerosol Layers from the GLAS Spaceborne Lidar in the Indian Ocean Region; *Geophys. Res. Lett.* **2005**, *32*, L22S06; doi: 10.1029/2005gl023671.
 134. Spinhirne, J.D.; Palm, S.P.; Hart, W.D.; Hlavka, D.L.; Welton, E.J. Cloud and Aerosol Measurements from GLAS: Overview and Initial Results; *Geophys. Res. Lett.* **2005**, *32*, L22S03; doi: 10.1029/2005gl023507.
 135. Hoff, R.M.; Palm, S.P.; Engel-Cox, J.A.; Spinhirne, J. GLAS Long-Range Transport Observation of the 2003 California Forest Fire Plumes to the Northeastern US; *Geophys. Res. Lett.* **2005**, *32*, L22S08; doi: 10.1029/2005gl023723.
 136. Winker, D.M.; Hunt, W.H.; McGill, M.J. Initial Performance Assessment of CALIOP; *Geophys. Res. Lett.* **2007**, *34*, L19803; doi: 10.1029/2007gl030135.
 137. CALIPSO Data Products; National Aeronautics and Space Administration; available at <http://www-calipso.larc.nasa.gov/products/> (accessed January 30, 2009).
 138. Redemann, J.; Vaughan, M.A.; Zhang, Q.; Russell, P.B.; Livingston, J.M.; Remer, L.A.; Christopher, S.A. Comparisons of MODIS and CALIPSO Level 2 Aerosol Products and their Combined Use for Calculating Direct Aerosol Radiative Effects. In *Proceedings of the Fall Meeting of the American Geophysical Union (AGU)*; AGU: Washington, DC, 2008; Vol. 89, Abstract No. A21G-05.
 139. Kittaka, C.; Winker, D.; Omar, A.; Liu, Z.; Vaughan, M.; Trepte, C. Global Aerosol Distributions Derived from the CALIPSO Observations. In *Proceedings of the Fall Meeting of the American Geophysical Union (AGU)*; AGU: Washington, DC, 2008; Vol. 89, Abstract A41A-0078.
 140. Chow, J.C.; Engelbrecht, J.P.; Freeman, N.C.G.; Hashim, J.H.; Jantunen, M.; Michaud, J.P.; de Tejada, S.S.; Watson, J.G.; Wei, F.S.; Wilson, W.E.; Yasuno, M.; Zhu, T.; Chapter One: Exposure Measurements; *Chemosphere* **2002**, *49*, 873-901.
 141. Chow, J.C.; Engelbrecht, J.P.; Watson, J.G.; Wilson, W.E.; Frank, N.H.; Zhu, T. Designing Monitoring Networks to Represent Outdoor Human Exposure; *Chemosphere* **2002**, *49*, 961-978.
 142. Bachmann, J. 2007 Critical Review: Will the Circle Be Unbroken: a History of the U.S. National Ambient Air Quality Standards; *J. Air & Waste Manage. Assoc.* **2007**, *57*, 652-697; doi: 10.3155/1047-3289.57.6.652.
 143. *Critical Satellite Climate Change Datasets*; Subcommittee on Commerce, Justice, Science, and Related Agencies; U.S. Congress: Washington, DC, 2009.
 144. Treatment of Data Influenced by Exceptional Events, Final Rule. CFR, Parts 50 and 51, Title 40, 2007.
 145. *Ambient Air Monitoring Strategy for State, Local, and Tribal Air Agencies*; U.S. Environmental Protection Agency; Office of Air Quality Planning and Standards: Research Triangle Park, NC, 2008.
 146. Sister, J.F.; Malm, W.C. Interpretation of Trends of PM_{2.5} and Reconstructed Visibility from the IMPROVE Network; *J. Air & Waste Manage. Assoc.* **2000**, *50*, 775-789.
 147. Baumgardner, R.E.; Isil, S.S.; Bowser, J.J.; Fitzgerald, K.M. Measurements of Rural Sulfur Dioxide and Particle Sulfate: Analysis of CAST-Net Data, 1987 through 1996; *J. Air & Waste Manage. Assoc.* **1999**, *49*, 1266-1279.
 148. Hansen, D.A.; Edgerton, E.S.; Hartsell, B.E.; Jansen, J.J.; Kandasamy, N.; Hidy, G.M.; Blanchard, C.L. The Southeastern Aerosol Research and Characterization Study. Part 1: Overview; *J. Air & Waste Manage. Assoc.* **2003**, *53*, 1460-1471.
 149. Brown, J., Air Quality Criteria for Ozone; U.S. Environmental Protection Agency; available at <http://cfpub.epa.gov/ncea/cfm/recordisplay.cfm?deid=149923> (accessed 2009).
 150. Al-Saadi, J.A.; Rosen, R.; Bohnenkamp, C.; Szykman, J.; Chu, D.A.; Hair, J.; Hostetler, C.; Ferrare, R.; Arcemont, G.; Kittaka, C.; Lewis, L.

- Application of Satellite Aerosol Optical Depth and Airborne Lidar Data for Monitoring Fine Particulate Formation and Transport in San Joaquin Valley, California. Presented at the 10th Conference on Atmospheric Chemistry; American Meteorological Society: Boston, MA, 2008.
151. Prados, A.I.; Huff, A. Air Quality Forecasting and Mapping (Optional Training Session). Presented at the National Air Quality Conference; U.S. Environmental Protection Agency/National Association of Clean Air Agencies: Dallas, TX, 2009.
 152. Koelemeijer, R.B.A.; Homan, C.D.; Matthijsen, J. Comparison of Spatial and Temporal Variations of Aerosol Optical Thickness and Particulate Matter over Europe; *Atmos. Environ.* **2006**, *40*, 5304-5315.
 153. Chu, D.A.; Kaufman, Y.J.; Zibordi, G.; Chern, J.D.; Mao, J.; Li, C.C.; Holben, B.N. Global Monitoring of Air Pollution over Land from the Earth Observing System-Terra Moderate Resolution Imaging Spectroradiometer (MODIS); *J. Geophys. Res. Atmos.* **2003**, *108*, 4661; doi: 10.1029/2002jd003179.
 154. Wang, J.; Christopher, S.A. Intercomparison between Satellite-Derived Aerosol Optical Thickness and PM_{2.5} Mass: Implications for Air Quality Studies; *Geophys. Res. Lett.* **2003**, *30*, 2095; doi: 10.1029/2003gl018174.
 155. Hutchison, K.D. Applications of MODIS Satellite Data and Products for Monitoring Air Quality in the State of Texas; *Atmos. Environ.* **2003**, *37*, 2403-2412.
 156. Hutchison, K.D.; Smith, S.; Faruqui, S. The Use of MODIS Data and Aerosol Products for Air Quality Prediction; *Atmos. Environ.* **2004**, *38*, 5057-5070.
 157. Hutchison, K.D.; Smith, S.; Faruqui, S.J. Correlating MODIS Aerosol Optical Thickness Data with Ground-Based PM_{2.5} Observations across Texas for Use in a Real-Time Air Quality Prediction System; *Atmos. Environ.* **2005**, *39*, 7190-7203.
 158. Hutchison, K.D.; Pekker, T.; Smith, S. Improved Retrievals of Cloud Boundaries for MODIS for Use in Air Quality Modeling; *Atmos. Environ.* **2006**, *40*, 5798-5806.
 159. Hutchison, K.D.; Faruqui, S.J.; Smith, S. Improving Correlations between MODIS Aerosol Optical Thickness and Ground-Based PM_{2.5} Observations through 3D Spatial Analyses; *Atmos. Environ.* **2008**, *42*, 530-543.
 160. Engel-Cox, J.A.; Hoff, R.M.; Haymet, A.D.J. Recommendations on the Use of Satellite Remote-Sensing Data for Urban Air Quality; *J. Air & Waste Manage. Assoc.* **2004**, *54*, 1360-1371.
 161. Engel-Cox, J.A.; Holloman, C.H.; Coutant, B.W.; Hoff, R.M. Qualitative and Quantitative Evaluation of MODIS Satellite Sensor Data for Regional and Urban Scale Air Quality; *Atmos. Environ.* **2004**, *38*, 2495-2509.
 162. Engel-Cox, J.A.; Young, G.S.; Hoff, R.M. Application of Satellite Remote-Sensing Data for Source Analysis of Fine Particulate Matter Transport Events; *J. Air & Waste Manage. Assoc.* **2005**, *55*, 1389-1397.
 163. Engel-Cox, J.A.; Hoff, R.M.; Rogers, R.; Dimmick, F.; Rush, A.C.; Szykman, J.J.; Al-Saadi, J.; Chu, D.A.; Zell, E.R. Integrating Lidar and Satellite Optical Depth with Ambient Monitoring for 3-Dimensional Particulate Characterization; *Atmos. Environ.* **2006**, *40*, 8056-8067.
 164. Al-Saadi, J.; Szykman, J.; Pierce, R.B.; Kittaka, C.; Neil, D.; Chu, D.A.; Remer, L.; Gumley, L.; Prins, E.; Weinstock, L.; MacDonald, C.; Wayland, R.; Dimmick, F.; Fishman, J. Improving National Air Quality Forecasts with Satellite Aerosol Observations; *Bull. Am. Meteor. Soc.* **2005**, *86*, 1249-1261.
 165. *Infusing Satellite Data into Environmental Applications (IDEA)*; National Oceanic and Atmospheric Administration; available at <http://www.star.nesdis.noaa.gov/smcd/spb/aa/> (accessed January 30, 2009).
 166. Hoff, R.; Zhang, H.; Jordan, N.; Prados, A.; Engel-Cox, J.; Huff, A.; Weber, S.; Zell, E.; Kondragunta, S.; Szykman, J.; Johns, B.; Dimmick, F.; Wimmers, A.; Al-Saadi, J.; Kittaka, C. Applications of the Three-Dimensional Air Quality System (3D-AQS) to Western U.S. Air Quality: IDEA, Smog Blog, Smog Stories, AirQuest, and the Remote Sensing Information Gateway; *J. Air & Waste Manage. Assoc.*, in press.
 167. Knapp, K.R.; Frouin, R.; Kondragunta, S.; Prados, A. Toward Aerosol Optical Depth Retrievals over Land from GOES Visible Radiances: Determining Surface Reflectance; *Int. J. Rem. Sens.* **2005**, *26*, 4097-4116.
 168. Prados, A.I.; Kondragunta, S.; Ciren, P.; Knapp, K.R. GOES Aerosol/Smoke Product (GASP) over North America: Comparisons to AERONET and MODIS Observations; *J. Geophys. Res. Atmos.* **2007**, *112*, D15201; doi: 10.1029/2006jd007968.
 169. Liu, Y.; Sarnat, J.A.; Kilaru, A.; Jacob, D.J.; Koutrakis, P. Estimating Ground-Level PM_{2.5} in the Eastern United States Using Satellite Remote Sensing; *Environ. Sci. Technol.* **2005**, *39*, 3269-3278.
 170. Grover, B.D.; Kleinman, M.; Eatough, N.L.; Eatough, D.J.; Hopke, P.K.; Long, R.W.; Wilson, W.E.; Meyer, M.B.; Amb, J.L. Measurement of Total PM_{2.5} Mass (Nonvolatile Plus Semivolatile) with the Filter Dynamic Measurement System Tapered Element Oscillating Microbalance Monitor; *J. Geophys. Res. Atmos.* **2005**, *110*, D07S03; doi: 10.1029/2004jd004995.
 171. Gupta, P.; Christopher, S.A.; Wang, J.; Gehrig, R.; Lee, Y.; Kumar, N. Satellite Remote Sensing of Particulate Matter and Air Quality Assessment over Global Cities; *Atmos. Environ.* **2006**, *40*, 5880-5892.
 172. Gupta, P.; Christopher, S.A.; Box, M.A.; Box, G. P. Multiyear Satellite Remote Sensing of Particulate Matter Air Quality over Sydney, Australia; *Int. J. Rem. Sens.* **2007**, *28*, 4483-4498.
 173. Gupta, P.; Christopher, S.A. Seven Year Particulate Matter Air Quality Assessment from Surface and Satellite Measurements; *Atmos. Chem. Phys.* **2008**, *8*, 3311-3324.
 174. van Donkelaar, A.; Martin, R.V.; Park, R.J. Estimating Ground-Level PM_{2.5} Using Aerosol Optical Depth Determined from Satellite Remote Sensing; *J. Geophys. Res. Atmos.* **2006**, *111*, D21201; doi: 10.1029/2005jd006996.
 175. Kumar, N.; Chu, A.; Foster, A. An Empirical Relationship between PM_{2.5} and Aerosol Optical Depth in Delhi Metropolitan; *Atmos. Environ.* **2007**, *41*, 4492-4503.
 176. Kumar, N.; Chu, A.; Foster, A. Remote Sensing of Ambient Particles in Delhi and its Environs: Estimation and Validation; *Int. J. Remote Sens.* **2008**, *29*, 3383-3405.
 177. Paciorek, C.J.; Liu, Y.; Moreno-Macias, H.; Kondragunta, S. Spatio-temporal Associations between GOES Aerosol Optical Depth Retrievals and Ground-Level PM_{2.5}; *Environ. Sci. Technol.* **2008**, *42*, 5800-5806.
 178. Zhang, H.; Hoff, R.M.; Engel-Cox, J.A. The Relation between MODIS Aerosol Optical Depth and PM_{2.5} over the United States: a Geographical Comparison by EPA Regions; *J. Air & Waste Manage. Assoc.*, in press.
 179. An, X.; Zhu, T.; Wang, Z.; Li, C.; Wang, Y. A Modeling Analysis of a Heavy Air Pollution Episode Occurred in Beijing; *Atmos. Chem. Phys.* **2007**, *7*, 3103-3114.
 180. Schaap, M.; Apituley, A.; Timmermans, R.M.A.; Koelemeijer, R.B.A.; de Leeuw, G. Exploring the Relation between Aerosol Optical Depth and PM_{2.5} at Cabauw, the Netherlands; *Atmos. Chem. Phys.* **2009**, *9*, 909-925.
 181. Apituley, A.; Schaap, M.; Koelemeijer, R.; Timmermans, R.; Schoemaker, R.; de Leeuw, G. Construction of Satellite Derived PM_{2.5} Maps using the Relationship between AOD and PM_{2.5} at the Cabauw Experimental Site for Atmospheric Research (CESAR)—the Netherlands. Presented at Geoscience and Remote Sensing Symposium, 2008, IGARSS 2008, IEEE International: Boston, MA, 2008; Vol. 3, pp III-507-III-510.
 182. Charlson, R.J.; Schwartz, S.E.; Hales, J.M.; Cess, R.D.; Coakley, J.A., Jr.; Hansen, J.E.; Hofmann, D.J. Climate Forcing by Anthropogenic Aerosols; *Science* **1992**, *255*, 423-430.
 183. Eder, B.; Kang, D.; Mathur, R.; Pleim, J.; Yu, S.; Otte, T.; Poulou, G. A Performance Evaluation of the National Air Quality Forecast Capability for the Summer of 2007; *Atmos. Environ.* **2009**, *43*, 2312-2320.
 184. Gupta, P. Thesis, University of Alabama-Huntsville, Huntsville, AL, 2008.
 185. *AIRNow Particles Now*; U.S. Environmental Protection Agency; available at <http://www.airnow.gov/index.cfm?action=airnow.showmap&pollutant=PM2.5> (accessed January 31, 2009).
 186. McMillan, W.W.; Warner, J.X.; Comer, M.M.; Maddy, E.; Chu, A.; Sparling, L.; Eloranta, E.; Hoff, R.; Sachse, G.; Barnett, C.; Razenkov, I.; Wolf, W. AIRS Views Transport from 12 to 22 July 2004 Alaskan/Canadian Fires: Correlation of AIRS CO and MODIS AOD with Forward Trajectories and Comparison of AIRS CO Retrievals with DC-8 In Situ Measurements during INTEX-A/ICARTT; *J. Geophys. Res. Atmos.* **2008**, *113*, D20301; doi: 10.1029/2007jd009711.
 187. *Infusing Satellite Data into Environmental Applications*; National Oceanic and Atmospheric Association; available at <http://www.star.nesdis.noaa.gov/smcd/spb/aa/> (accessed January 30, 2009).
 188. Liu, Z.Y.; Omar, A.; Vaughan, M.; Hair, J.; Kittaka, C.; Hu, Y.X.; Powell, K.; Trepte, C.; Winker, D.; Hostetler, C.; Ferrare, R.; Pierce, R. CALIPSO Lidar Observations of the Optical Properties of Saharan Dust: a Case Study of Long-Range Transport; *J. Geophys. Res. Atmos.* **2008**, *113*, D07207; doi: 10.1029/2007jd008878.
 189. McMillan, W.W.; Pierce, R.; Sparling, L.; Osterman, G.; McCann, K.; Fischer, M.; Rappengluck, B.R.; Newsom, R.; Turner, D.; Kittaka, C.; Evans, K.; Andrews, A.; Oltmans, S.; Biraud, S.; Lefer, B.; Barnett, C. Satellite Observations of Continental-Scale Pollution Transport Contributions to an Ozone Exceedance Episode in Houston, Texas on 1 September 2006 during TEXAQS II; *J. Geophys. Res. Atmos.*, in press.
 190. Xia, X.G.; Eck, T.F.; Holben, B.N.; Phillippe, G.; Chen, H.B. Analysis of the Weekly Cycle of Aerosol Optical Depth Using AERONET and MODIS Data; *J. Geophys. Res. Atmos.* **2008**, *113*, D14217; doi: 10.1029/2007jd009604.
 191. Konovalov, I.B.; Beekmann, M.; Burrows, J.P.; Richter, A. Satellite Measurement Based Estimates of Decadal Changes in European Nitrogen Oxides Emissions; *Atmos. Chem. Phys.* **2008**, *8*, 2623-2641.
 192. Richter, A.; Burrows, J.P.; Nuss, H.; Granier, C.; Niemeier, U. Increase in Tropospheric Nitrogen Dioxide over China Observed from Space; *Nature* **2005**, *437*, 129-132; doi: 10.1038/nature04092.
 193. Mathur, R.; Yu, S.; Kang, D.; Schere, K.L. Assessment of the Wintertime Performance of Developmental Particulate Matter Forecasts with the

- Eta-Community Multiscale Air Quality Modeling System; *J. Geophys. Res. Atmos.* **2008**, *113*, D02303; doi: 10.1029/2007jd008580.
194. Mathur, R. Estimating the Impact of the 2004 Alaskan Forest Fires on Episodic Particulate Matter Pollution over the Eastern United States through Assimilation of Satellite-Derived Aerosol Optical Depths in a Regional Air Quality Model; *J. Geophys. Res. Atmos.* **2008**, *113*, D17302; doi: 10.1029/2007jd009767.
195. McKeen, S.; Chung, S.H.; Wilczak, J.; Grell, G.; Djalalova, I.; Peckham, S.; Gong, W.; Bouchet, V.; Moffet, R.; Tang, Y.; Carmichael, G.R.; Mathur, R.; Yu, S. Evaluation of Several PM_{2.5} Forecast Models Using Data Collected during the ICARTT/NEAQS 2004 Field Study; *J. Geophys. Res. Atmos.* **2007**, *112*, D10s20; doi: 10.1029/2006jd007608.
196. Yu, S.C.; Mathur, R.; Schere, K.; Kang, D.W.; Pleim, J.; Young, J.; Tong, D.; Pouliot, G.; McKeen, S.A.; Rao, S.T. Evaluation of Real-Time PM_{2.5} Forecasts and Process Analysis for PM_{2.5} Formation over the Eastern United States Using the Eta-CMAQ Forecast Model during the 2004 ICARTT Study; *J. Geophys. Res. Atmos.* **2008**, *113*, D06204; doi: 10.1029/2007jd009226.
197. Wang, J.; Christopher, S.A. Mesoscale Modeling of Central American Smoke Transport to the United States: 2. Smoke Radiative Impact on Regional Surface Energy Budget and Boundary Layer Evolution; *J. Geophys. Res. Atmos.* **2006**, *111*, D14S92; doi: 10.1029/2005jd006720.
198. Newchurch, M.A.B.; Khan, M.S.; Koshak, B.; Nair, U.S.; Fuller, K.; Wang, L.; Park, Y.; Williams, R.; Christopher, S.; Kim, J.; Liu, X.; Byun, D.; Pierce, B.; Chance, K.; Kurosu, T.P.; McMillan, W.W. Improvements in Air-Quality Forecasts from Satellite Observations. Presented at the Community Modeling and Analysis Conference, Chapel Hill, NC, October 6–8, 2008.
199. Justice, C.O.; Giglio, L.; Korontzi, S.; Owens, J.; Morisette, J.T.; Roy, D.; Descloitres, J.; Alleaume, S.; Petitcolin, F.; Kaufman, Y. The MODIS Fire Products; *Remote Sens. Environ.* **2002**, *83*, 244–262.
200. Zhang, X.Y.; Kondragunta, S. Estimating Forest Biomass in the USA Using Generalized Allometric Models and MODIS Land Products; *Geophys. Res. Lett.* **2006**, *33*, L09402; doi: 10.1029/2006gl025879.
201. Reid, J.S.; Prins, E.M.; Westphal, D.L.; Schmidt, C.C.; Richardson, K.A.; Christopher, S.A.; Eck, T.F.; Reid, E.A.; Curtis, C.A.; Hoffman, J.P. Real-Time Monitoring of South American Smoke Particle Emissions and Transport Using a Coupled Remote Sensing/Box-Model Approach; *Geophys. Res. Lett.* **2004**, *31*, L06107; doi: 10.1029/2003gl018845.
202. Wang, J.; Christopher, S.A.; Nair, U.S.; Reid, J.S.; Prins, E.M.; Szykman, J.; Hand, J.L. Mesoscale Modeling of Central American Smoke Transport to the United States: 1. “Top-Down” Assessment of Emission Strength and Diurnal Variation Impacts; *J. Geophys. Res. Atmos.* **2006**, *111*, doi: 10.1029/2005jd006416.
203. Stein, A.F.; Rolph, G.D.; Draxler, R.R.; Stunder, B.; Ruminski, M. Verification of the NOAA Smoke Forecast: Model Sensitivity to the Injection Height; *Weather Forecast.* doi: 10.1175/2008WAF222166.1.
204. Kondragunta, S.; Lee, P.; McQueen, J.; Kittaka, C.; Prados, A.I.; Ciren, P.; Laszlo, I.; Pierce, R.B.; Hoff, R.; Szykman, J.J. Air Quality Forecast Verification Using Satellite Data; *J. Appl. Meteor. Clim.* **2008**, *47*, 425–442.
205. Schmidt, H.; Martin, D. Adjoint Sensitivity of Episodic Ozone in the Paris Area to Emissions on the Continental Scale; *J. Geophys. Res. Atmos.* **2003**, *108*, 8561; doi: 10.1029/2001jd001583.
206. Hollingsworth, A.; Engelen, R.J.; Textor, C.; Benedetti, A.; Boucher, O.; Chevallier, F.; Dethof, A.; Elbern, H.; Eskes, H.; Flemming, J.; Granier, C.; Kaiser, J.W.; Morcrette, J.J.; Rayner, P.; Peuch, V.H.; Rouil, L.; Schultz, M.G.; Simmons, A.J. Toward a Monitoring and Forecasting System for Atmospheric Composition: the GEMS Project; *Bull. Am. Meteor. Soc.* **2008**, *89*, 1147–1164.
207. Stavrakou, T.; Muller, J.F.; Boersma, K.F.; De Smedt, I.; van der A, R.J.; Assessing the Distribution and Growth Rates of NO_x Emission Sources by Inverting a 10-Year Record of NO₂ Satellite Columns; *Geophys. Res. Lett.* **2008**, *35*, L10801; doi: 10.1029/2008gl033521.
208. Liu, Y.; Franklin, M.; Kahn, R.; Koutrakis, P. Using Aerosol Optical Thickness to Predict Ground-Level PM_{2.5} Concentrations in the St. Louis Area: a Comparison between MISR and MODIS; *Rem. Sens. Environ.* **2007**, *107*, 33–44; doi: 10.1016/j.rse.2006.05.022.
209. Rossow, W.B.; Duenas, E.N. The International Satellite Cloud Climatology Project (ISCCP) Website—An Online Resource for Research; *Bull. Am. Meteor. Soc.* **2004**, *85*, 167–172.
210. Rossow, W.B.; Schiffer, R.A. Advances in Understanding Clouds from ISCCP; *Bull. Am. Meteor. Soc.* **1999**, *80*, 2261–2287.
211. Gupta, P.; Christopher, S.A. An Evaluation of Terra-MODIS Sampling for Monthly and Annual Particulate Matter Air Quality Assessment over the Southeastern United States; *Atmos. Environ.* **2008**, *42*, 6465–6471.
212. Kaufman, Y. J. Satellite Sensing of Aerosol Absorption; *J. Geophys. Res.* **1987**, *92*, 4307–4317.
213. Fraser, R.S.; Kaufman, Y.J. The Relative Importance of Aerosol Scattering and Absorption in Remote Sensing; *IEEE Trans. Geosci. Remote Sens.* **1985**, *5*, 625–633.
214. Lyapustin, A.; Williams, D.L.; Markham, B.; Irons, J.; Holben, B.; Wang, Y. A Method for Unbiased High-Resolution Aerosol Retrieval from Landsat; *J. Atmos. Sci.* **2004**, *61*, 1233–1244.
215. Lyapustin, A.; Wang, Y.; Frey, R. An Automatic Cloud Mask Algorithm based on Time Series of MODIS Measurements; *J. Geophys. Res. Atmos.* **2008**, *113*, D16207; doi: 10.1029/2007jd009641.
216. Test Specifications for PM₁₀, PM_{2.5} and PM_{10–2.5} Candidate Equivalent Methods. CFR, Part 53, Title 40, 2006, Appendix C-4.
217. Lamsal, L.N.; Martin, R.V.; van Donkelaar, A.; Steinbacher, M.; Celarier, E.A.; Bucsela, E.; Dunlea, E.J.; Pinto, J.P. Ground-Level Nitrogen Dioxide Concentrations Inferred from the Satellite-Borne Ozone Monitoring Instrument; *J. Geophys. Res. Atmos.* **2008**, *113*, D16308; doi: 10.1029/2007jd009235.
218. Blond, N.; Boersma, K.F.; Eskes, H.J.; van der A, R.J.; Van Roozendael, M.; De Smedt, I.; Bergametti, G.; Vautard, R. Intercomparison of SCIAMACHY Nitrogen Dioxide Observations, in Situ Measurements and Air Quality Modeling Results over Western Europe; *J. Geophys. Res. Atmos.* **2007**, *112*, D10311; doi: 10.1029/2006jd007277.
219. *Risk and Exposure Assessment to Support the Review of the NO₂ Primary National Ambient Air Quality Standard*; U.S. Environmental Protection Agency: Research Triangle Park, NC, 2008.
220. Whiteman, D.N.; Veselovskii, I.; Cadirola, M.; Rush, K.; Comer, J.; Potter, J.R.; Tola, R. Demonstration Measurements of Water Vapor, Cirrus Clouds, and Carbon Dioxide Using a High-Performance Raman Lidar; *J. Atmos. Oceanic Tech.* **2007**, *24*, 1377–1388.
221. Ansmann, A.; Wandinger, U.; Le Rille, O.; Lajas, D.; Straume, A.G. Particle Backscatter and Extinction Profiling with the Spaceborne High-Spectral-Resolution Doppler Lidar ALADIN: Methodology and Simulations; *Appl. Opt.* **2007**, *46*, 6606–6622.
222. Marini, A.E. ATLID: the Technology Development Programme for ESA's Satellite-Borne Atmospheric Lidar; *ESA Bull. Eur. Space Agency* **1998**, *95*, 113–118.
223. Schmit, T.J.; Li, J.; Gurka, J.J.; Goldberg, M.D.; Schrab, K.J.; Li, J.L.; Feltz, W.F. The GOES-R Advanced Baseline Imager and the Continuation of Current Sounder Products; *J. Appl. Meteor. Clim.* **2008**, *47*, 2696–2711.
224. *Overview of the “Ibuki” (GOSAT)*; Japan Aerospace Exploration Agency; available at http://www.jaxa.jp/countdown/f15/overview/ibuki_e.html (accessed January 31, 2009).
225. *ESA Satellite Missions*; European Space Agency; available at <http://earth.esa.int/missions/> (available at January 31, 2009).
226. *NSSDC Master Catalog Search*; National Space Science Data Center; available at <http://nssdc.gsfc.nasa.gov/nmc/spacecraftSearch.doc> (accessed January 31, 2009).
227. Volz, F.E. Economical Multispectral Sun Photometer for Measurements of Aerosol Extinction from 0.44 μm to 1.6 μm and Precipitable Water; *Appl. Opt.* **1974**, *13*, 1732–1733.
228. Krotkov, N. Earth Observatory: Sulfur Dioxide Emissions, Bulgaria; National Aeronautics and Space Administration; available at <http://earthobservatory.nasa.gov/IOTD/view.php?id=36790> (accessed January 31, 2009).
229. Chu, D.A.; Szykman, J.; Kittaka, C.; Chin, M.; Liu, H.-C.; Remer, L.; Al-Saadi, J.; Winker, D. Developing Aerosol Height Product from MODIS and Synergy of MODIS and CALIPSO Measurements for Global Application. In *Atmospheric Remote Sensing for Air Pollution and Human Health*, IGARSS '08, SPIE: Boston, MA, 2008; pp IV-303–IV-306.

About the Authors

Raymond M. Hoff is a professor with the Department of Physics, the director of the Joint Center for Earth Systems Technology, and the director of the Goddard Earth Sciences and Technology Center at University of Maryland/ Baltimore County. Sundar A. Christopher is a professor with the Department of Atmospheric Sciences and the associate director of Earth System Science Center at the University of Alabama-Huntsville. Please address correspondence to: Raymond M. Hoff, Joint Center for Earth Systems Technology, 1000 Hilltop Circle, Baltimore, MD 21250; phone: +1-410-455-1610; e-mail: hoff@umbc.edu.